Doctoral Dissertation
Doctoral Program in Materials Science and Technology (38th Cycle)

From waste to resources: Tailored recycling strategies for polyolefins

Giulia Bernagozzi
* * * * * *

Supervisors
Prof. Rossella Arrigo, Supervisor
Prof. Alberto Frache, Co-Supervisor

Politecnico di Torino
2026

I hereby declare that, the contents and organisation of this dissertation constitute my own original work and does not compromise in any way the rights of third parties, including those relating to the security of personal data.

…….....

Giulia Bernagozzi

Turin, 2026

Summary

Plastic itself is not the problem; rather, the way plastic waste is managed represents the real challenge. Polymers are indispensable materials in modern society, yet their sustainability is critically undermined by ineffective end-of-life management and the limited performance of recycled materials. This thesis addresses these challenges by focusing on the mechanical recycling of polyolefins - specifically polypropylene (PP) and high-density polyethylene (HDPE) - which dominate plastic production. The work is grounded in a critical analysis of current plastic production, waste management, and recycling practices, highlighting how, despite increasing regulatory pressure and ambitious policy targets, the plastics economy remains largely linear. It is now well established that meaningful sustainability improvements must rely on enhanced circularity rather than indiscriminate material substitution. Within this context, mechanical recycling is identified as the most mature and energy-efficient recycling route.

The experimental work systematically investigates the thermo-mechanical degradation of polypropylene during repeated extrusion cycles, revealing that PP degradation is dominated by random chain scission, leading to progressive reductions in molecular weight, without significant oxidative modification of the polymer. To counteract these effects, a reactive repair additive is evaluated under conditions representative of both pre-consumer and post-consumer mechanical recycling. The results demonstrate that the additive is effective in mitigating viscosity loss, partially rebuilding molecular weight, and inducing controlled modifications of the macromolecular architecture.

Beyond short-term processing behavior, the long-term performance of recycled polypropylene is assessed through photo-oxidative aging experiments. The evolution of chemical structure, thermal response, and mechanical properties is systematically analyzed, providing clear evidence that the introduction of the repair additive is also able to maintain adequate mechanical properties for long

periods under photo-oxidative degradation. In this way, the useful life of films produced with recycled plastic can be extended, greatly reducing the loss of elongation at break and stress at break even when exposed to solar UV light and condensation cycles.

This work further explores the mechanical recycling of high-density polyethylene, whose degradation behavior is characterized by the coexistence of chain scission, branching, and crosslinking reactions, leading to highly heterogeneous microstructures. By tailoring processing conditions, these degradation-induced reactions are deliberately exploited to promote long-chain branching. As a result, recycled HDPE with enhanced melt strength and increased ductility is obtained, enabling its use in processing technologies dominated by elongational flow.

In addition, the thesis investigates the functional upgrading of recycled PP through the incorporation of different flame-retardant systems. For each formulation, rheological behavior, morphology, and fire retardancy are systematically compared with those of virgin PP-based systems. The results demonstrate that effective flame retardancy can be achieved in recycled matrices, while also revealing how polymer degradation influences the efficiency and stability of flame-retardant additives.

Finally, the end-of-life mechanical recycling of flame-retarded PP is examined by subjecting an intumescent flame-retardant system to multiple extrusion cycles. The evolution of rheological, mechanical, morphological, and fire-retardant properties during repeated reprocessing highlights the combined effects of polymer degradation and additive redistribution. These findings provide critical insights into the recyclability of functionalized plastics and underline the importance of designing flame-retardant systems that remain compatible with mechanical recycling across multiple life cycles.

Overall, unlike conventional re-stabilization approaches, which merely slow down further degradation, the strategies developed in this PhD thesis actively enable structural recovery and functional upgrading. The results reported in this PhD dissertation prove that through targeted microstructure control and functional design, recycled polyolefins can achieve enhanced performance, extended application potential, and higher added value. These findings demonstrate that mechanical recycling can evolve from a downcycling practice into a robust technological pillar for a circular plastics economy.

Acknowledgment

First of all, I would like to thank my supervisors Prof. Rossella Arrigo and Prof. Alberto Frache for the trust you placed in me from the very beginning, and for all the guidance, teaching, and support you have provided since the first moment we met. Having you as my supervisors throughout this journey has certainly been one of the best things that has ever happened to me.

I would also like to acknowledge those who financially supported my PhD program. This project was carried out within the MICS (Made in Italy – Circular and Sustainable) Extended Partnership and received funding from the European Union Next-GenerationEU (PIANO NAZIONALE DI RIPRESA E RESILIENZA (PNRR) – MISSIONE 4 COMPONENTE 2, INVESTIMENTO 1.3 – D.D. 1551.11-10-2022, PE00000004).

I would also like to sincerely thank Nexam Chemical for providing their additives for use in my PhD project and for all the fruitful discussions that I had the honor to take part in.

A special thanks goes to Prof. Miaojun Xu for hosting me in his laboratories in Harbin, China, where I carried out part of my research. I am deeply grateful to all the people who made me feel at home even thousands of kilometers away.

My heartfelt thanks go to the entire research group All-Polymer. Thank you for your patience and for filling my days with joy.

I would also like to thank everyone working at PoliAL.

Finally, I thank my friends and my family for their constant support.

To little Giagia

Contents

List of Tables

List of Figures

List of Abbreviations

The main abbreviations used in the thesis are classified alphabetically.

APP	Ammonium polyphosphate
ATR-FTIR	Attenuated total reflection – Fourier Transform Infrared Spectroscopy
DR	Draw ratio
DSC	Differential Scanning Calorimetry
EDX	Energy Dispersive X-Ray Analysis
EHC	Effective heat of combustion [MJ/kg]
FIGRA	Fire growth rate index [$kW/m^2/s$]
FPI	Fire performance index [m^2*s/kW]
FR	Flame-retardant
FRI	Flame retardancy index
G’	Rheological storage modulus [Pa]
G’’	Rheological loss modulus [Pa]
HDPE	High-density polyethylene
HRR	Heat release rate
IFR	Intumescent flame-retardant
LCB	Long-chain branching
LOI	Limiting oxygen index [%]
MARHE	Maximum average rate of heat emission [kW/m^2]
$Mg(OH)_2$	Magnesium hydroxide
MLR	Mass loss rate [g/s]
MPP	Melamine pyrophosphate
MS	Melt strength

M_w	Molecular weight
NEX	Nexamite® additives
PE	Polyethylene
PER	Pentaerythritol
PET	Polyethylene terephthalate
PP	Polypropylene
PAPP	Piperazine pyrophosphate
rPP	Recycled polypropylene
SEA	Specific smoke extinction area [m^2/kg]
SEM	Scanning Electron Microscopy
SPR	Smoke production rate [m^2/s]
TGA	Thermogravimetric analysis
TSP	Total smoke production [m^2]
TSR	Total smoke release [m^2/m^2]
THR	Total heat release [MJ/m^2]
TTI	Time to ignition [s]
T_{onset}	Temperature of initial degradation
T_{max}	Temperature of maximum degradation rate
TSE	Twin-screw extruder
UL-94	Vertical burning test
vPP	Virgin polypropylene
wt. %	Weight percentage [%]
Xc	Crystallinity degree [%]
ΔH_m	Melting enthalpy [J/g]
$\Delta H_{100\%}$	Melting enthalpy for a 100% crystalline [J/g]
$\lambda H(\lambda)$	Weighted relaxation spectra
η^*	Complex viscosity [Pa*s]
η_0	Zero-shear viscosity [Pa*s]
ω	Angular frequency [rad/s]

Chapter 1

Introduction

1.1 Critical issues in plastic waste management

Plastics occupy a central and irreplaceable position in modern material systems, supporting countless industrial sectors and consumer applications due to their versatility, durability, low density, and cost-effective manufacturing. These features have enabled plastics to deliver significant societal and environmental benefits, including light weighting in transportation, food preservation through high-performance packaging, and improved safety and comfort in diverse applications. Yet these same characteristics also contribute to the escalating environmental burden associated with their end-of-life management. In 2024, global plastic production reached approximately 430.9 million tonnes (Mt), while European demand alone amounted to 54.6 Mt [1]. The total magnitude of this production inevitably gives rise to vast quantities of post-consumer waste. In addition, a recent study estimates that the annual global demand and the waste generation of polymers are expected to double by 2100 [2]. Despite progressively expanding collection schemes and recycling infrastructures across Europe, substantial fractions of discarded plastics continue to be landfilled or incinerated, causing the irreversible loss of valuable materials and the amplification of climate and pollution impacts [3].

Recent statistics illustrate that although meaningful progress has been made, significant gaps remain in achieving a truly circular plastics economy. In 2024, only 7.7 Mt were successfully reincorporated into new products, corresponding to an effective recycled-content rate of roughly 14% [1]. While this represents an improvement compared with previous years, as shown in Figure 1, the discrepancy between collected and reused material remains substantial. It reflects systemic inefficiencies throughout the plastics value chain, including limited recyclability embedded in product design, inadequate sorting technologies, contamination issues that impair recyclate quality, and persistent price competition with low-cost virgin polymers. Achieving a circular plastics system

demands not only improved waste collection, sorting, and reprocessing technologies, but also fundamental shifts in product-design philosophies, regulatory frameworks and business models across the entire plastics economy [4–6]. There is growing recognition of the relevance of designing for durability, reusability and recyclability to ensure that materials retain their functional and economic value over multiple life cycles [7,8]. Nevertheless, global market data confirm that the plastics economy remains overwhelmingly linear, with more than half of annual plastic production accumulating as unrecovered waste [1]. Thus, improving recycling performance and expanding the availability of high-quality secondary materials remain central pillars in the transition toward a sustainable circular economy.

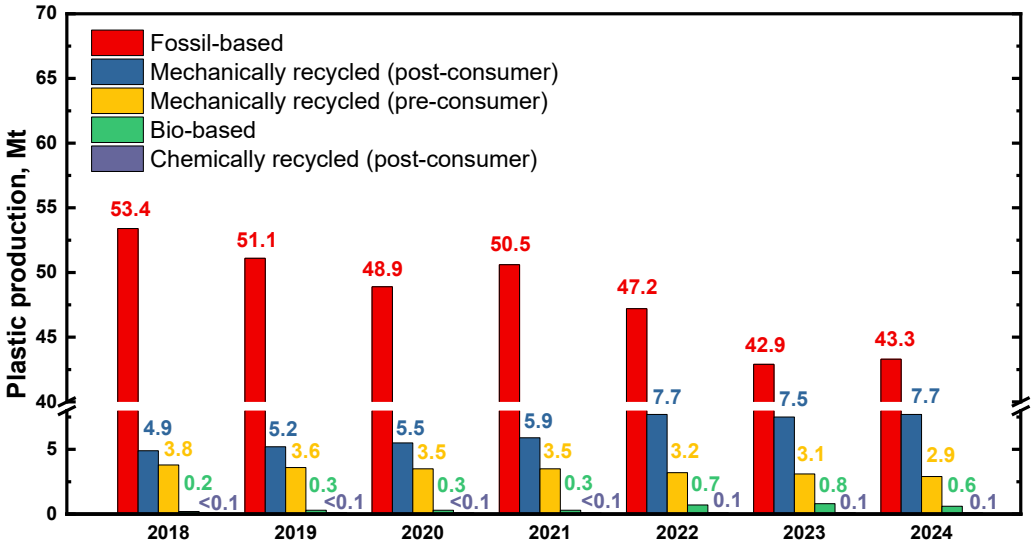

Figure 1. European plastic production from 2018 to 2024 (adapted from [1]).

Within this context, mechanical recycling constitutes the most mature, widely implemented and energy-efficient route for polymer recovery and reuse [5,8,9]. Mechanical recycling of plastics typically involves four main stages. First, waste materials are collected from post-consumer or post-industrial streams. They are then sorted to separate different polymer types and remove non-plastic fractions. The sorted plastics undergo washing, which removes surface contaminants such as residues, labels, and dirt. Finally, the cleaned materials are shredded, melt reprocessed and pelletized into secondary raw materials suitable for manufacturing new plastic products [10]. Ideally, mechanically recycled plastics should be capable of substituting virgin materials in equivalent applications. In practice, however, polymer degradation during service life and repeated processing cycles continues to pose significant technical and economic constraints. Thermal oxidation, chain scission and other degradation mechanisms modify molecular weight and impair mechanical, thermal and aesthetic properties, thereby limiting the range of feasible end-uses for recovered materials [11,12]. These challenges undermine the competitiveness of recycled polymers and

highlight the need for further advances in stabilization strategies, compatibilization technologies, and processing enhancements. From an economical point of view, the ability to generate recycled materials whose performance approaches or surpasses that of virgin plastics is crucial for sustaining market demand and accelerating the adoption of secondary raw materials.

Another major issue related to plastics that should definitely be mentioned is the dissemination of microplastics, which is now recognized as one of the main environmental and health concerns associated with the widespread use and dispersion of plastics. All the plastics waste that leaks into the environment each year progressively fragment into smaller particles. It has been estimated that in 2010 a percentage between 1.7 % and 4.6 % of the total plastic waste generated, corresponding to a range between 4.8 and 12.7 Mt, entered the ocean, where they gradually degrade in microplastics [13]. These particles are now detected in marine ecosystem, freshwater systems and even the atmosphere, raising concerns about their ingestion and inhalation by living organisms. Recent studies also highlight that recycling itself can be a source of microplastics: during some steps of mechanical recycling processes, such as crushing and grinding, plastic waste undergoes strong mechanical stresses that generate large numbers of microplastic fragments [14]. Mechanical recycling processes can release particles into wastewater and airborne dust within recycling facilities. Consequently, the potential exposure of workers to aerosolized microplastics in recycling plants is emerging as an important occupational health issue, highlighting the need for improved monitoring, containment strategies, and protective measures.

1.1.1 Current status and outlook of plastic recycling in Europe

Over the years, notable improvements in plastic waste management and recycling have been achieved, as evidenced by the analysis *Circular Economy for Plastics – A European Analysis* (2024) [15]. Between 2018 and 2022, the availability of post-consumer recycled plastics in Europe increased by more than 70%, reaching 6.8 Mt, while circular plastic content in new products rose to 13.5%. Mechanical recycling capacity expanded significantly, with mechanically recycled plastics reaching roughly 8.7 Mt in 2022 - an increase of more than 57% since 2018 (Figure 2). By contrast, chemical recycling remained at an early stage, representing only 0.1% of European plastics production in 2022. Waste-management data further indicate that, for the first time, more plastics were recycled than landfilled in 2022, as the overall recycling rate reached 26.9%. Although these developments mark important milestones, challenges remain, including persistently high incineration rates (up 15% since 2018), inadequate sorting capacity and limited uptake of recycled content in certain sectors such as automotive.

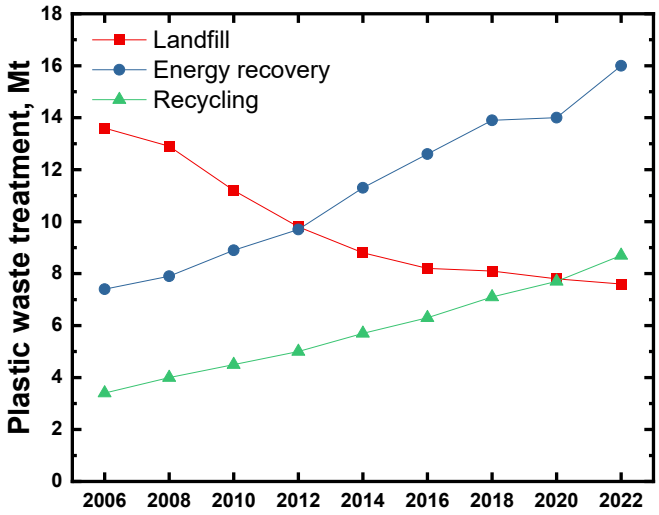

Figure 2. Evolution of post-consumer plastics waste treatment from 2006 to 2022 (adapted from [15]).

The *Plastics Transition* roadmap evaluated by Plastics Europe [16] outlines an ambitious and quantitatively detailed forecast for the scale-up of plastic recycling as a core mechanism for achieving both circularity and decarbonization within the European plastics system. The roadmap shown in Figure 3 anticipates that recycling, both mechanical and chemical recycling technologies, will become one of the dominant sources of polymer feedstock by 2050, fundamentally reshaping material flows and reducing dependence on fossil-based plastics. Between 2021 and 2030, the share of circular plastics is projected to more than double from 12% to 25%, driven by significant improvements in waste collection and sorting. Mechanical recycling is expected to increase from 5 Mt to 9 Mt, while chemical recycling is projected to rise from negligible levels to 3 Mt by 2030, marking a decisive technological shift towards processes capable of handling more heterogeneous and contaminated waste streams. The long-term outlook intensifies this trajectory: by 2050, mechanical recycling is forecast to reach 15 Mt and chemical recycling 12 Mt, together supplying approximately 27 Mt of recyclate - around 40% of total plastics demand - and forming a key component of the roadmap's projection that 65% of all plastics consumed in Europe will be produced from circular feedstocks. This structural evolution is positioned not only as a material-circularity strategy but also as one of the most effective levers for reducing greenhouse gas emissions across the plastics life cycle, particularly through the displacement of virgin fossil feedstocks and the avoidance of incineration emissions. The roadmap emphasizes that achieving these recycling targets will require coordinated systemic changes, including large-scale investment in new recycling capacity, harmonized EU-wide regulatory frameworks, the phase-out of landfill and incineration for recyclable plastics, and improved integration across the entire value chain, from polymer producers to waste-management operators. Overall, the forecast positions recycling as a central pillar of Europe's transition to a climate-neutral and resource-efficient plastics

economy, while acknowledging that its success depends on enabling policy conditions, technological innovation, and cross-sectoral collaboration.

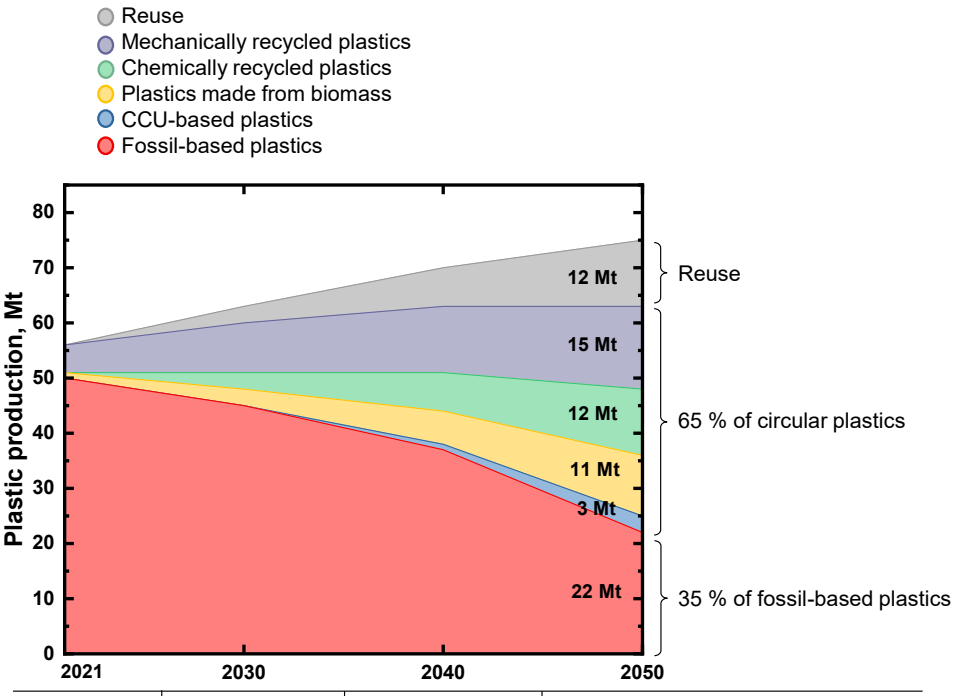

57 Mt	60 Mt	62 Mt	65 Mt	Converter's use (in Mt)
12%	25%	40%	65%	% of circular plastics compared to total converter's use

Figure 3. European plastic recycling forecast (adapted from [16]).

The European union (EU), in turn, is committed to publishing new regulations which set recycled-plastic content targets for different sectors. In the packaging and single-use sector, Single-Use Plastics Directive (SUPD, Directive (EU) 2019/904) introduces necessary recycled-content targets specifically for beverage bottles, namely 25% recycled plastic in polyethylene terephthalate (PET) beverage bottles by 2025 and 30% recycled plastic in all plastic beverage bottles by 2030. Besides, the Packaging and Packaging Waste Regulation (PPWR, Regulation (EU) 2025/40) is the current cornerstone of EU legislation governing packaging materials, including plastics: from 2030, plastic packaging placed on the EU market must contain a minimum percentage of post-consumer recycled plastic, with the specific threshold to be published. The other targets defined in the regulation are 30% recycled plastic for bottles, 10% for plastics in contact with food (non-PET), and 35% for other plastic packaging by 2030, rising further by 2040. Beyond recycled content mandates, the PPWR also includes design and recyclability requirements to ensure that packaging is suitable for mechanical recycling, which reinforces the connection between product design and achievable recycled content. During 2025, also a new regulation for End-of-Life vehicles (ELV) was published, in which a mandatory minimum recycled-plastic content will be introduced for new vehicles placed on the EU market. The target should

amount to at least 15% recycled plastic within six years of the regulation's entry into force, rising to 25% within ten years. Of this recycled content, a defined proportion (e.g., 20% of the overall target) may need to come specifically from plastics recovered from end-of-life vehicles or post-use automotive components, reinforcing closed-loop recycling within the automotive system. The new ELV Regulation also incorporates design for recycling provisions and extended producer responsibility to ensure that vehicles are easier to dismantle and recycle.

It is evident that meeting all mandated targets requires coordinated efforts across multiple fronts; nevertheless, the current European situation has reached a critical moment. The *Plastics Recycling Industry Figures 2024* analysis [17] reveal the first major stagnation of the recycling sector after years of growth across Europe. Despite an extensive infrastructure composed of an installed capacity of 13.5 Mt, recyclate output decreased from 7.7 Mt in 2023 to around 7.5 Mt in 2024. This contraction was driven primarily by falling market demand, high production and energy costs, and escalating competition from low-priced imported recyclates, which forced numerous producers to reduce or suspend operations. Turnover fell by 5.5%, marking the second consecutive year of economic decline. Polymer-specific analyses reveal stagnant or declining performance across multiple streams, including polyolefin films, PET, polypropylene (PP) and high-density polyethylene (HDPE). Polyolefin film recycling capacity plateaued at 3.5 Mt, representing roughly 26% of Europe's total installed capacity. PET, the second largest stream, exhibited a modest capacity increase from 3.2 to 3.3 Mt, yet PET recyclers faced heightened market pressures due to the growing importation of low-priced recycled PET, which led to unprecedented stock accumulations. These dynamics threatened the viability of domestic PET recyclers, especially those producing food-contact grade materials subject to stringent regulatory requirements. Rigid PP and HDPE capacities remained relatively stable at 1.8 and 1.75 Mt, respectively, though many HDPE recyclers reported reduced turnover and performance. Other polymer streams either stagnated or exhibited limited growth. At the same time, waste exports increased sharply, up 15% relative to 2023 and 36% relative to 2022, while the share of imported polymers rose to 24%, exacerbating domestic underutilization and destabilizing secondary-material markets. Particularly concerning were widespread facility closures in 2024, amounting to 0.3 Mt of lost capacity - double the figure recorded in 2023 - with projections suggesting the volume of closures could triple by 2025 without intervention. These developments collectively expose the fragility of Europe's recycling ecosystem and cast doubt on the achievability of mandated recycling and recycled-content targets.

1.1.2 The challenge of replacing plastics

In any case, plastics occupy a central and irreplaceable position in contemporary material systems due to their exceptional versatility, low density, tunable mechanical and barrier properties, and cost-effective manufacturing. An

expanding body of Life Cycle Assessment (LCA) literature [18] demonstrates that their functional advantages frequently translate into net environmental benefits when compared with conventional alternatives. In their work, Meng et al. [19] show that the plastic products result in fewer greenhouse gas emission if compared to their alternatives - paper, aluminum, steel, glass among few to mention - in 15 of the 16 applications considered, demonstrating also that in some applications no suitable alternatives to plastics exist.

In the packaging sector, polymers such as PE, PET, and polyamide (PA) provide excellent barrier performance against oxygen, moisture, and microbial contamination [20,21], thereby extending shelf life and reducing spoilage in perishable foods [22,23]. This is particularly critical because the environmental burdens embedded in food production often exceed those associated with packaging by one or more orders of magnitude; for instance, the FAO estimates that global food waste accounts for roughly 8-10% of anthropogenic greenhouse gas emissions, making preservation technologies indispensable for sustainability [24]. LCA studies show that even modest increases in food shelf life obtained through plastic packaging systems, such as modified-atmosphere trays or high-barrier multilayer films, lead to net reductions in lifecycle greenhouse gas emissions, water consumption, and land occupation, often far surpassing the impacts generated by the packaging materials themselves [23,25]. Furthermore, when compared with heavier alternatives such as glass or metal, plastics deliver substantial reductions in transport-related emissions and energy use due to their lower mass, which contributes significantly to overall environmental efficiency [26].

Similarly, in the automotive sector, plastics such as PP, polyurethane (PU), or acrylonitrile butadiene styrene (ABS) have become essential enablers of light weighting strategies aimed at reducing vehicle mass and, consequently, operational energy demand. Vehicle weight remains a key determinant of fuel consumption for internal combustion engine vehicles and of battery capacity for electric vehicles, and LCA studies demonstrate that the operational-phase emission savings resulting from lightweight plastic components far outweigh their production-phase environmental impacts [27]. Moreover, plastics offer design freedom, corrosion resistance, and crash-energy absorption characteristics that cannot easily be replicated by metals, thereby improving not only environmental performance but also safety and comfort.

In the textile industry, synthetic fibers such as polyesters, PA, and PP have transformed global apparel and technical textile markets due to their durability, controlled performance properties, and economic accessibility. When evaluated through LCA, these fibers often outperform natural alternatives such as cotton, which requires large quantities of water, pesticides, and arable land, contributing to substantial environmental pressure in major producing regions [28]. Cotton's agricultural phase is particularly impactful: its water footprint is among the highest of any fiber crop, and intensive pesticide use remains a widespread challenge, whereas synthetic fibers - despite relying on petrochemical feedstocks - exhibit lower water consumption, no agricultural land use, and significantly

longer product lifetimes, which contribute to reduced overall environmental burdens [29,30].

Across these diverse application sectors, LCAs consistently converge on a similar conclusion: plastics, when used appropriately across their full life cycle, provide environmental and functional benefits that cannot readily be matched by alternative materials. Their roles in minimizing food waste, reducing energy consumption in transportation, and enabling safety and design flexibility in healthcare applications illustrate that plastics are not only deeply embedded in modern society but fundamentally necessary for achieving broader sustainability objectives. Consequently, the challenge for research and policy is not merely to reduce plastic usage indiscriminately, but to optimize material selection, improve recyclability and circularity.

Bio-based and biodegradable plastics are frequently promoted as sustainable alternatives to conventional fossil-derived polymers. However, the scientific literature shows that these materials cannot currently provide a comprehensive solution to the environmental challenges posed by plastics. Bio-based polymers such as polylactic acid (PLA) and polyhydroxyalkanoates (PHA) often exhibit inferior mechanical performance compared with widely used fossil-based polymers like PE and PP. PLA, for instance, is brittle and has low impact resistance, making it unsuitable for applications requiring ductility or toughness unless costly additives or blending strategies are employed [31,32]. Similarly, PHAs suffer from thermal instability and narrow processing windows, complicating industrial-scale manufacturing and limiting their ability to replace fossil-based polymers in high-performance applications [33,34]. These mechanical and processing limitations restrict the applicability of most bioplastics to niche markets and prevent them from matching the broad versatility and durability of conventional polymers.

In addition to performance constraints, biodegradability claims surrounding bioplastics are frequently misunderstood or overstated. Many biodegradable materials require highly controlled industrial composting conditions to achieve meaningful degradation. PLA shows negligible biodegradation in ambient soil, freshwater, or marine environments, persisting for long periods under natural conditions [35,36]. Even certified compostable plastics may fail to degrade in home composting or natural ecosystems, undermining the assumption that they will reduce pollution or microplastic formation.

Furthermore, the idea that bioplastics inherently offer lower environmental impacts than fossil-derived polymers is not universally supported by LCA studies. While bio-based plastics can reduce reliance on fossil resources, their production frequently involves high agricultural inputs, including land use, fertilizer application, irrigation, and energy-intensive biomass processing [37]. These factors contribute to eutrophication, greenhouse-gas emissions, and competition with food and feed production. Thus, the environmental benefits of bioplastics are strongly dependent also on feedstock origin.

It is worth mentioning that the current and foreseeable availability of biopolymers remains insufficient to satisfy global plastic demand. Global plastic

production exceeds 400 Mt per year, whereas total biopolymer production capacity accounts for less than 1% of this volume, corresponding to only a few million tonnes annually [38]. This disparity reflects fundamental constraints related to feedstock availability. Moreover, even optimistic growth scenarios indicate that biopolymer production is unlikely to scale rapidly enough to replace a significant fraction of conventional plastics in high-volume applications such as packaging, automotive, and construction [16]. Consequently, while biopolymers can play a role in single-use or application-specific contexts, they cannot realistically substitute fossil-based plastics at the scale required by modern society.

Despite growing public and political pressure to reduce plastic use, the accumulated scientific evidence clearly indicates that plastics remain essential materials for the society. Their unique combination of low density, mechanical versatility, chemical resistance, barrier performance, and cost efficiency has enabled widespread applications that cannot be readily replicated by alternative materials without incurring significant environmental or functional penalties. Life cycle assessment studies consistently demonstrate that replacing plastics with heavier or less durable materials often leads to increased energy consumption, higher greenhouse gas emissions, and greater resource use, particularly in sectors such as packaging, transportation, healthcare, and construction. As a result, a strategy based solely on substitution or material avoidance is neither technically feasible nor environmentally robust at a systemic level.

Given the inevitability of continued plastic use, recycling must be regarded as a central and unavoidable pillar of a sustainable plastics economy. Among available technologies, mechanical recycling is currently the most mature, energy-efficient, and economically viable route for plastic recovery; however, its performance is fundamentally constrained by the quality and compatibility of waste streams. Degradation phenomena occurring during service life and reprocessing, together with inappropriate material and product design choices, significantly undermine recyclate quality and prevent high value-added reuse. Consequently, the transition toward a truly circular plastics economy does not hinge on eliminating plastics themselves, but on fundamentally rethinking how they are designed, used, managed, and reintegrated at end of life.

1.2 Mechanical recycling of polyolefins

Among all polymers, polyolefins, including the different types of polyethylene (PE) and polypropylene (PP), account for almost half of the European plastic production, as observable in Figure 4 [1]. Owing to their advantageous chemical and physical properties, such as low density, durability, chemical resistance, and low production cost, polyolefins are widely employed across numerous industrial sectors, including packaging, automotive, healthcare, and electronics [12,39,40]. In particular, polypropylene exhibits excellent chemical and thermal resistance combined with good mechanical properties,

which has led to its extensive use in high-volume applications [40]. Similarly, high-density polyethylene is one of the most widely used thermoplastic polymers in the plastic market, valued for its mechanical strength, chemical resistance, and versatility. The broad range of applications of polyolefins has driven a continuous increase in production volumes and related waste over recent decades [12].

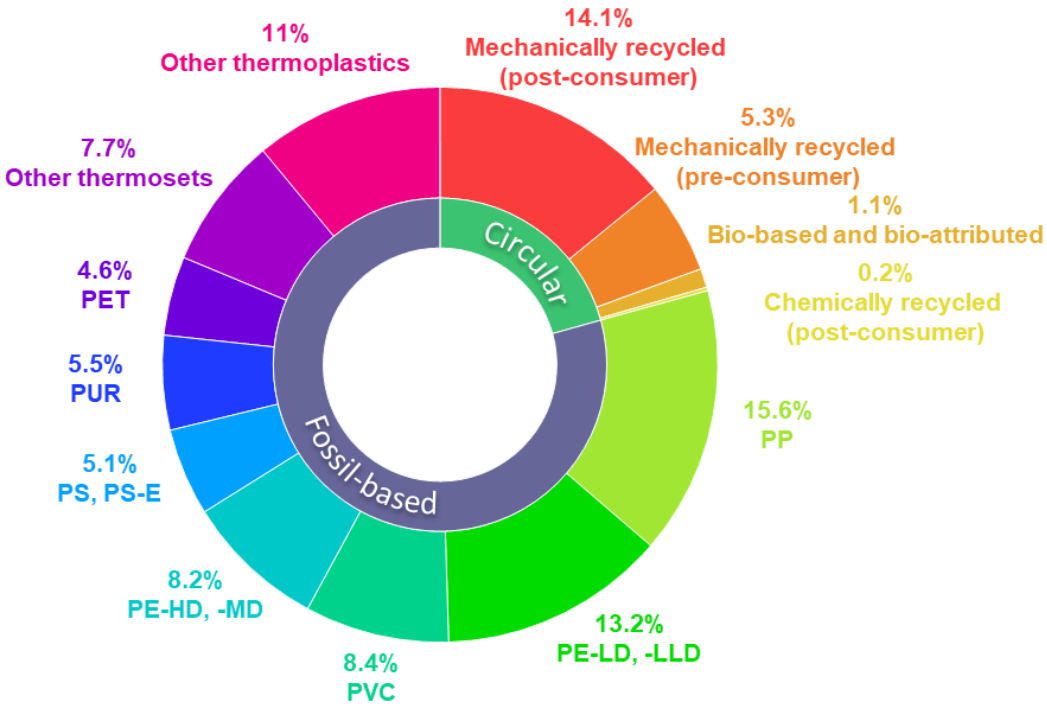

Figure 4. European plastic production by polymer in 2024 (adapted from [1]).

It is worth highlighting a fundamental difference with important implications for circularity between polyolefins and polyesters, which are also widely used in the packaging sector, which in turn represents one of the largest end-use markets for plastics. Unlike polyolefins, polyesters - most notably PET - can undergo molecular-weight restoration through reactive processing, making true closed-loop recycling technically feasible. In the case of PET, hydrolytic and thermal degradation during use and reprocessing primarily leads to chain scission, resulting in reduced intrinsic viscosity [41]. However, this degradation can be effectively counteracted through solid-state polycondensation or reactive extrusion with chain extenders, which promote end-group reactions and rebuild polymer chains. These processes enable the production of recycled PET with molecular weight and mechanical performance comparable to virgin material, thereby allowing its reuse in demanding applications [42].

As a result, bottle-to-bottle recycling of PET is already industrially established, particularly for food-contact packaging. Post-consumer PET bottles can be mechanically recycled, decontaminated, and subsequently upgraded through solid-state polycondensation to meet stringent regulatory and performance requirements [43]. This closed-loop recycling route has enabled high recycled-content levels in beverage bottles, supported by EU regulatory targets

and well-developed collection and sorting systems. In contrast, no analogous molecular rebuilding mechanism exists for polyolefins. For PP and PE, degradation-induced modifications cannot be reversed through selective end-to-end reattachment, and available modification routes, such as peroxide-induced branching or crosslinking, alter molecular architecture without restoring the original chain structure. Consequently, while polyesters such as PET demonstrate that high-quality closed-loop recycling is achievable through molecular repair, polyolefin recycling remains constrained by irreversible degradation phenomena.

1.2.1 Recycling-induced degradation effects

During their service life, plastic products are exposed to various degrading phenomena that depend on the polymer type and application environment, where polymers could be exposed to heat, oxygen, mechanical stress, and UV radiation. This exposure initiates oxidation phenomena, in which the polymer chains undergo degradation through a series of radical reactions [44]. In particular, during photo-oxidation, UV light generates free radicals within the polymer matrix, leading to chain scission and the formation of oxygen-containing functional groups such as carbonyls, hydroperoxides, and alcohols. These chemical changes progressively alter the polymer's structure, resulting in discoloration, surface cracking, and a significant decrease in mechanical properties [44]. Additional degradation occurs during mechanical recycling, where repeated thermal and mechanical stresses affect the polymer microstructure, leading to changes in molecular weight, crystallinity, chain topology, and, in some cases, the formation of new functional groups [40,45–47]. These degradation mechanisms differ significantly between PP and PE, influencing their recyclability and final performance of the resulting recyclates.

During mechanical recycling, polypropylene is repeatedly subjected to elevated temperatures and shear stresses, conditions that promote thermo-mechanical degradation dominated by chain scission reactions (Figure 5). Owing to its chemical structure, PP is particularly susceptible to this degradation pathway. The presence of tertiary carbon atoms along the polymer backbone creates weak points where C–C bond cleavage can readily occur under thermal or mechanical stress. The degradation mechanism typically initiates with hydrogen abstraction from tertiary carbon atoms, generating macroradicals along the polymer chain [48,49]. Then β-scission of the macroradicals leads to the cleavage of the polymer backbone, producing shorter chains and unsaturated end groups, without significant recombination or crosslinking. As a result, PP degradation proceeds primarily through random chain scission, leading to a progressive reduction in molecular weight with each reprocessing cycle [48].

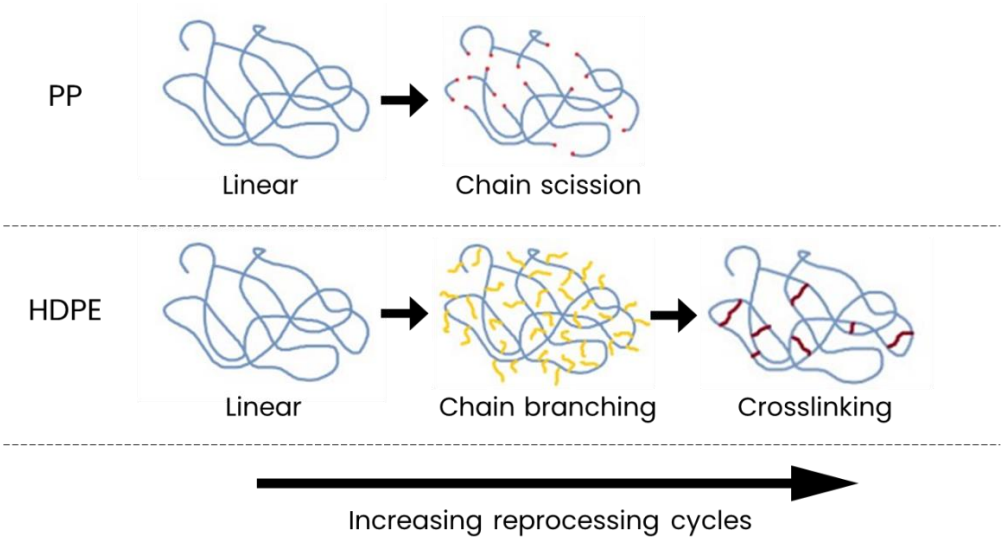

Figure 5. Effects of reprocessing on PP and HDPE macromolecular architecture.

Experimentally, chain scission in recycled PP manifests as a systematic increase in melt flow index (MFI) [45,47,50,51] and a corresponding decrease in viscosity [51–54] as the number of extrusion cycles increases. These microstructural changes and the reduction in molecular weight lead to a deterioration of mechanical properties and a gradual loss of added value, confining recycled PP primarily to applications with lower engineering requirements compared to virgin PP. As a consequence, the mechanical recycling of polypropylene is often regarded as a downcycling process. Importantly, spectroscopic analyses have demonstrated that the chemical structure of PP does not undergo significant oxidative modification during reprocessing. Minimal or negligible formation of oxygen-containing functional groups has been observed, indicating that structural degradation via chain scission is the dominant mechanism, rather than oxidative functional degradation [45–47,50].

In contrast to PP, the degradation behavior of HDPE during mechanical recycling is more complex. During reprocessing, degradation proceeds through free-radical mechanisms that differ fundamentally from those observed in polypropylene, as shown in Figure 5. Owing to the absence of tertiary carbon atoms along its backbone, HDPE exhibits a lower intrinsic tendency toward β-scission; instead, degradation is governed by a competition between chain scission, radical recombination, branching, and crosslinking reactions, resulting in significant alterations of macromolecular architecture [55–60]. The relative contribution of these mechanisms depends on several factors, including polymerization catalyst type [59], concentration and type of unsaturated groups, and reprocessing conditions [55,56,58,60]. The degradation process initiates with cleavage of C–C or C–H bonds, generating macroradicals along the polyethylene backbone [61]. In the early stages of degradation, chain scission reactions dominate, producing shorter polymer chains and increasing the concentration of macroradicals. However, unlike polypropylene, these radicals in HDPE have a strong tendency to undergo recombination reactions, particularly in the melt state

where chain mobility is high. A key pathway leading to long-chain branching (LCB) involves the reaction between a macroradical and a vinyl end group generated during earlier scission events [59]. This mechanism results in the formation of both short- and long-chain branches, depending on the location and length of the reacting chains. As degradation progresses and radical concentration increases, crosslinking reactions may occur. Crosslinking arises from radical–radical recombination between two macromolecular chains, leading to the formation of permanent covalent networks. This process reduces chain mobility and can ultimately result in gel formation if crosslink density becomes sufficiently high, affecting processability [57].

The simultaneous occurrence of chain scission, branching, and crosslinking leads to a complex evolution of HDPE macromolecular architecture during mechanical recycling. In most cases, the melt flow rate (MFR) value decreases [57,62–65] and the viscosity increases [58,65–67], indicating a reduction in the macromolecular mobility due to chain branching and crosslinking. Since the reported increase in viscosity and the modified macromolecular architecture can lead to the unsuccessful reprocessing of recycled HDPE with the same technology of its virgin counterpart, in most cases it is necessary to select different, downgraded technologies for the production of recycled materials with low added value and limited engineering requirements. Anyway, the adjustment of processing parameters is typically required when dealing with this kind of recyclates [63]. In addition, it is worth pointing out that the final mechanical properties of recycled HDPE are usually poorer than those of the virgin polymer; once again, this can be ascribed to the heterogeneous microstructure characterizing the recycled material [58,68].

1.2.2 Valorization strategies

Several strategies for the valorization of recycled PP have been explored. The most used approach (also at industrial level) involves the introduction of virgin PP in blend with the recycled one, resulting in an increase of the properties and performances as compared to unmodified recycled PP [51,69]. In particular, it has been demonstrated that the mechanical performances of virgin PP can be maintained by creating a blend containing up to 70 wt.% of recycled PP [53]. Interestingly, blends of virgin/recycled PP have been also exploited for 3D printing processes, demonstrating the possibility of valorizing a typical low added-value material through its use for innovative manufacturing approaches [70].

A further approach concerns the blending of recycled PP with long-chain branched PP, inducing an enhancement of the rheological and mechanical properties as compared to recycled PP, paving the way for the use of these materials in applications where high melt strength values are required [71]. In this context, it has been demonstrated the possible upcycling strategy of recycled PP through blending with long-chain branched PP, leading to an increase of the melt

strength but a decrease in the mechanical properties because of the presence of PE-based impurities within the post-consumer household waste [72]. The PP waste valorization can be even carried out by means of functionalization or addition of compatibilizers or fillers [54,73,74].

Furthermore, the reactive extrusion route can be followed. In particular, enhanced mechanical properties can be achieved if contaminated recycled PP is melt-compounded with chemical species, like peroxide, that can lead to the formation of long-chain branching [75,76]. Besides, PP waste has been upcycled by means of reactive extrusion obtaining long-subchain hyper-branched polypropylene starting from thermally degraded products as precursor [77].

Nevertheless, it should be highlighted that for PP there is currently no solution available to restore the molecular weight, apart from traditional cross-linking strategies (e.g. through peroxides) that, however, are not selective and do not rebuild the molecular weight through an end-to-end reattachment mechanism [78–80]. Surely, the so-called re-stabilization methods allow preventing chain cleavage during the reprocessing (by adding, as an example, fresh antioxidant or re-stabilization additives) but do not have any effects in restoring the original molecular weight, hence processability, of the virgin polymer [81].

Just like for PP, one of the most established valorization routes for recycled HDPE involves blending with virgin polymer, which allows partial recovery of mechanical and rheological properties while enabling higher recycled-content incorporation and the use of recycled HDPE in the same initial application [82]. This strategy is commonly employed in rigid packaging and construction products, where performance requirements can be met through optimized blend ratios [83]. However, blending alone does not address the intrinsic microstructural heterogeneity of recycled HDPE and therefore remains a compromise rather than a definitive solution for a full plastic circularity. For example, it has been shown that, for the formulation of bottles for cleaning products, high levels of environmental stress cracking resistance are mandatory. However, due to the modifications of the polymer microstructure induced by degradation, this property is typically inferior in post-consumer recycled plastics, thus limiting their effective exploitation in the rigid-packaging industry [84]. Similarly, recycled HDPE recovered from pressure pipes is not currently utilized for the same applications, mainly due to the high structural and loading requirements (in terms of slow crack growth and rapid crack propagation resistances) that must be guaranteed [85].

As well as PP, compatibilizers, antioxidants and a variety of fillers have been successfully employed to enhance mechanical and thermal properties of recycled HDPE [86].

More advanced valorization strategies focus on tailoring the macromolecular architecture of recycled HDPE to improve processability and performance. In particular, the introduction of long-chain branching (LCB) has been shown to significantly enhance melt strength, extensional viscosity, and strain-hardening behavior, which are critical for processing technologies such as blow molding, film blowing, foaming, and fiber spinning [87]. The formation of long-chain

branching can be successfully obtained through the addition of peroxides both on virgin [88] and recycled HDPE [89]. Furthermore, the reactive extrusion of recycled HDPE with various contents of peroxides, aiming to introduce LCB, results in increased melt strength and extensional viscosity and the appearance of a strain-hardening behavior [90]. Therefore, the presence of LCB induces a significant modification of the processability of these products, allowing the employment of polymers in several industrially relevant processing technologies dominated by elongational flow [91–93]. In the context of mechanical recycling, the introduction of LCBs on a recycled polymer could open new perspectives towards closed-loop recycling strategies or upcycling approaches, resulting in high-added-value products that can be employed in applications with high-engineering requirements.

1.2.3 Functional upgrading and end-of-life challenges: the case of flame-retardant systems

As highlighted in some recent reviews [94], current interest in the literature lies also in investigating how plastics derived from recycling processes can be transformed into new functional polymeric formulations, such as flame retardant (FR) systems, with the aim of upcycling plastic waste and producing enhanced-functionality recycled products. In fact, the different forms of degradation underwent from polymers during their service life, as well as the thermomechanical degradation typically experienced during mechanical recycling processes, usually result in chemical or structural modifications of the macromolecular chains, thereby potentially impacting the FR effectiveness. Therefore, understanding the relationship between the degradation extent of a recycled polymer and its flame-retardant properties is a key factor for assessing the viability of using recyclates in fire-risk applications. In fact, when dealing with applications where plastics could be subjected to combustion and fire, the utilization of flame-retardant additives becomes a mandatory requirement. This is essential in order to delay the flashover time and increase the fire resistance of the materials [95]. As a result, over the years, several commercial FRs have been developed to meet these demands. These additives can be differentiated based on their modes of action and chemical compositions [96,97], and their selection depends on various factors, including regulatory requirements, specific performance standards, and the potential fire scenarios that the materials are expected to face. A few works dealing with the introduction of different FR systems in recycled polymers are reported in the literature. For instance, Casetta et al. [98] investigated the flame retardancy of virgin and recycled PP/ethylene propylene rubber blends containing different contents of an intumescent flame retardant (IFR) system. The obtained results indicated an increase of the time to ignition and a decrease of the peak of heat release rate for recycled PP-based blends as compared to their virgin counterpart. Similarly, Bodzay et al. [99] demonstrated the effectiveness of an IFR system on a PP-based waste derived

from the light fraction of end-of-life vehicles, by achieving a decrease of the peak of heat release rate of about 80% as compared to recycled PP matrix. Also recycled PP-based composites containing wood flour, halogen-free flame retardants and synergistic agents with superior flame retardancy properties and mechanical performances were successfully developed by Ren et al. [100]. Interestingly, Combeau et al. [101] demonstrated that the incorporation of polyhedral oligomeric silsesquioxane into intumescent flame-retardant systems effectively enhances the fire performance of both virgin and recycled high-density polyethylene, enabling improved flame retardancy in terms of heat release rate peak and keeping adequate mechanical properties for recycled material.

However, the presence of functional additives, such as FR, complicates both the recyclability and the end-of-life behavior of many polymeric systems. The primary function of FR is expected to manifest at the final stage of a product's life, specifically under fire conditions, where FRs act to suppress or delay combustion. Nevertheless, a substantial amount of FR-containing plastics never encounters a fire scenario during their service life. Consequently, these additives may remain chemically active and structurally intact when the plastic components enter waste streams and undergo recycling processes [94]. Their persistence raises significant concerns regarding the recyclability and circularity of FR polymers. The presence of active flame retardants can alter the physico-chemical properties of recycled materials, potentially compromising their performances, processability and safety [102]. Therefore, a more comprehensive understanding of the fate, behavior, and potential reactivity of flame retardants during end-of-life treatment is urgently needed. Such knowledge is helpful for promoting a higher degree of material circularity and decreasing the dependence on virgin polymers in the manufacture of new products. Current studies indicate that the vast majority of plastic products formulated with FR-containing polymers are not effectively recycled [94]. Instead, these materials typically follow linear disposal pathways: they are either landfilled, where FRs may accumulate and pose long-term environmental risks, or incinerated, which can lead to the release of hazardous by-products depending on the type of flame retardant and combustion conditions [103]. Considering the plastic derived from WEEE (waste from electrical and electronic equipment), in 2020, only around 2 kilotons are effectively recycled out of a total of 220 kilotons [104], with the main limitations given by both the presence of hazardous substances, such as brominated FR, and the complex microstructures of the polymeric blend usually employed in these applications. The low recycling rate of FR plastics underscores the pressing need for innovative and sustainable strategies for their recovery, reuse, and reintegration into production cycles. The easiest strategy could lie in the development of FR plastics which are surely mechanically recyclable at their end-of-life.

In this context, there is an urgent need to gain a deeper and more systematic understanding of the chemical and physical transformations that FR polymers undergo during their useful life and then mechanical recycling processes. A growing number of research papers has investigated the ageing behavior of flame-retarded polymer-based composites, demonstrating how thermal and thermo-

oxidative ageing mechanism can affect both the polymer matrix and the efficacy of flame-retardant system, especially those incorporating intumescent flame-retardant (IFR) [105–108]. On the other hand, the studies about the effects of mechanical recycling on flame retardancy are few and old [106,109,110]. Although mechanical recycling represents a key strategy for reducing plastic waste and conserving resources, it is well established that repeated processing steps can induce structural degradation of polymer chains, modify the distribution and effectiveness of additives, and ultimately alter the functional performance of the recycled material [111]. These phenomena are particularly critical in the case of FR-polymers, in which the complex interplay between polymer matrix, flame retardants, and thermo-mechanical stresses during reprocessing can lead to unpredictable changes in material behavior. In particular, the thermo-mechanical degradation and the changes in the molecular weight distribution during successive reprocessing cycles can be further exacerbated by the presence of FRs. These transformations may impact not only the mechanical performances of the recycled polymer but also its combustion behavior, which is of paramount importance for applications where fire safety is mandatory. For example, degradation of the polymer or partial volatilization and redistribution of FR additives during extrusion may significantly affect ignition behavior, heat release rate, and charring efficiency. Such alterations may lead to markedly different responses under fire scenarios, diminishing the effectiveness of the original flame-retardant system [106,109]. Furthermore, the repeated exposure of FR polymers to high shear and thermal stresses during multiple reprocessing cycles can negatively impact their processability. Typical manifestations include decreased melt viscosity and reduced thermal stability, which may hinder the ability to manufacture high-quality recycled materials [112]. As the number of recycling cycles increases, these effects tend to accumulate, making it essential to adapt processing conditions, such as temperature profile, residence times, and screw configuration, to maintain acceptable material properties and avoid further degradation.

1.3 PhD framework and objectives

The growing environmental pressure associated with plastic production and waste generation, combined with the structural limitations of current recycling technologies, has highlighted the urgent need for advanced strategies to improve the performance, reliability, and added value of recycled polymers. In this context, the main objective of this PhD thesis is to investigate degradation mechanisms in recycled polyolefins (polypropylene and high-density polyethylene) and find effective methods for their valorization and functional upgrading. Specifically considering mechanical recycling strategies, the main scope is the use of industrially viable methods exploitable in the immediate for obtaining materials with tailored properties and *ad-hoc* designed processability, aiming at effectively enhancing the value added of the recyclates and, hence, their

industrial appealing. The work aims to overcome the traditional downcycling paradigm by tailoring polymer microstructure, stabilization strategies, and functional modifications to enable higher value-added reuse of recycled polyolefins.

The thesis is organized into a sequence of interconnected chapters, each addressing a specific aspect of polyolefin degradation, valorization, and functional upgrading within the context of mechanical recycling. The progression of the work starts from fundamental degradation phenomena, moving toward properly modify of recycled polyolefins microstructure for achieving a desired processability, and finally addressing functional upgrading and recyclability of flame-retardant formulations.

Firstly, in **Chapter 2.1**, the thermo-mechanical degradation of polypropylene during mechanical recycling was investigated, with particular emphasis on the evolution of molecular weight and macromolecular architecture under repeated extrusion cycles. This chapter establishes the fundamental understanding of PP degradation phenomena typically encountered during recycling and the development of approaches aimed at rebuilding the polymer molecular weight.

Chapter 2.2 extends the investigation to the long-term performance of recycled polypropylene, addressing the aging resistance. In this chapter, recycled PP films are subjected to photo-oxidative aging under humid conditions. The evolution of chemical structure, thermal behavior, and mechanical properties is analyzed.

Chapter 2.3 shifts the focus to high-density polyethylene, whose degradation behavior during mechanical recycling differs fundamentally from that of polypropylene, involving the obtainment of a very heterogeneous microstructure. This chapter investigates the possibility of valorizing recycled HDPE through controlled modification of its macromolecular architecture, exploiting thermo-mechanical degradation reactions to promote long-chain branching.

Chapters 3.1, **3.2** and **3.3** are dedicated to the functional upgrading of recycled polypropylene through the introduction of flame-retardant additives, addressing the need to expand the application range of recycled polymers beyond conventional, low value-added uses. These last chapters investigate the effectiveness of three different flame-retardants into recycled polypropylene in comparison with its virgin counterpart. Together, these chapters provide a comprehensive assessment of how different flame-retardant additives interact with recycled PP in terms of rheology, morphology and fire behavior, evaluating the suitability of recycled PP for advanced and safety-critical applications.

Finally, a key challenge for plastic circularity that is often neglected was addressed in **Chapter 3.4**: the mechanical recycling of flame-retarded polymers at end of life. In this chapter, polypropylene containing an intumescent flame-retardant system is subjected to multiple extrusion cycles to simulate repeated mechanical recycling. The evolution of rheological behavior, morphology, mechanical and flame retardancy performances is analyzed after each reprocessing step.

Overall, this thesis develops a coherent and comprehensive framework that connects degradation phenomena, microstructure control, aging resistance, and functional upgrading of recycled polyolefins. By focusing on industrially relevant materials, additives and processing routes, the work contributes to the advancement of realistic recycling strategies capable of increasing the value, performance and application potential of recycled polypropylene and high-density polyethylene, thereby supporting the transition toward a more robust and sustainable circular plastics economy.

The materials and instruments used for the experimental trials, as well as the characterization methods employed, are reported in the **Appendix A**.

Chapter 2

Tailoring the microstructure of recycled polyolefins

Part of the work described in the Chapter 2 has been previously published in:

'Bernagozzi G., Arrigo R., Ponzielli G., Frache A. Towards effective recycling routes for polypropylene: Influence of a repair additive on flow characteristics and processability. Polymer Degradation and Stability, 2024, 223, 110714' [113]

'*Bernagozzi G., Arrigo R., Frache A. High melt strength recycled high-density polyethylene: evaluation of a novel route for targeting the polymer microstructure. Polymers 2025, 17, 382'* [114]

2.1 Rebuilding the molecular weight of recycled polypropylene

The aim of this chapter is to evaluate the thermomechanical degradation that PP undergoes during multiple reprocessing cycles and the effects of a commercially available additive (Nexamite® R201, hereinafter called NEX), usually employed for the enhancement of the processability and properties of recycled PP. Nexamite® R201 additive is currently the only industrially-relevant available solution to modify the molecular weight and viscosity of recycled PP. NEX is an ethylene copolymer comprising hydrolysable silicon-containing groups, thus its mechanism during recycling should involve silane hydrolysis and silanol condensation reactions. Firstly, the effect of multiple extrusions on the rheological behavior and thermal properties of PP was assessed. Then, the additive was introduced within PP following two different routes, mimicking the primary (i.e. pre-consumer) and the secondary (or post-consumer) mechanical recycling process, respectively. Therefore, the recyclates used as benchmark in this first study are two different recycled PP, derived from controlled laboratory reprocessing simulating the primary and secondary mechanical recycling

conditions. The additive-induced microstructural modifications of PP during the reprocessing cycles were monitored through rheological, thermal, and spectroscopic analyses. Finally, an in deep characterization of the rheological behavior and of the relaxation dynamics of the PP macromolecules with and without the additive as a function of the residence time during the processing was performed, aiming at correlating the achieved microstructural evolutions to the processability of the recycled PP.

The mechanical recycling of PP (Moplen HP500N), with and without NEX, was simulated by subjecting the material up to 9 re-processing cycles performed using a twin-screw extruder. Table 1 reports the codes of the investigated materials. The samples without NEX will be distinguishable from the number of cycles reported at the end of the name (e. g. rPP n9). To investigate the effects of NEX, two strategies were followed. More specifically, the additive was introduced during the first reprocessing cycle of PP (rPP+NEX@n1), aiming at simulating the conditions that the material usually undergone during the pre-consumer or primary recycling. The sample have been named rPP+NEX@n1, where @n1 indicate the cycle in which NEX was added. Then the so-obtained material was reprocessed up to 9 times and the number of cycles will be reported at the end of the name of the sample (e.g. rPP+NEX@n1 – n9). The second strategy attempts to simulate the conditions of a post-consumer mechanical recycling process; to this aim, NEX was introduced in PP already subjected to 8 reprocessing cycles, therefore on ninth cycle (rPP+NEX@n9). The effect of NEX on the microstructure and macromolecular architecture of PP was also evaluated using a twin-screw mini-extruder equipped with a recirculation channel that allows selecting the desired residence time, more specifically 3 and 9 minutes. Hereinafter the specimens processed with mini-extruder will be named adding the residence time at the end of the codes: PP 3 min, PP+NEX 3 min, PP 9 min and PP+NEX 9 min.

Table 1. Samples codes of virgin and reprocessed PP with and without NEX.

Number of cycles	Pristine PP	NEX@n1	NEX@n9
0	PP n0	-	-
1	rPP n1	rPP+NEX@n1 – n1	-
4	rPP n4	rPP+NEX@n1 – n4	-
6	rPP n6	rPP+NEX@n1 – n6	-
9	rPP n9	rPP+NEX@n1 – n9	rPP+NEX@n9

2.1.1 Multiple reprocessing of pristine PP

First of all, PP was subjected to reprocessing in a twin-screw extruder up to 9 cycles to simulate the conditions that the polymer undergone during a typical mechanical recycling process. The modification of the material microstructure was monitored through rheological analyses. Figure 6a reports the trend of the complex viscosity as a function of the frequency for the virgin sample (PP n0) and for those collected at cycle 1, 4, 6 and 9. As expected, virgin PP shows a typical Newtonian behavior at low and intermediate frequencies, followed by a mild shear thinning at higher frequency. When increasing the number of reprocessing cycles, a progressive decrease of the complex viscosity at low frequencies can be observed. Besides, the material reprocessed for a higher number of cycles shows a progressively more pronounced Newtonian behavior. As widely reported in the literature [51–54], both these features indicate a gradual decrease of the molecular weight of PP due to the chain-scission reactions occurring during the reprocessing. In fact, the decrease of the chain length induced by the thermomechanical degradation of PP causes a reduction of the mass average molecular weight (hence, of the complex viscosity) and, consequently, a reduction of the entanglements and intermolecular interactions. This last results in an enhancement of the macromolecular mobility, leading to a progressive more pronounced Newtonian behavior. Furthermore, the analysis of the curves depicted in Figure 6a highlights that the differences between the complex viscosity curves of the different samples subjected to various reprocessing cycles tend to minimize in the high frequency region, indicating a different effect on the shear thinning region. According to the literature, this behavior can be ascribed to a progressive widening of the molecular weight distribution [51].

Figure 6b reports the FTIR spectra collected in the range 4000-400 cm^{-1} for PP n0 and for the rPP samples. As can be clearly noticeable, no significant variations can be observed as a function of the number of reprocessing cycles. Furthermore, the collected spectra indicate that no oxidative reactions occur during the reprocessing, as testified by the lack of peaks associated with oxygen-containing functional groups. Therefore, the obtained results suggest that during multiple extrusion steps the structural degradation of the polymer, strongly affecting its molecular weight, is significantly predominant as compared to functional degradation that can be practically neglected.

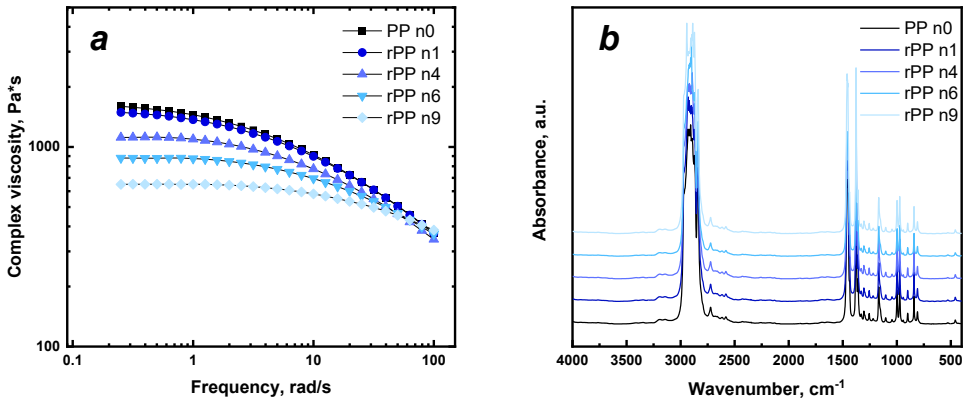

Figure 6. (a) Complex viscosity curves collected at 190°C and (b) FTIR spectra of virgin and multi-extruded rPP as a function of reprocessing cycles. Reprinted under CC BY 4.0 license.

2.1.2 Effect of the reactive additive during multiple reprocessing cycles

Following the first approach, the conditions of a pre-consumer or primary mechanical recycling process have been simulated by the addition of 5 wt.% NEX directly during the first processing cycle, therefore on virgin PP. Then, the so-obtained material (rPP+NEX@n1) was subjected up to 9 reprocessing cycles. The complex viscosity curves of the samples containing NEX collected at cycles 1, 4, 6 and 9, reported in Figure 7 (the complex viscosity curve of virgin PP is reported for sake of comparison), indicate a slight increase of the complex viscosity for the sample collected after the first reprocessing cycle, especially in the low frequency region. Then, a gradual decrease of the complex viscosity when increasing the number of reprocessing cycles can be observed. However, as compared to the scenario depicted in Figure 6a, the complex viscosity is remarkably less affected by the number of reprocessing cycles, and a significant lower viscosity decreasing rate is observed. Additionally, the trend of the complex viscosity as a function of the frequency is almost unmodified as a function of the reprocessing cycles, without the amplification of the Newtonian behavior already noticed for pristine PP. Therefore, the obtained results suggest, as also discussed for pristine PP, a progressive decrease in the molecular weight with increasing the number of reprocessing cycles because of the slight decrease in viscosity, but the introduction of NEX seems to be effective in preventing the dramatic drop of the complex viscosity, hence of the molecular weight, observed for PP reprocessed without NEX.

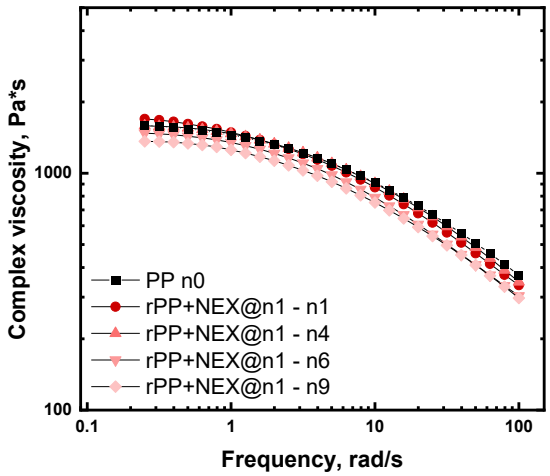

Figure 7. Complex viscosity curves collected at 190 °C of rPP+NEX@n1 as a function of reprocessing cycles. Reprinted under CC BY 4.0 license.

According to the second proposed strategy, the conditions that plastic parts usually experience during their secondary mechanical recycling have been simulated introducing 5 wt.% of NEX within PP already reprocessed up to eight times, therefore on ninth cycle (rPP+NEX@n9). Figure 8a shows the trend of complex viscosity for rPP+NEX@n9 along with the curves of virgin PP (PP n0) and of pristine PP extruded 9 times (rPP n9), that are reported for completeness and clarity in the interpretation of the results. Compared to rPP reprocessed 9 times without the additive (rPP n9), the sample containing NEX exhibits higher complex viscosity values in the low frequency region. Additionally, a less pronounced Newtonian behavior and a more prominent shear thinning at high frequency can be noticed. Besides, the trend of the complex viscosity curve tends to become very similar to that of pristine virgin PP. All these features testify that NEX is able to rebuild the molecular weight of reprocessed PP, effectively preventing the thermomechanical degradation of the polymer during the reprocessing. To further evaluate the effect of NEX also on the stability of the molecular weight of PP at high temperatures, time sweep tests have been carried out and the obtained results are depicted in Figure 8b. For both investigated systems, a gradual decrease of the complex viscosity over time is observed. Apart from the differences in the values of complex viscosity, already observed in Figure 8a, the introduction of NEX results in a lower rate of decrease of the viscosity as a function of the time, indicating that the beneficial effect of the additive is maintained also if the material is kept at high temperature for long times.

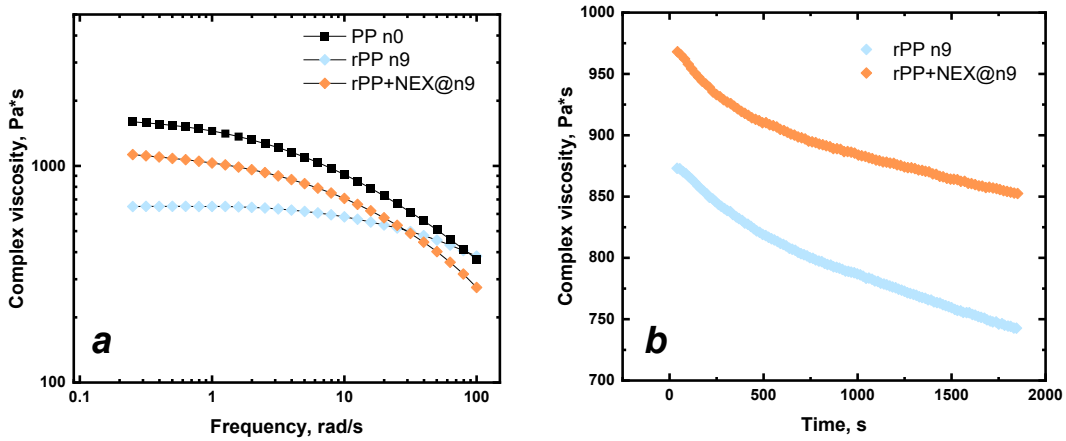

Figure 8. Complex viscosity curves of rPP+NEX@n9 collected at 190 °C (a) as a function of frequency and (b) as a function of time. Reprinted under CC BY 4.0 license.

2.1.3 Additive-induced evolution of PP macromolecular architecture

The results of the rheological characterization of the different samples subjected to multiple reprocessing cycles demonstrated that the introduction of NEX, for both exploited strategies, is beneficial in mitigating the decrease of the molecular weight of PP induced by the thermomechanical degradation experienced during the reprocessing. Aiming at quantitatively evaluating this effect, the complex viscosity data showed in Figure 6a, Figure 7 and Figure 8a were fitted through the Carreau model:

$$\eta(\omega) = \eta_0[1 + (\lambda\omega)^2]^{\frac{n-1}{2}} \quad (1)$$

where: η_0 is the zero-shear viscosity (which provides useful information about the polymer molecular weight), λ is the characteristic relaxation time and n is the power law index. Figure 9 plots the values of η_0 as a function of the number of reprocessing cycles for rPP with and without the additive, following the two exploited strategies. Considering pristine PP, a sharp decrease of the η_0 can be clearly noticed, indicating a dramatic drop of the PP molecular weight passing from the virgin material to the one reprocessed 9 times. For rPP+NEX@n1, an increase in zero-shear viscosity was observed for the material that underwent 1 reprocessing cycle, suggesting the obtainment of higher molecular weight as compared to reprocessed pristine virgin PP. With increasing the number of the reprocessing cycle, a decrease of η_0 is detected also for this sample. However, as already inferred from the analysis of the complex viscosity curves reported previously, the introduction of the additive on virgin PP was beneficial in mitigating the loss of PP molecular weight. In fact, although also in this case the η_0 values show a decreasing trend as a function of the reprocessing cycle, the reduction is significantly less pronounced with respect to that of pristine PP.

As far as the rPP+NEX@n9 is concerned, also in this case a significant recover of the polymer molecular weight as compared to the pristine PP subjected to the same number of reprocessing cycles can be observed. This result confirms that the used additive is able to rebuild the structure of PP macromolecules also if it is introduced within a heavily degraded sample, hence suggesting its possible application for the recovery of the molecular weight of post-consumer recycled PP.

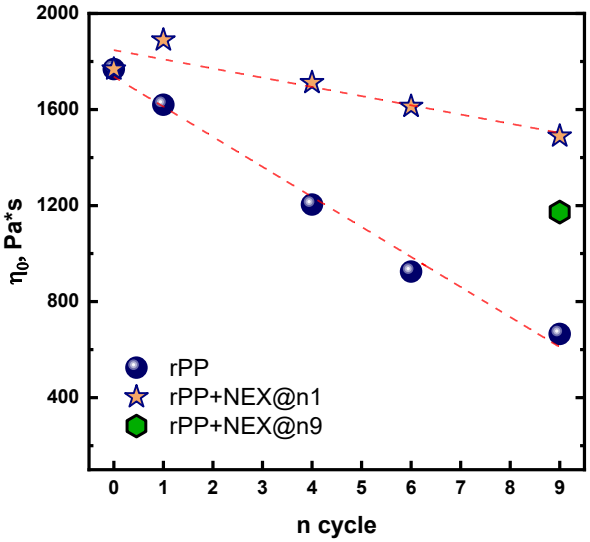

Figure 9. Zero-shear viscosity (η_0) as a function of the number of reprocessing cycles for virgin and multi-extruded rPP, rPP+NEX@n1 and rPP+NEX@n9. Reprinted under CC BY 4.0 license.

As widely documented in the literature [115], the polymer molecular weight can be estimated from the zero-shear viscosity through the application of the Mark-Houwink equation:

$$\eta_0 = k\, M_w^a \qquad (2)$$

where η_0 is the zero-shear viscosity, M_w is the molecular weight, and k and a are constant values for a given polymer. For polymer macromolecules characterized by a linear topology, the Mark-Houwink equation predicts a linear relation in a η_0-M_w plot, while deviations from this linear relationship may indicate the presence of different topologies, involving branched structures [116–120]. As observable in Figure 10, the data for reprocessed pristine PP lie on a straight line, obeying to the Mark-Houwink relation. This behavior indicates that a progressive shortening of the PP chains occurs during the reprocessing, without any alteration of the typical linear topology of the PP macromolecules. Differently, the data for the materials containing NEX introduced at cycle n1 lie below the line for the linear samples and the deviation from the linear behavior is progressively more pronounced for the samples subjected to increasing reprocessing cycles. More specifically, the data of the material rPP+NEX@n1 -

n1 lies on the straight line, suggesting no apparent variation of the linear structure. As PP+NEX@n1 is being reprocessed, all the data progressively tend to distance from the straight line, lying below it. This result demonstrates that NEX is able to promote some modification of the macromolecular architecture of the PP chains [121,122]. In particular, as demonstrated by Gabriel and Münstedt [123], a position of η_0-M_w data beneath the linear relation indicates a branched treelike topology. Therefore, the introduction of NEX into virgin PP and the subsequent reprocessing of the material caused not only a partial recovery of the molecular weight of the polymer, mitigating the effect of the thermomechanical degradation, but also a remarkable alteration of the macromolecular architecture through the introduction of branched structures. Interestingly, this further effect of NEX could be profitably exploited to modulate the processability of recycled PP. In fact, it is very known that the introduction of branched structures is beneficial for the processing of polymeric materials through some industrially relevant technologies in which the elongational flow is dominant (such as film blowing or melt spinning) [87,124]. Therefore, the proposed approach could allow for obtaining recycled PP endowed with a specific processability, paving the way for an effective valorization of recyclates through a widening of their typical application field.

Finally, also the data for rPP+NEX@n9 lies below the straight line, demonstrating that even when NEX is introduced in a PP sample which has already experienced a severe degradation (i.e., typical postconsumer recycled polymers) some modification of the macromolecular architecture of PP chains occurs, involving also in this case the obtainment of branched structures.

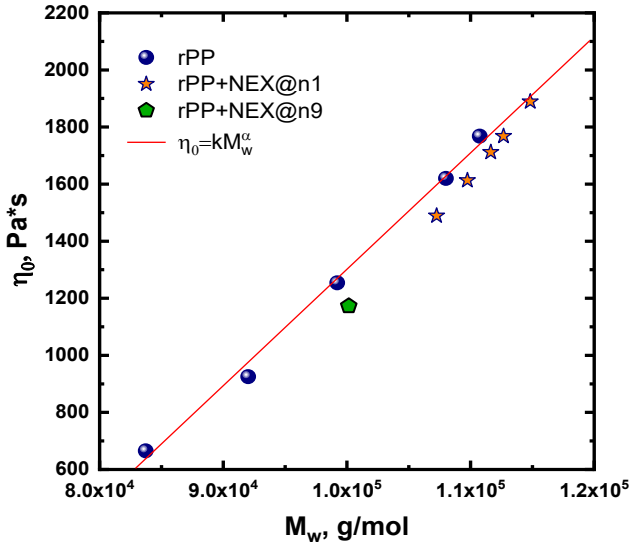

Figure 10. Mark-Houwink plot for virgin and multi-extruded rPP, rPP+NEX@n1 and rPP+NEX@n9. Reprinted under CC BY 4.0 license.

Since the inferred alteration of the PP chains topology induced by the introduction of NEX is expected to promote some differences in the relaxation behavior of the polymer macromolecules, the weighted relaxation spectra for the materials processed at different residence times were derived. This kind of analysis could be useful in gaining some further insights on the effect of NEX on the modification of the PP chains topology, considering the possible influence of the time interval in which the polymer and the additive are processed together.

The weighted relaxation spectra of PP with and without NEX processed for 3 or 9 min with a twin-screw mini-extruder are reported in Figure 11. When PP is processed for 3 min, a single broad peak is obtained (Figure 11a). This last, according with the literature [125,126], can be associated with the relaxation dynamics of a single population of macromolecular chains. For the system PP+NEX processed for the same time interval, a shift of the peak towards longer relaxation times can be observed, suggesting the already inferred increase of the molecular weight of PP which causes a retarded relaxation of the polymer macromolecules.

Looking at the spectra for the materials processed for 9 min (Figure 11b), it can be noticed that the main relaxation peak of PP (in the material without NEX) is shifted towards lower times; additionally, a secondary peak, attributable to the presence of short chains relaxing in a lower time interval, appears. In presence of NEX, the main relaxation of PP chains occurs at longer times, indicating the achievement of longer chains relaxing in a longer time interval. Besides, a distinct tail rising over the considered range is observed (Figure 11b). This last suggests the introduction of a new dynamic specie with restricted mobility which is not able to fully relax in the tested time interval [122,127,128]. Therefore, the introduction of the additive and the processing at long residence time could promote some melt-structuring phenomena associable with the formation of treelike branched structures, as already inferred from the analysis of the Mark-Houwink plot, or also some crosslink points.

Results obtained from the analysis of the relaxation spectra thus indicate that the microstructure of PP can be profitably tuned through the introduction of NEX, depending on the residence time during the processing step, allowing for achieving different macromolecular architectures and chain topologies as a function of the processing conditions.

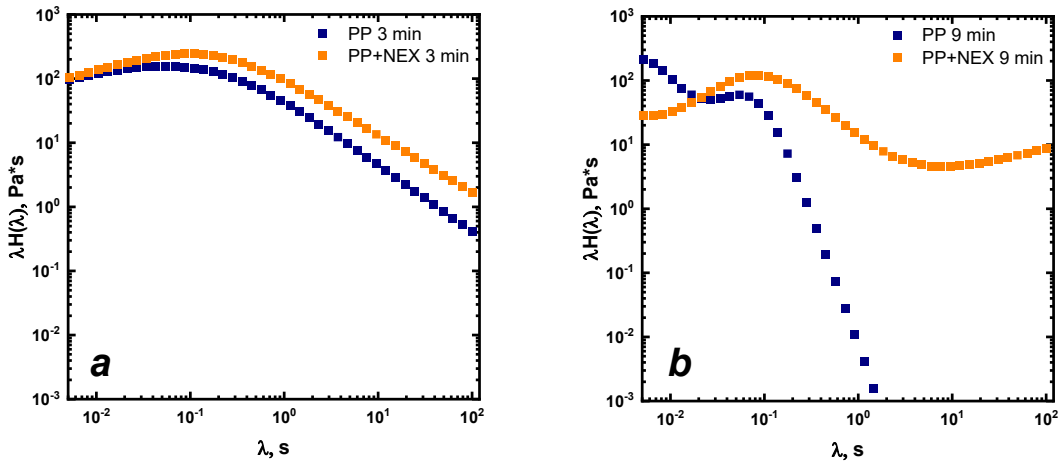

Figure 11. Weighted relaxation spectra of PP processed for: (a) 3 minutes with and without NEX; (b) 9 minutes with and without NEX. Reprinted under CC BY 4.0 license.

To further confirm the microstructural modifications occurring in PP upon the introduction of NEX, DSC analyses have been carried out. Figure 12 shows the trend of the melting enthalpy ΔH_m as a function of the number of cycles for PP reprocessed 9 times and for the systems rPP+NEX containing the additive introduced at n1 and at n9. Furthermore, Table 2 reports the melting and crystallization temperatures, as well as the crystallization enthalpy for all the investigated materials. Considering pristine PP, when the number of reprocessing cycles increases, higher values of ΔH_m were detected until sixth cycle, then a decrease of ΔH_m can be noticed. This result can be associated with a variation of the crystallinity degree of PP with increasing the number of reprocessing cycles. In this context, other authors have already reported a similar variation of the PP crystallinity, resulting from the polymer degradation [45,47,54,129]. In particular, the increase of ΔH_m and, hence, of crystallinity can be ascribed to the occurrence of chain scission reactions, predominantly involving the amorphous portion, which causes the formation of short chains whose crystallization is enhanced as compared to primitive long macromolecular chains. On the other hand, the decrease of ΔH_m noticed at high reprocessing cycles can be explained considering that the polymer is heavily degraded at this stage; thus, the chain scission mechanism affects also the crystalline portion, with an overall decrease of the crystallinity degree of the material.

The introduction of NEX during the first reprocessing cycle results in an initial decrease of ΔH_m if compared to virgin PP. Then ΔH_m shows a slightly increase until n4 and a subsequent decrease. The lower values of ΔH_m and hence of crystallinity for rPP+NEX@n1 as compared to pristine PP can be ascribed to the already inferred increase of the molecular weight of the reprocessed PP, and also to the formation of branched structures (which are not able to crystallize) induced by the presence of NEX. For the sample rPP+NEX@n1 reprocessed 9

times, instead, the crystallinity is higher than that of pristine rPP, although the rheological characterization indicated a higher molecular weight. This result further demonstrates that the introduction of NEX is beneficial in preventing the degradation of PP during reprocessing, avoiding severe chain scission mechanisms affecting also the PP crystalline portion.

When the additive is introduced in PP already subjected to 9 reprocessing cycles (rPP+NEX@n9), ΔH_m decreases slightly with respect to rPP n9. Also in this case, the lower crystallinity of this sample as compared to reprocessed pristine PP can be attributed to the formation of branches and to the maintenance of a higher molecular weight promoted by the presence of NEX.

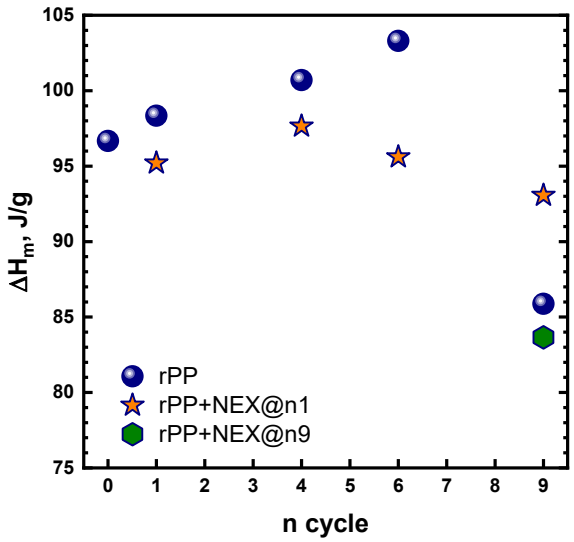

Figure 12. Melting enthalpy values (ΔH_m) as a function of the number of cycles for virgin and multi-extruded rPP, rPP+NEX@n1 and rPP+NEX@n9. Reprinted under CC BY 4.0 license.

Besides, DSC analysis have been carried out also on the samples produced through the mini-extruder at different processing times. Table 3 reports the melting enthalpy values of virgin PP (PP n0) and of PP processed for 3 and 9 min with and without NEX.

For pristine PP, the processing for 3 min causes an increase of the enthalpy and thus crystallinity, due to the decrease of the chain length. Differently, longer processing times induce a decrease of the melting enthalpy, likely because, as already described for the samples experiencing severe thermomechanical degradation, the chain scission reactions affected also the crystalline portion. When NEX is added to PP, both for 3 and 9 min, lower melting enthalpies compared to virgin PP are obtained. The presence of the additive, in fact, can lead to an increase of the molecular weight. Moreover, comparable melting enthalpy values are obtained for either short or long residences time. This last result demonstrates that NEX is able to promote an increase of the molecular weight of PP and maintain it, without loss, even for longer processing times.

Table 2. Values of crystallization temperature, crystallization enthalpy, melting temperature and melting enthalpy for all investigated materials.

	T_c (°C)	ΔH_c (J/g)	T_m (°C)	ΔH_m (J/g)
PP n0	112	99	166	97
rPP n1	114	102	165	98
rPP n4	114	104	165	101
rPP n6	115	106	164	103
rPP n9	114	87	165	86
rPP+NEX@n1 – n1	114	97	165	95
rPP+NEX@n1 – n4	114	98	165	98
rPP+NEX@n1 – n6	117	97	165	96
rPP+NEX@n1 – n9	116	95	166	93
rPP+NEX@n9	115	85	165	84
PP 3 min	110	102	167	98
PP 9 min	112	97	167	91
PP+NEX 3 min	114	96	167	94
PP+NEX 9 min	111	95	165	94

Table 3. Melting enthalpy values (ΔH_m) of virgin PP and PP processed for 3 and 9 minutes with and without NEX.

	ΔH_m (J/g)	
PP n0	96,7	
	Pristine	*with NEX*
PP 3 min	98,1	94,3
PP 9 min	91,1	93,6

2.1.4 Mechanistic considerations

Considering all the obtained results about the coupled effects of the thermo-mechanical degradation experienced during multiple extrusion cycles and of the introduction of NEX on the microstructure of PP, the following insights concerning the mechanistic of the observed behaviors emerged:

(i) the mechanical recycling of PP involves a severe thermo-mechanical degradation, which mainly involves the occurrence of chain-scission reactions causing a progressive reduction of the polymer molecular weight. This phenomenon, in turn, induces a gradual decrease of the PP complex viscosity and an amplification of its Newtonian

rheological behavior, dramatically compromising the processability of recycled PP that cannot longer be processed through the same processing technology as its virgin counterpart.

(ii) The introduction of NEX in a slightly degraded PP (i.e., in a recycled pre-consumer PP) significantly alleviates the loss of the polymer molecular weight and, consequently, of its viscosity. In fact, the decrease of the viscosity over the reprocessing cycles is less pronounced with respect to the pristine PP and, after 9 reprocessing cycles, the material containing NEX shows a zero-shear viscosity which could still allow processing of the recycled PP through the same processing technology of its virgin counterpart. Additionally, the additive induces some modifications of the macromolecular architecture of PP chains, promoting the introduction of branched structures. Therefore, in this case, a double effect of NEX can be recognized: it is able to rebuild the molecular weight of PP and, at the same time, it introduces some branches onto the backbone of the polymer. It is important to highlight that the observed NEX-induced microstructural modifications are beneficial for the future processability of recycled PP, since the achievement of a branched topology ensures the proper flow characteristics required for the processing of the polymer through technological processes in which high values of melt strength are mandatory, such as, for instance, blow molding or film blowing.

(iii) When NEX is introduced in a heavily degraded PP (i.e., in a recycled post-consumer PP) a partial recovery of the initial viscosity of the virgin polymer is obtained. Besides, the presence of the additive helps in maintaining the viscosity of the polymer at high temperature for a longer time as compared to pristine recycled PP, exerting a sort of melt stabilization action. However, in this case, NEX seems to act as a classical chain-extender additive, able to repair the molecular weight of the PP macromolecules strongly affected by the chain scission reactions occurring during the processing. Therefore, the addition of NEX to recycled post-consumer PP allows the further utilization of the material through a processing technology requiring the same flow characteristics of the virgin polymer.

(iv) Interestingly, it has been demonstrated that the additive-induced microstructural modifications of PP can be tuned on purpose varying the processing conditions during the melt compounding. In fact, it has been shown that, depending on the residence time within the extruder, different macromolecular architectures can be obtained. More specifically, while low residence times mainly cause the formation of linear chains, an increment of the processing time promotes the appearance of melt structuring phenomena, involving the introduction of branched structures and, also, some crosslink points. This last result

testifies that recycled PP with adjustable processability can be easily obtained through the proper selection of the processing conditions.

2.1.5 Conclusions

In this first chapter, the effect of a commercially available additive in rebuilding the molecular weight of a PP sample subjected to multiple reprocessing cycles was evaluated and discussed. Firstly, the microstructural changes induced by the thermo-mechanical degradation that PP undergoes during a typical mechanical recycling process were evaluated through rheological and thermal analyses. The obtained results confirmed that the main mechanism of degradation of PP involves the occurrence of chain scission reactions, which result in a severe progressive decrease of the polymer molecular weight. FTIR analyses suggested that the structural degradation affecting the polymer molecular weight is predominant as compared to the functional degradation, since the oxidative degradation of PP is quite negligible. Then, the effects of the repair additive on the microstructural modifications experienced by PP during reprocessing were evaluated following two different approaches, simulating the mechanical recycling process of pre-consumer and the post-consumer polymers, respectively. A detailed rheological study allowed demonstrating that the introduction of NEX can effectively prevent the decrease of the molecular weight of PP, especially when the additive is added in a low degraded PP (i.e. in the case of pre-consumer recycling). Furthermore, it was also showed that NEX can induce some melt structuring phenomena, involving the obtainment of branched structures or crosslink points, especially if the melt processing is carried out for long residence times. Finally, the results coming from DSC analyses confirmed the inferred modification of the PP macromolecular architecture.

In all, the proposed approach demonstrated the possibility of achieving recycled PP with different macromolecular architectures and, hence, flow characteristics, endowed with tunable and adaptable processability. The obtained results can thus open new perspectives toward an effective valorization of recycled PP through different processing technologies, allowing its employment also in applications with high-engineering requirements.

2.2 Retention of mechanical properties for recycled polypropylene upon photo-oxidative degradation

Photo-oxidative aging of polypropylene involves complex chemical reactions initiated by UV irradiation, resulting in chain scission, formation of oxygen-containing functional groups, and progressive embrittlement of the material. In recycled PP, these effects are exacerbated by the presence of pre-existing oxidative defects and a broader molecular weight distribution inherited from previous processing and use cycles. As a consequence, maintaining adequate mechanical performance, particularly ductility and strength, over extended outdoor exposure remains a key challenge for the high-value reuse of rPP.

In the previous chapter, the effectiveness of a functional additive, namely Nexamite® R201 (NEX), capable of modifying the macromolecular architecture of recycled polyolefins, was demonstrated. More specifically, in the case of reprocessed PP under laboratory-controlled mechanical recycling, this additive has shown the ability to partially restore the polymer molecular weight, promoting at the same time long-chain branching or melt structuring phenomena, ultimately improving the processability of the recycled material. However, the influence of such additives on the photo-oxidative degradation behavior of recycled polypropylene, particularly under combined UV radiation and moisture conditions, has not yet been systematically investigated.

In this context, the present work aims to evaluate the photo-oxidative degradation behavior of post-consumer recycled polypropylene films, both pristine and modified with Nexamite® R201, under accelerated weathering conditions. In contrast to the previous chapter, the recyclate used as reference in this study is a genuine post-consumer recycled PP derived from packaging trays. Then, cast extruded films of rPP and rPP containing NEX (rPP+NEX) were obtained using a twin-screw extruder equipped with a flat die, and a three-roll calendaring unit. The aging process was carried out using a QUV instrument with exposure cycles combining UVA irradiation and water condensation to simulate outdoor environments. Each sample has been named by designating at the end of the name the total time of aging, i.e. rPP t0 has not undergone any type of aging, instead rPP t24 have been collected after 24 hours of aging. The evolution of chemical, thermal, rheological, mechanical, and morphological properties was monitored to elucidate the role of the additive during photo-aging. Particular attention was devoted to assessing the ability of NEX to preserve key mechanical properties, such as elongation at break and stress at break, over prolonged exposure times.

2.2.1 Preliminary characterizations of post-consumer rPP

First of all, the recycled PP flakes (rPP) were characterized through spectroscopic and thermal analyses. The ATR-FTIR spectrum of the rPP flakes, reported in Figure 13, shows the characteristics peak of PP. In fact, according to

the literature [130–132], the following signals can be recognized: (i) a peak at 2950 cm^{-1}, attributed to the asymmetric stretching vibration mode of -CH_3; (ii) a peak at 1375 cm^{-1} related to -CH_3 symmetric bending vibration mode; (iii) a peak at 1455 cm^{-1}, associated to -CH_3 asymmetric bending mode; (iv) two peaks at 2838 and 2917 cm^{-1}, attributed to –CH_2– symmetric and asymmetric stretching, , respectively. Therefore, from the analysis of the ATR-FTIR spectrum, it can be inferred that no other plastic contaminations are present in the rPP flakes. Besides, the broad band appearing in the range 1550-1750 cm^{-1} can be associated with the presence of carbonyl and vinyl products resulting from some thermo- and/or photo-oxidative degradation underwent by the polymer during its service life [133]. Regarding the characterization of the thermal properties carried out on rPP flakes as received, the DSC analysis revealed an endothermic peak at about 165°C recorded during heating, and an endothermic crystallization peak during cooling at approximately 131°C. These are typical results attributable to the only presence of polypropylene in the rPP flakes, according to the literature [51,134]. The measured crystallization temperature can be considered slightly high if compared to virgin PP, but given the origin of the material considered in this study which derived from a recycled product, a small presence of contaminants that could act as nucleating agents promoting crystallization cannot be excluded [47].

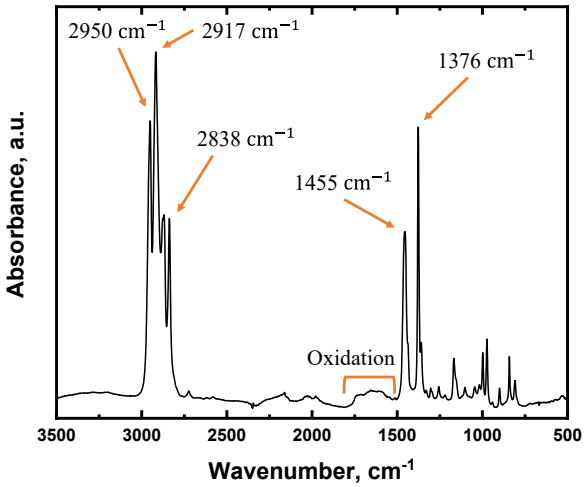

Figure 13. ATR spectrum of rPP flakes.

2.2.2 rPP macromolecular architecture: variations induced by processing and additive introduction

Rheological analyses were carried out in order to evaluate the macromolecular architecture of rPP as received (rPP t0 (flakes)), after the film extrusion step (rPP t0 (film)) and upon the introduction of NEX (rPP+NEX t0 (film)). In Figure 14a, the complex viscosity of all investigated materials is reported as a function of the frequency. All the curves display the typical Newtonian behavior of polypropylene, with a pronounced Newtonian plateau at low and intermediate frequencies and a decrease of the complex viscosity when

the frequency increases (shear thinning). When comparing rPP as received in the form of flakes with the film of rPP obtained after a cycle of extrusion, a decrease of the complex viscosity throughout all the investigated frequency range can be observed. This result can be explained considering some thermo-mechanical degradation phenomena, involving chain-scission reactions [135], occurred during the processing step.

The effect of NEX when it was added to rPP can be clearly observable from the complex viscosity curves reported in Figure 14a, where an overall increase can be noticed over all the investigated frequencies: the additive is able to increase the complex viscosity, hence the molecular weight, of rPP, but without reaching the original values of rPP as received (flakes). The resulting increased viscosity is in agreement with the findings of the study reported in the previous chapter on simulated recycled PP [113]. The ability to rebuild the molecular weight of PP has been demonstrated effective also on a real recycled PP.

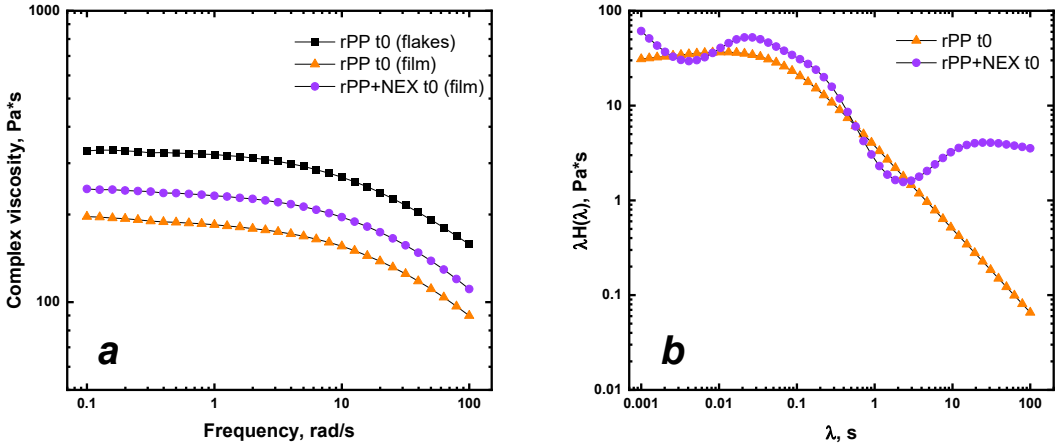

Figure 14. (a) Complex viscosity curves collected at 190 °C of rPP as received (rPP t0 (flakes)) and after film extrusion without (rPP t0 (film)) and with NEX (rPP+NEX t0 (film)); (b) weighted relaxation spectra of pristine rPP film (rPP t0) and rPP film with NEX (rPP+NEX t0).

Moreover, in order to evaluate if the additive is also able to promote some variations in the relaxation behavior of the macromolecules or in the chain's topology, the weighted relaxation spectra of rPP with and without the additive were derived and depicted in Figure 14b. The relaxation spectra of rPP is featured by a broad peak, associable with the relaxation dynamics of a single population of macromolecular chains. The introduction of NEX within the system resulted in a completely different relaxation behavior, which is characterized by a shift of the first peak towards longer relaxation time and a separate second peak at even higher times. Firstly, the shifting of the first peak confirms the already inferred increase in the molecular weight, because of the presence of longer chains relaxing in a longer time interval. On the other hand, the appearance of a second peak denoted the introduction of new dynamic species, characterized by a restricted mobility, which are not able to fully relax in the considered time

interval. Therefore, in accordance with the previous work, the additive NEX is also able to promote some melt-structuring phenomena associable with branched structured or some crosslinking points even when used with a real recycled polypropylene.

2.2.3 Effects of photo-oxidation on chemical, thermal and mechanical properties

Post-consumer recycled PP without and with NEX have been then subjected to an accelerated weathering test through a QUV apparatus in order to evaluate their behavior under photo-oxidative degradation in moisture environment. Different chemical, thermal and mechanical features have been monitored and evaluated. The main objective is to understand what could happen when a recycled PP is used in film applications under outdoor exposure conditions and what varied when introducing an additive, that can definitely change the processability of the recycled PP, by reconstructing the molecular weight and establishing some melt-structuring phenomena.

First of all, from FTIR analysis two new broad band appears when increasing the aging time, namely around 3300-3600 cm^{-1} and in the region between 1650-1800 cm^{-1}. The first band is associated with the hydroxyl groups, correlated to the formation of hydroperoxide and hydroxyl species [136]. Regarding the band around 1712 cm^{-1}, this is related to the formation of carbonyl species [136]. The hydroperoxide and carbonyl groups are, in fact, the main photo-oxidative products of PP during weathering [44]. The evolution of carboxylic acid peak (1712 cm^{-1}) was used to investigate the chemical modifications induced by the aging, expressed as carbonyl index (Figure 15a). The carbonyl index was measured by normalizing the intensities of carbonyl group peak with respect to the intensity of CH bending and stretching modes absorption band of polypropylene at 2722 cm^{-1}, as it does not change during the aging process [133,137]. The typical trend of the carbonyl index, featured by an induction period then followed by a growth stage [137], was found for both rPP and rPP+NEX. As already mentioned, an initial photo-oxidative degradation can be detected within the post-consumer rPP flakes, thus nonzero values can be found in the graphs also for the unaged samples (0 hours). As observable in Figure 15a, the carbonyl index remained almost constant both for pristine rPP and for rPP+NEX before accelerated weathering test begins to about 200 hours of aging. From this point, both rPP without and with the additive exhibited progressively increasing carbonyl indexes but with different rate of growth. In fact, the additive seemed to promote a faster formation of carboxylic acid in aged rPP. These results can be also displayed in the detailing of the FTIR spectra of rPP (Figure 15b) and rPP+NEX (Figure 15c) reporting the zone of carbonyl groups. For the first 200 hours of aging time, all the spectra overlapped. Then, the increase of the peak at 1712 cm^{-1}, related to the carboxylic acid, can be appreciated for both materials but in a more pronounced manner for rPP containing NEX. This phenomenon could be explained considering the

degradation of silicon-containing materials already reported in the literature [138,139], because of hydrolysis, condensations and thermal oxidation in the presence of moisture and UV irradiation. Moreover, there could be a photo-initiating effect of carbonyl group, following the Norrish reaction, in the additive itself [140]. All these degradation phenomena of the silicon groups inside NEX could thus accelerated the formation of carbonyl group in rPP, likely also speeding up the overall photo-oxidation as already observed in polyolefins-based nanocomposites with SiO_2 [136,141].

The functional degradation, involving the formation of new oxidative chemical species, can be negligible until about 200 hours, without any substantial difference between rPP with and without the additive. Then a marked chemical modification affected both materials, denoting the beginning of functional degradation after 200 hours, which corresponds to approximately 130 hours of UV exposure and 65 hours of H_2O condensation.

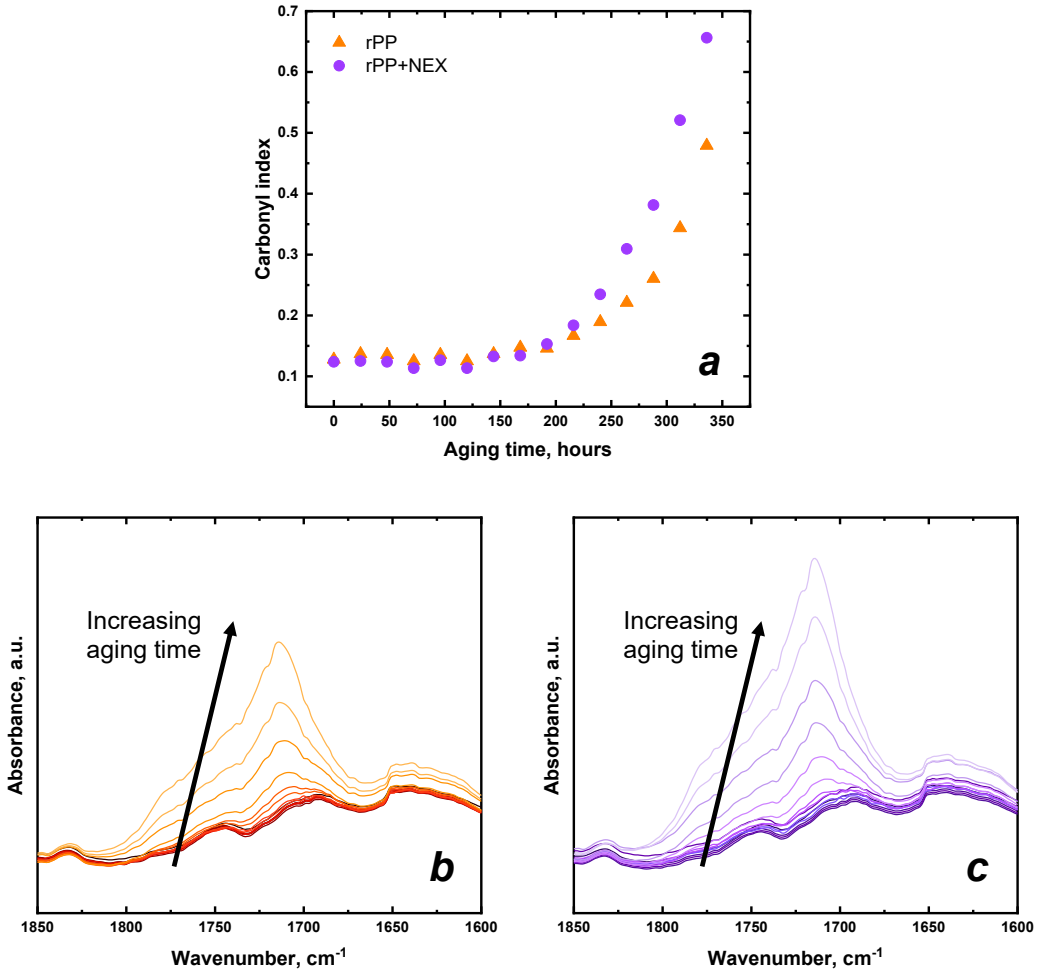

Figure 15. (a) Carbonyl index as a function of the aging time; details of FTIR spectra: carbonyl group peak evolution when increasing the aging time of (b) rPP and (c) rPP+NEX.

In order to evaluate the possible evolution of the material thermal properties during the aging, DSC analysis have been carried out on the samples of rPP and

rPP+NEX before the photo-oxidative treatment and after 96, 144 and 192 hours. In Figure 16 the DSC thermograms recorded during the first heating and cooling scans are reported for all the investigated materials. Let's first analyze the behavior of rPP without any additive. Figure 16a shows the melting peak recorded during the first heating cycle. The melting temperature did not change passing from the unaged rPP to the samples subjected to photo-oxidative degradation in moisture environment for 144 hours. A variation in the shape of the melting peak and a decrease in the melting temperature were observed when the aging time reached 192 hours. These phenomena can be associated with the reduction of the thickness of the lamellae, which caused a broadening of the melting peak. This last showed an irregular shape and a second peak appeared, indicating the formation of smaller crystallites because of prolonged aging [44]. The crystallization temperature of rPP (Figure 16b) was not affected by the aging.

On the other hand, the thermal properties of the system containing NEX displayed some differences as the aging time increased. In particular, the accelerated weathering resulted in more several changes in the thermal behavior of rPP when NEX is added before the aging with respect to pristine rPP. In Figure 16c, a progressive decrease of the melting temperature and a variation in the shape of the melting peak can be observed. This phenomenon of smaller crystallites with reduced lamellae thickness was already explained for pristine rPP, but in the system containing NEX every sample collected at different aging time resulted in different melting behavior. The observed decrease in the melting temperature when increasing the aging time depends on the degradation occurring at the lamellar fold surfaces, which involved the scission of the tie molecules and the increase of the surface free energy of the crystals because of the reactions of photo-oxidation on the crystal surface [140,142]. The crystallization temperature (Figure 16d) also displayed big variations when increasing the aging time, firstly increasing but then decreasing by more than 10 °C. The reduction in both melting and crystallization temperatures during aging of rPP+NEX was caused also by the accumulation of structural defects within the material due to photo-oxidative degradation [143]. These crystal defects could include the formation of oxygen-containing functional groups, the introduction of double bonds, an increase in chain terminations and the development of branching sites. As a result, the crystals that formed become smaller and contain more defects. The crystallization temperature was also found out to be decreased because of crosslinking or branching effect [144], characteristics of the rPP+NEX macromolecular architecture already inferred from rheological analysis before the aging.

In contrast, the crystallinity degree underwent slight variations due to aging for both pristine rPP and rPP+NEX (Table 4). A slight increase can be observed for pristine rPP after almost 200 hours of aging and this increase could be associated with the chemio-crystallization phenomena [142,145,146]. In fact, photo-oxidation often lead to the process of chemio-crystallization, in which after the degradation-induced chain scission some segments of entangled and tie chain molecules are release in the amorphous region and can arrange into new crystalline phases. Regarding aged rPP+NEX, instead, some fluctuations in the

crystallinity degree were found, with no specific trend agreeing with no trend found for melting and crystallization temperatures. This phenomenon could be explained considering that the presence of chemical irregularities, already stated to be more present in the samples with NEX with respect to pristine rPP, acted as an obstacle to the progressive increase in the crystallinity. As suggested in other works, two competitive mechanism could happen during photo-oxidation of rPP+NEX: the chemio-crystallization and the formation of impurities [145,147,148]. Finally, also crosslinking phenomena could modify or inhibit the crystallization [148].

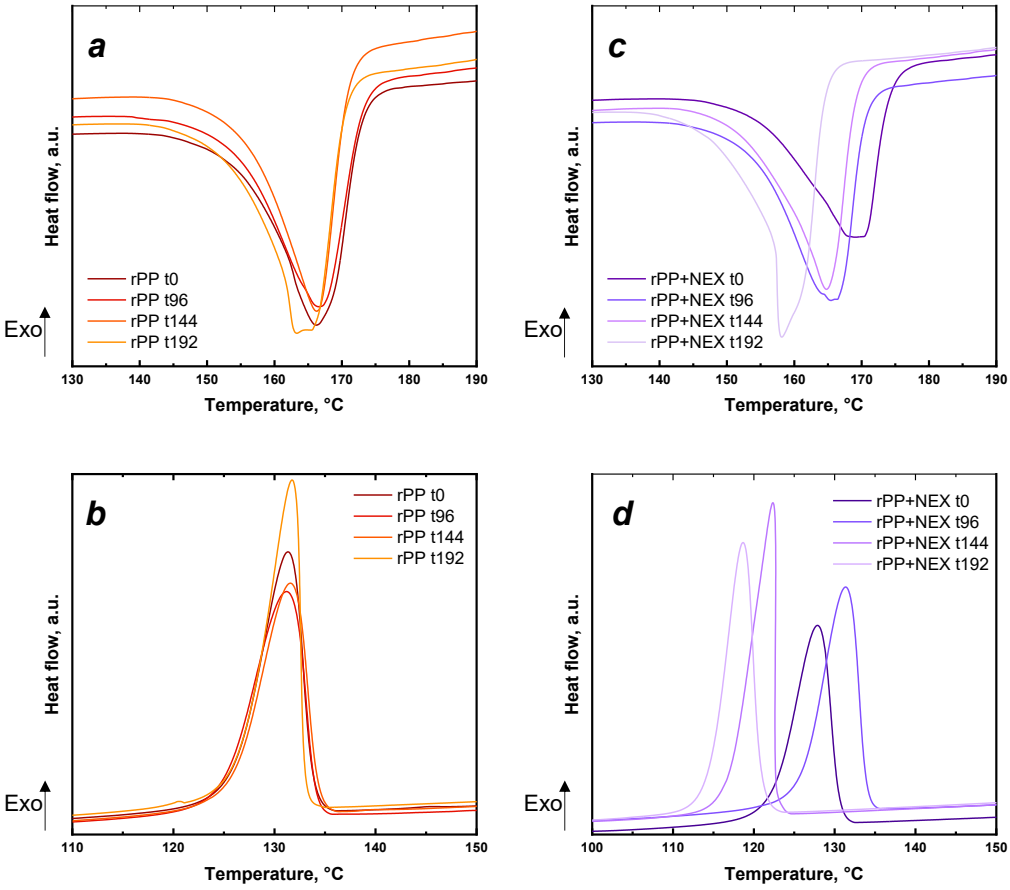

Figure 16. DSC thermograms recorded during the first heating and cooling scans for rPP (a, b) and rPP+NEX (c, d), respectively, at different aging time.

Table 4. Crystallinity degree of rPP and rPP+NEX at different aging time.

	Crystallinity degree [%]	
Aging hours	***rPP***	***rPP+NEX***
0	42	38
96	42	42
144	41	39
192	44	42

The mechanical properties as a function of the aging time have been evaluated through tensile tests, and the mean values of elastic modulus, elongation at break and stress at break are reported in Figure 17. In order to better assess the variation in these properties as a function of the aging time, Figure 17 reports normalized values, obtained by dividing the actual value of the property by the value of the unaged sample (reported for the sake of completeness in Table 5). Evaluating how the mechanical properties change if compared to the values before the accelerated weathering is of crucial importance to try to predict their tensile behavior before the material become too fragile to withstand the application for which the films are provided. In fact, the typical effect of the photo-oxidative degradation in terms of mechanical properties is an overall embrittlement of the material over time [143,149] because of chain scission phenomena, increase in crystallinity and the formation of cracks on the surface of aged samples [44,145–147,150].

Noteworthy observations can be highlighted regarding the results obtained through tensile testing of the aged sample when NEX is introduced in rPP. The elastic modulus of rPP both without and with NEX reported in Figure 17a is not so much affected by the aging time, remaining in a range included between +18% and -10% of the original value for pristine rPP and in a range between +15% to -4% for rPP+NEX in the considered aging time (until 192 hours).

The trend of the elongation at break (EB) is displayed in Figure 17b. Firstly, for both the systems there is an increase of EB after 48 hours of exposure. Then, for pristine rPP a gradual decrease of EB can be observed as aging time increased. At 168 hours of exposure the material lost more than 99% of its initial value and the completely fragile behavior is observed also at 192 hours of aging time: the EB of pristine rPP varied from 470% to 2% from t0 to t192. Surprisingly, the presence of NEX inside rPP is able to maintain increased value of EB also after 72 hours (+9%) and an additional gain of 31% if compared to the original value is noted after 96 hours of exposure. From that point also the samples containing NEX displayed a gradual decrease of EB, even if after 144 hours the loss of EB is maintained within 40% of its initial value, increasing the exposed period in which this kind of material can be used in outdoor applications without exhibiting an embrittlement. At the same aging time, EB of pristine rPP is reduced by almost 80%. At 168 and 192 hours of exposure, also rPP containing NEX became fragile by losing 97% and 98% of its original value, respectively: the EB for rPP+NEX varied from 520% (t0) to 9% (t192).

Regarding the stress at break (SB), reported in Figure 17c, a progressive decrease when exposure in QUV increased can be observed for rPP with and without NEX. At 144 hours of exposure, both rPP without and with NEX lost approximately 20% of the initial value of SB, but for increasing hours of aging two completely different trends can be observed. On one side, the stress at break of pristine rPP decreased by 38% at 168 hours, reaching a loss of 65% at 192 hours. On the other hand, the introduction of NEX led to the maintenance of almost constant values of SB up to 192 hours of aging: at 144 aging hours the samples with NEX lost 28% of SB's original value and after 192 hours of exposure SB decreased by only 32%. For a better understanding of the different

tensile behavior with or without NEX, Figure 18 shows the stress-strain curves of samples aged for 192 hours.

The reason behind the higher elongation at break during aging and the higher stress at break after 192 hours of exposure must be sought in the microstructural modifications induced by the additive NEX even during the photo-oxidative degradation. In fact, a similar silicon groups-containing additive was employed in another study dealing with recycled HDPE, and also in that case a marked increase in the elongation at break was found out [114]. The additive, in that case, was able to drive the thermo-mechanical degradation reactions towards the formation of long chain branches which, in turn, are able to form tie-molecules. The presence of such tie-molecules has been proved to increase both the elongation at break and the tensile strength [151,152], playing a role in the stress transmission during the tensile deformation [153]. Moreover, tie-molecules play an important role also in the recrystallization behavior of photo-oxidized PP, as the chain scission and the sliding diffusion of tie molecules during aging can result in reorganization of the crystal domains and the growth of thin lamellae [154]. As a result, the increase in the elongation and stress at break reported in this study is a consequence of some rearrangement of the crystalline phases and the tie-molecules formed thanks to the ability of the additive to induce some melt structuring phenomena, like side branches. These noteworthy findings are very relevant for the use of recycled PP in applications requiring exposure to outdoor environments. The maintenance of mechanical properties for long periods becomes essential to ensure the effective use of recycled plastics, thus increasing their circularity. The introduction of NEX can be positioned in this context as it is actually able to extend the useful life of films produced with recycled plastic, greatly reducing the loss of elongation at break and stress at break even when exposed to solar UV light and condensation cycles.

Table 5. Mean values of Young modulus, elongation at break, and strength at break for the unaged (t0) samples without (rPP) and with NEX (rPP+NEX).

	Modulus [MPa]	**Elongation at break [%]**	**Strength at break [MPa]**
rPP t0	1053 ± 45	470 ± 20	40.0 ± 1.9
rPP+NEX t0	915 ± 39	526 ± 26	44.1 ± 2.1

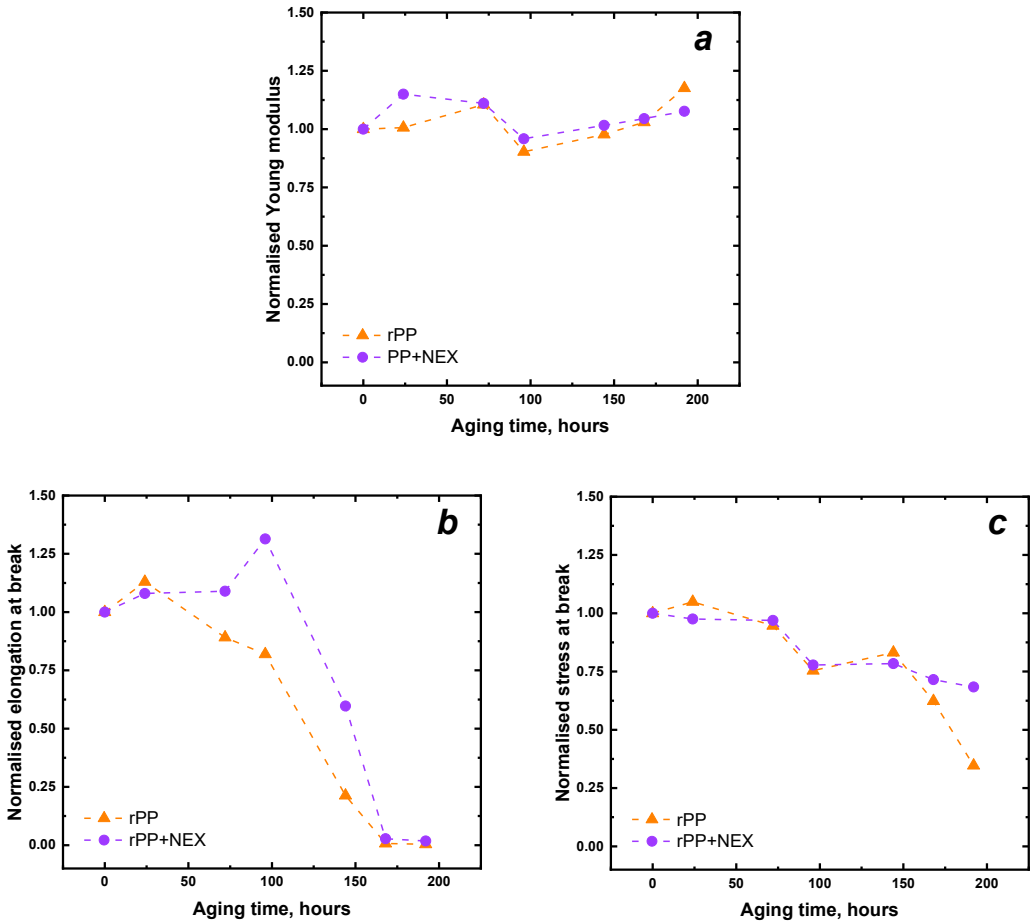

Figure 17. Normalized mechanical tensile properties of rPP and rPP+NEX as a function of the aging time: (a) elastic modulus, (b) elongation at break (EB) and (c) stress at break (SB).

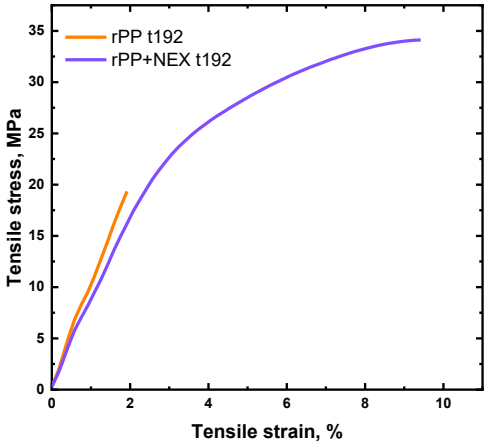

Figure 18. Tensile stress-strain curves of rPP and rPP+NEX aged for 192 hours.

At the end, in order to understand the main possible reason of such a decrease of the elongation at break values between 168 and 192 aging hours, the exposed surface of the aged films have been analyzed with SEM. One of the main reasons of the embrittlement of PP after photo-oxidation is the formation of cracks. The spontaneous cracking of the exposed surface is the direct consequence of chemio-crystallization, because of the contraction of the surface layers due to internal stresses and a reduction of plasticity in the amorphous phase [133,147,148]. The SEM images of the films of rPP without and with NEX after 192 aging hours are displayed in Figure 19. For both films, the typical cracking phenomena of the photo-oxidative degradation began to be evident after 192 hours of exposure under UV light and H_2O condensation cycles. In the SEM images of both materials, the developed cracks are perpendicular to the material flow, and they are the first crack appearing after photo-oxidation, named "transversal cracks". The second type of cracks which are perpendicular to the material flow, namely "longitudinal cracks", instead have not been observed in the samples, likely because they started to appear at higher exposure time.

Therefore, the ultimate decrease in the elongation at break for both rPP with and without NEX can be ascribed to the reduced molecular weight, because of β chain scission reactions (inferred from the decrease in the melting temperature) and also because of the formation of cracks on the exposed surface, as already reported by other authors [133,147].

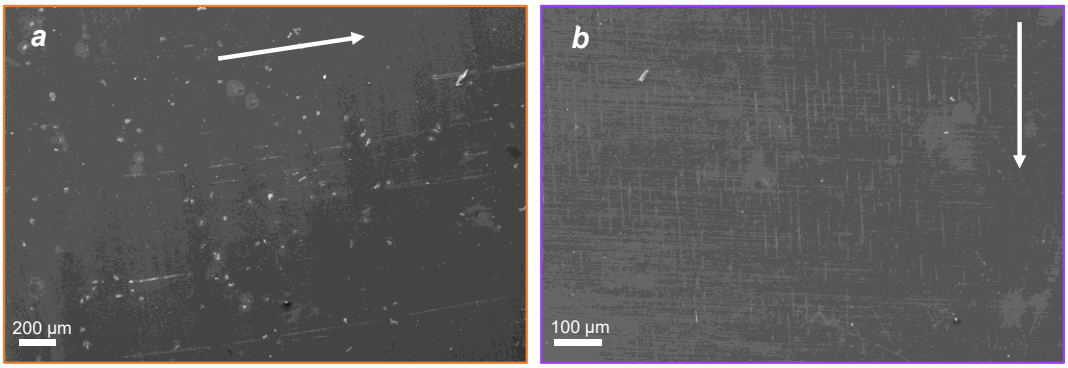

Figure 19. SEM images of the film's exposed surface of (a) rPP and (b) rPP+NEX after 192 hours of aging (the arrows indicate the stretching direction).

2.2.4 Conclusions

Under photo-oxidative degradation in moisture environment, the behavior of post-consumer recycled PP films and their counterparts containing a commercially available additive Nexamite® R201 can be summarized as follows:

- The functional degradation evaluated trough FTIR analysis, involving the formation of carbonyl group because of photo-oxidative reactions, started after about 200 hours of UVA-H_2O exposure cycles, with a higher carbonyl index growth rate when NEX is added to rPP, likely

because of the presence of hydrolysable silicon-containing groups in the additive;

- The effects of aging on DSC characterizations revealed smaller variations in the main thermal properties for pristine rPP with respect to rPP+NEX, thus suggesting that the introduction of the additive has a more pronounced impact on the evolution of the crystalline phases when gradually exposed to UVA-H_2O cycles;
- Remarkable results have been obtained in term of tensile properties of the aged films, more specifically with the introduction of NEX elongation at break and stress at break can be retained at higher values over extended periods: after about 150 hours of exposure, elongation at break is reduced by only 40% with NEX, as opposed to pristine rPP that lost almost 80% of its original value, whereas the stress at break after about 200 aging hours passed from a reduction of 65% for pristine rPP to 32% in the presence of NEX;
- Transversal cracking phenomenon appeared on the exposed surface of both rPP with and without NEX after 192 hours of UVA-H_2O exposure cycles, being the main cause of films' embrittlement.

2.3 High melt strength recycled high-density polyethylene

In the context of mechanical recycling, the introduction of long-chain branching (LCB) on a recycled polymer could open new perspectives towards closed-loop recycling strategies or upcycling approaches, resulting in high-added-value products that can be employed in applications with high-engineering requirements.

In this chapter, the effects of the thermo-mechanical degradation of HDPE (Eraclene MS80U) occurring during a typical mechanical recycling process were evaluated. Moreover, an effective and industrially viable strategy for obtaining recycled HDPE with a high melt strength, and hence improved processability upon elongational flow, was proposed. To this aim, another commercially available additive, namely Nexamite® R305, was used. Nexamite® R305 (NEX) is characterized by hydrolysable silicon-containing groups, and it is supplied specifically to improve the processability and the quality of recycled polyethylene. NEX was introduced in a degraded HDPE sample, and the so-obtained material was subjected to further reprocessing. The evolution of the macromolecular architecture of the polymer was monitored through rheological and spectroscopic analyses. Then, the melt strength of the recycled HDPE (with and without the additive) was evaluated, and the materials were subjected to non-isothermal elongational flow for obtaining fibers at different draw ratios, which were further characterized through tensile tests.

The virgin HDPE pellets, which did not experience any processing, were named HDPE_V. This sample was subjected to 30 subsequent extrusion cycles in a twin-screw extruder, until reaching a high extent of degradation, and the so-obtained material was named HDPE_D. Such intensive processing served to mimic advanced aging, providing a consistent and repeatable baseline of polymer degradation. Subsequently, HDPE_D was further processed for 1 min or 5 min without (HDPE_R1 and HDPE_R5, respectively) and with 5 wt.% of the additive (HDPE_RN1 and HDPE_RN5, respectively). In addition, HDPE_R5 and HDPE_RN5 fibers with diameters ranging from 200 to 800 μm were collected.

2.3.1 Effect of degradation on the mechanical properties of HDPE

One of the main issues affecting the reutilization of recycled HDPE in the same application as the original material is the dramatic loss of mechanical performance, particularly in terms of ductility, compared to the virgin polymer [58,155]. To verify this feature, tensile and Izod impact tests were carried out on both degraded and virgin HDPE. Figure 20 depicts the stress–strain curves of the two samples, and Table 6 reports the averaged values of the tensile modulus and strength, elongation at break, and impact energy. An overall decrease in all the measured mechanical properties was observed when thermo-mechanical degradation occurred in HDPE. More specifically, while the tensile modulus remained almost unchanged, the elongation at break suffered a substantial

reduction of 95%, passing from the virgin material to the degraded one. Likewise, the tensile strength decreased by 12% for HDPE_D. Conversely, the impact energy remained almost unchanged.

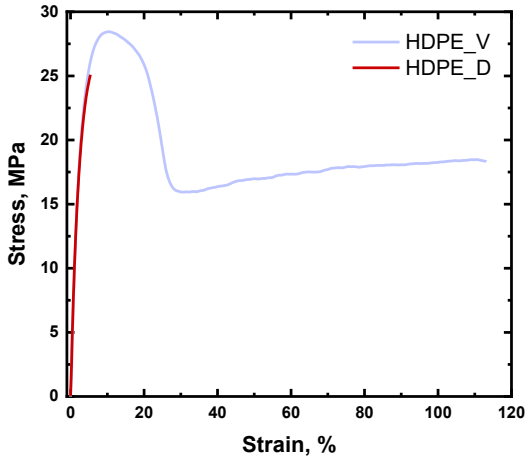

Figure 20. Stress–strain curves for virgin and degraded HDPE (HDPE_V and HDPE_D). Reprinted under CC BY 4.0 license.

Table 6. Mean values of tensile modulus and strength, elongation at break, and impact energy for virgin and degraded HDPE (HDPE_V and HDPE_D).

	Young modulus [MPa]	**Elongation at break [%]**	**Tensile strength [MPa]**	**Impact energy [J]**
HDPE_V	1113 ± 22	114.5 ± 28.0	28.2 ± 0.4	1.04 ± 0.54
HDPE_D	1101 ± 32	5.4 ± 0.9	24.9 ± 1.2	0.93 ± 0.38

According to the literature [57,58], the thermo-mechanical degradation experienced by HDPE, involving a severe modification of the polymer microstructure, resulted in a severe worsening of the mechanical performances of the material. In particular, as testified by the dramatic decrease in the elongation at break, HDPE_D shows a completely brittle behavior, implying that the reutilization of this recycled material is only limited to applications with low-engineering requirements, such as the formulation of low-performance products.

2.3.2 Evolution of the HDPE macromolecular architecture upon degradation and NEX introduction

In order to evaluate the evolution of the HDPE macromolecular architecture induced by thermo-mechanical degradation and the possible effects of the introduction of the additive, rheological investigations were performed. Figure 21 displays the trend of the complex viscosity as a function of the frequency for all the formulated samples.

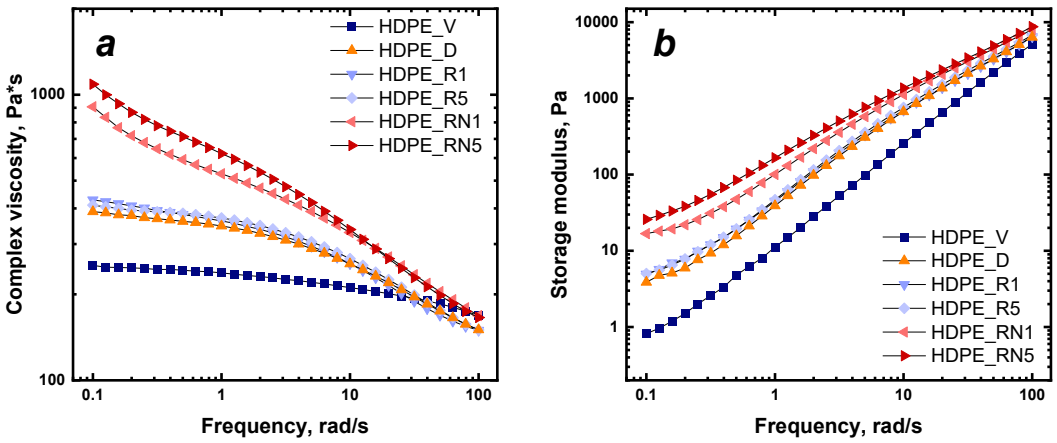

Figure 21. (a) Complex viscosity and (b) storage modulus as a function of the frequency collected at 190 °C for virgin (HDPE_V), degraded (HDPE_D), and recycled (HDPE_R1; HDPE_R5; HDPE_RN1; and HDPE_RN5) HDPE without and with NEX. Reprinted under CC BY 4.0 license.

Virgin HDPE (HDPE_V) features a typical Newtonian behavior at low and intermediate frequencies, with mild shear thinning when the frequency increases. The rheological behavior of HDPE_V reflects the high melt flow rate (27 g/10 min) and, thus, the low molecular weight of this polymer [156–158]. Concerning the degraded HDPE (HDPE_D), the complex viscosity increases in the low- and medium-frequency region with respect to HDPE_V, whereas, at higher frequencies, the curves almost overlay. The observed behavior can be attributed to the modification of the macromolecular architecture of the HDPE chains caused by thermo-mechanical degradation. In fact, as widely reported in the literature [58,65–67], when HDPE is reprocessed many times, different mechanisms can occur simultaneously: chain scission, the formation of long and/or short branches, and crosslinking. The higher viscosity of HDPE_D at low and intermediate frequencies compared to that of HDPE_V can thus be related to the decreased chain mobility caused by the formation of a branching structure or the introduction of some crosslinking. The inferred modification of the HDPE microstructure was further investigated through spectroscopic characterization, monitoring the extent of -CH_3 groups on the polymer chains. As observable in

Table 7 (the ATR-FTIR spectra are depicted in Figure 22), reporting the ratio between the intensities of the peaks related to the -CH_3 (1368 cm^{-1}) and -CH_2 (1463 cm^{-1}) groups, there is a progressive increase in this ratio when passing from virgin HDPE to its degraded counterpart. This result, coupled with the observed amplification of the non-Newtonian rheological behavior, suggests that chain scission and branching occur as competitive mechanisms during the thermomechanical degradation of HDPE. On the other hand, crosslinking phenomena cannot be excluded. Therefore, the macromolecules of the HDPE_D sample are characterized by a non-homogeneous architecture.

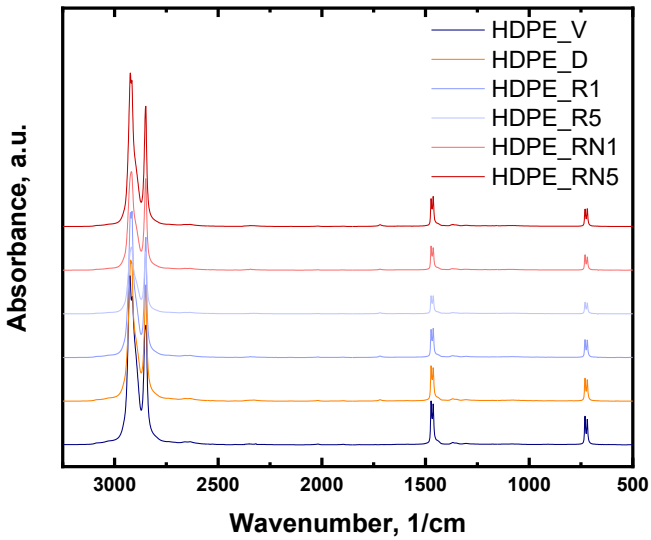

Figure 22. ATR-FTIR spectra for virgin (HDPE_V), degraded (HDPE_D), and recycled (HDPE_R1; HDPE_R5; HDPE_RN1; and HDPE_RN5) HDPE without and with NEX. Reprinted under CC BY 4.0 license.

Table 7. Ratio between the intensities of the peaks related to -CH_3 and -CH_2 for virgin (HDPE_V), degraded (HDPE_D), and recycled (HDPE_R1; HDPE_R5; HDPE_RN1; and HDPE_RN5) HDPE without and with NEX.

	-CH_3/-CH_2 ratio
HDPE_V	0.037
HDPE_D	0.045
HDPE_R1	0.040
HDPE_R5	0.041
HDPE_RN1	0.044
HDPE_RN5	0.041

In Figure 21, the trends of complex viscosity for recycled HDPEs are also reported. When simulating the recycling conditions for 1 min (HDPE_R1), the complex viscosity slightly increased only in the low-frequency zone compared to HDPE_D. Considering FTIR characterization (Table 7), the $-CH_3/-CH_2$ ratio decreased with respect to HDPE_D, suggesting that the crosslinking phenomenon was predominant over chain scission. When degraded HDPE was further processed for 5 min (HDPE_R5), the trend in the complex viscosity curve was very similar to that of HDPE_R1. Nevertheless, a slightly more pronounced Newtonian behavior could be observed, denoting a decrease in the molecular weight of recycled HDPE. In fact, from the FTIR analysis, the $-CH_3/-CH_2$ ratio barely increased with increasing the processing times, indicating a growth in the number of shorter chains. Therefore, the previous characterizations suggest that, as already reported in the literature [65], chain branching is the prevailing thermo-mechanical degradation mechanism for short degradation times, while chain scission becomes predominant when HDPE is heavily degraded.

The effects of the additive were evaluated considering, as the starting material, a degraded HDPE, therefore aiming to simulate the recycling of post-consumer HDPE. To achieve this, the additive was introduced within HDPE_D, and then the so-obtained material was further reprocessed for 1 and 5 min. Firstly, the complex viscosity displayed a significant increase in the whole tested frequency interval for the sample HDPE_RN1 (Figure 21a). Furthermore, a more pronounced shear-thinning behavior was noticed compared to HDPE_R1, and the Newtonian plateau almost disappeared. As widely reported in the literature [88,89,122,157,159–163], the increase in the viscosity at low frequencies and the magnified non-Newtonian characteristics could be related to the presence of long-chain branches on the polymer backbone. In fact, LCBs induce an increase in the number of chain entanglements, which prevent the mutual slipping of the macromolecules, thereby hindering their relaxation. Additionally, as reported by Stadler et al. [158], for LCB-PE samples, the typical shape of the viscosity function involves the appearance of a minimum and two distinct bends. In Figure 21a, an inflection point in the curve of HDPE_RN1 can be clearly observed. In addition, from the FTIR results reported in Table 7, an increase in the ratio between the intensities of the peaks related to methyl and methylene can be noticed for HDPE_RN1 compared to HDPE_R1, confirming the formation of LCB already inferred from the complex viscosity trend.

When the sample HDPE_RN1 was further processed, an additional increase in the complex viscosity at lower frequencies was detected, along with an amplification of the non-Newtonian features, as observable for HDPE_RN5 in Figure 21. Once again, all the noticed modifications of the rheological response could be attributed to the presence of species increasingly hindering the relaxation of the macromolecules. The amount of $-CH_3$ groups evaluated through FTIR analyses is diminished for HDPE_RN5 in comparison to HDPE_RN1, thereby indicating that the mean length of the side-chain branches is continuing increasing. Therefore, further processing for 5 min resulted in a higher extent of longer branches that induced an additional increase in the viscosity of the entire

system. Considering that NEX is an ethylene copolymer containing hydrolysable silicon groups, according to several papers dealing with the utilization of silanes in HDPE [164,165], it can be inferred that it may act by a mechanism involving silane hydrolysis and silanol condensation reactions, leading to the formation of long-chain branching.

LCBs also strongly affects the polymer melt elasticity. Looking at Figure 21b, depicting the trend in the storage modulus G′ as a function of the frequency, a progressive increase in the storage modulus in the low- and intermediate-frequency range is detected when passing from virgin HDPE (HDPE_V) to its degraded counterpart (HDPE_D). When considering the recycled HDPE (HDPE_R1, HDPE_R5), a slight increase in G′ can be observed compared to HDPE_D. On the other hand, as a result of the introduction of NEX into degraded HDPE (HDPE_RN1), the storage modulus deviates upward in the low-frequency zone, indicating a non-terminal rheological behavior. Also, in this case, the increase in G′ could be ascribed to the presence of long-chain branches and the consequent strengthening of the entanglement network [122,160,163,166]. When HDPE + NEX was further reprocessed for 5 min (HDPE_RN5), G′ displayed an additional increase at lower frequencies, indicating an even more elastic behavior due to the presence of longer side branches.

Overall, the analysis of the rheological response, coupled with the results of FTIR characterization, indicates that, when NEX is introduced within an already-degraded HDPE and the so-obtained material is further processed for different durations, the additive is able to drive the thermo-mechanical degradation reactions of HDPE towards the selective introduction of long-chain branches, promoting the achievement of a more homogeneous microstructure compared to pristine degraded HDPE.

In order to confirm this result, the Cole–Cole plot (displaying the imaginary component of the complex viscosity η″ as a function of the real one η′) was derived, and the obtained curves are reported in Figure 23. Typically, linear polymers show a semi-circular shape, while, for long-chain branched polymers, an upward tail (whose magnitude can qualitatively be related to the degree of long-chain branches) appears [167,168]. As shown in Figure 23, for HDPE_D, HDPE_R1, and HDPE_R5, the behavior expected for linear polymers was obtained, although the degraded and recycled materials exhibited some deviations from the semi-circular shape associable with the inferred heterogeneous microstructure encompassing some branches and crosslinking points. On the other hand, when NEX was added to the degraded HDPE (HDPE_RN1) and, even more, when the material was further processed (HDPE_RN5), a sudden increase in η″ in the high η′ region could be observed, clearly demonstrating the effect of the additive in promoting the formation of LCB, hampering the complete relaxation of the polymer macromolecules.

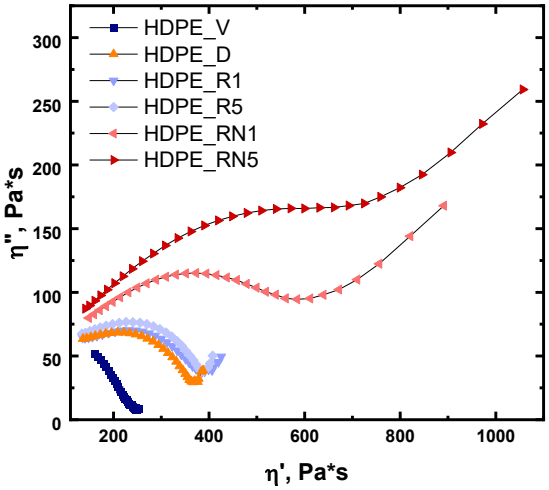

Figure 23. Cole-Cole plot of virgin (HDPE_V), degraded (HDPE_D), and recycled (HDPE_R1; HDPE_R5; HDPE_RN1; and HDPE_RN5) HDPE without and with NEX. Reprinted under CC BY 4.0 license.

The formation of LCB is also demonstrated by the analysis of the relaxation spectra and the Van Gurp–Palmen plots reported in Figure 24. Concerning the relaxation spectra, as compared to virgin HDPE, the peak related to the main relaxation mechanism of recycled HDPE shifts at longer times, likely due to the modifications of the chain architecture already described. Furthermore, the appearance of a distinct tail rising over the considered time range is observed. This last suggests the presence of a new dynamic specie with restricted mobility which is not able to fully relax in the tested time interval [169]. All these differences are even more pronounced for the materials containing NEX, confirming the effect of the additive in promoting the further formation of LCB hampering the complete relaxation of the polymer macromolecules.

Besides, in order to gain some information about the presence of LCB and the molecular weight distribution of the investigated materials, the Van Gurp-Palmen (VGP) plot reporting the phase angle δ as a function of the complex modulus G* was derived and displayed in Figure 24b. As widely known from the literature [170,171], this kind of representation is independent from the molecular weight, but it is affected by the molecular weight distribution and by the presence of LCB. Usually for linear-like polymers VGP plot results in a plateau at approximately 90°C, indicating a predominantly viscous behavior. As expected, HDPE_V shows the typical trend of a linear polymer. At variance, recycled HDPE samples exhibit a lower value of δ as compared to HDPE_V; besides, the decrease of the phase angle values starts at lower values of G* with respect to the virgin polymer, suggesting a widening of the molecular weight distribution for these materials. On the other hand, the samples containing NEX do not show a clear phase angle plateau and the overall values of δ are lower if compared to recycled HDPE samples without the additive. As already reported by other authors [122], no clear plateau is detected for polymers having a star-like macromolecular architecture.

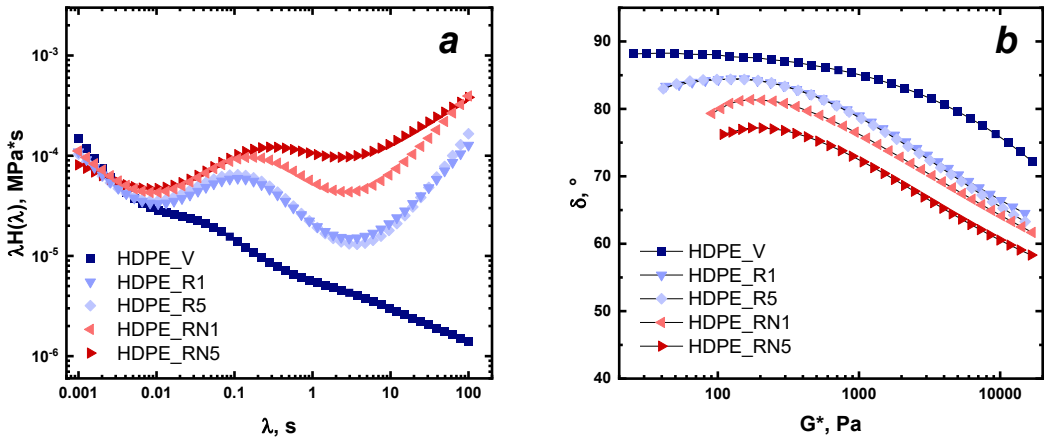

Figure 24. Stress relaxation spectra (a) and Van Gurp-Palmen plot (b) of virgin (HDPE_V), degraded (HDPE_D), and recycled (HDPE_R1; HDPE_R5; HDPE_RN1; and HDPE_RN5) HDPE without and with NEX. Reprinted under CC BY 4.0 license.

It is important to highlight that all the observed alterations in the HDPE chain architecture, promoted by thermo-mechanical degradation and the incorporation of the additive, did not affect neither the crystallization and melting temperatures nor the crystallinity degree of the formulated materials, as demonstrated by the DSC analysis (Table 8).

Table 8. Crystallization (T_c) and melting (T_m) temperatures, crystallization (ΔH_c) and melting (ΔH_m) enthalpies and crystallinity degree for virgin (HDPE_V), degraded (HDPE_D), and recycled (HDPE_R1; HDPE_R5; HDPE_RN1; and HDPE_RN5) HDPE without and with NEX.

	T_c [°C]	**ΔH_c [J/g]**	**T_m [°C]**	**ΔH_m [J/g]**	**Crystallinity [%]**
HDPE_V	115.3	207.0	131.0	213.7	73
HDPE_D	114.1	195.7	131.5	200.1	68
HDPE_R1	115.4	207.7	131.4	217.8	74
HDPE_R5	116.1	206.1	130.9	207.6	71
HDPE_RN1	116.0	204.2	130.1	209.6	71
HDPE_RN5	115.6	207.0	130.3	212.0	72

2.3.3 Processability evaluations and mechanical performances

The previously reported characterizations revealed the ability of NEX to selectively drive the thermo-mechanical degradation reactions of HDPE towards the achievement of an LCB microstructure. As widely reported in the literature [88,90,91,172], the introduction of LCB is beneficial for obtaining the high melt strength (MS) values that are required for the successful processing of polymers through technologies (such as film blowing and fiber spinning) dominated by elongational flow. MS is a very important technological parameter in such processing operations, since it is related to the force that a stretched polymer melt can withstand before breaking. In fact, the ability of the melt to avoid deformation under its own weight is of fundamental importance when stretching or drawing is applied during the processing. In this context, if the polymer melt is unable to withstand the elongation stresses to which it is subjected at the exit of the extrusion die (e.g., tendency to sag), various issues may arise, resulting in poor-quality products or unsuccessful processing.

The MS values of recycled HDPE, with and without NEX, were measured, obtaining 2.07 ± 0.27 and 4.32 ± 0.7 cN for HDPE_R5 and HDPE_RN5, respectively. Such result is quite striking and paves the way for the effective exploitation of NEX-containing recycled HDPE for further processing through technologies dominated by elongational flow. To further verify this feature, fibers of recycled HDPE without and with NEX (HDPE_R5 and HDPE_RN5) at different draw ratios were collected, and their tensile behavior was assessed. The obtained results in terms of elongation at break as a function of the draw ratio (DR) are depicted in Figure 25. As far as pristine recycled HDPE (HDPE_R5) was concerned, a slight reduction in the elongation at break with increasing the DR was observed, meaning constant or slightly reduced ductility as the diameter of the fibers decreased. However, higher values of elongation at break were obtained in the oriented samples with respect to their isotropic counterparts (see results reported in Table 6), indicating a beneficial effect of the macromolecules' orientation. On the other hand, noteworthy results were obtained for the sample containing NEX. In fact, in this case, the fibers showed a significant growth of the elongation at break as a function of the draw ratio. As an example, at a draw ratio equal to 60, a fifty-fold increase in the elongation at break was noticed for HDPE_RN5 with respect to HDPE_R5, reaching a value of 350%.

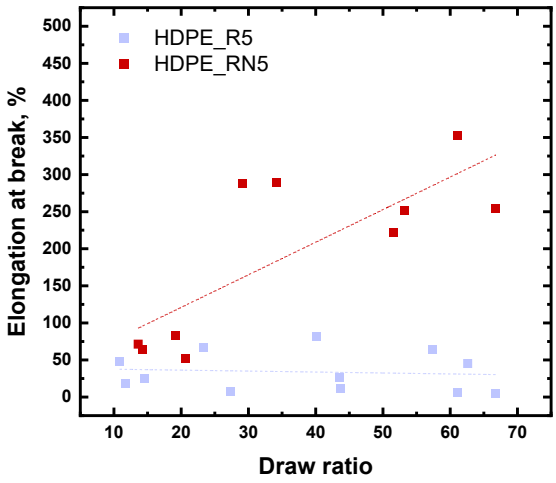

Figure 25. Elongation at break (%) as a function of the draw ratio for recycled HDPE without and with NEX (HDPE_R5 and HDPE_RN5). Reprinted under CC BY 4.0 license.

The observed behavior could be explained considering that the presence of LCB in the sample containing NEX promoted a greater orientation capability of the macromolecular chains during continuous stretching, which, in turn, led to increased ductility [87]. Furthermore, the possible effect of LCB on the polymer crystallization kinetics cannot be neglected. In this context, it has been demonstrated the ability of side branches to form tie molecules in the interlamellar region between different crystalline lamellae incorporating the linear backbone, resulting in increased mechanical properties [173–175]. Finally, it could be inferred that the observed buildup of the elongation at break as a function of the draw ratio could have also be related to a progressive increase in the content of the amorphous phase for thinner fibers, solidifying faster than thicker ones.

To summarize, the obtained results undoubtedly demonstrate that NEX can be profitably exploited for achieving an effective upcycling of HDPE. In fact, the used additive, promoting the attainment of an LCB microstructure, makes not only recycled HDPE suitable for applications (such as fibers and films) with high-engineering requirements but, even more importantly, allows for the formulation of materials based on recovered polyethylene endowed with mechanical performances comparable to those of their virgin counterparts.

2.3.4 Conclusions

In this work, an effective and industrially viable route for obtaining recycled HDPE with a high melt strength was proposed. In particular, the following key findings can be pointed out:

- The thermo-mechanical degradation experienced by HDPE during a typical mechanical recycling process involved the occurrence of different phenomena, achieving a heterogeneous microstructure that, ultimately,

resulted in brittle behavior. In particular, degraded HDPE exhibited a decrease of 95% in the elongation at break and of 12% in the tensile strength compared to the virgin material. This dramatic deterioration of mechanical properties severely limits any further reutilization of the recyclate for applications with high engineering requirements.

- The introduction of Nexamite® R305 was effective in selectively directing the thermo-mechanical degradation pathway of HDPE towards the achievement of a long-chain branching microstructure, which, in turn, promoted the obtainment of high melt strength values, thereby allowing the further processing of NEX-containing recycled HDPE through technologies dominated by elongational flow.
- Fibers obtained by subjecting recycled HDPE containing NEX to non-isothermal stretching exhibited a remarkably enhanced ductility compared to pristine recycled HDPE samples (elongation at break increased fifty-fold for fibers stretched at DR = 60), further demonstrating the beneficial effect of NEX in enabling high-value-added applications for recycled HDPE.

To sum up, this work clearly demonstrates the possibility of obtaining recycled HDPE potentially suitable for future applications characterized by high-engineering requirements, opening new perspectives for the effective upcycling of HDPE-based waste.

Chapter 3

Closing the loop with fire safety

3.1 Flame retardancy of recycled polypropylene with magnesium hydroxide

The transition toward a circular economy has intensified the use of recycled polymers in industrial applications; however, their deployment in safety-critical sectors remains limited by uncertainties related to performance reliability. Among these, fire behavior represents a major concern. As already discussed, recycled polypropylene might possess altered molecular weight and viscosity, potentially affecting the mechanisms through which flame retardants operate. As a result, flame-retardant systems originally developed and optimized for virgin polymers cannot be assumed to retain the same effectiveness when applied to recycled matrices. A systematic evaluation of standard, commercially employed flame retardants in recycled polymers is therefore necessary to determine whether established formulations remain valid and to ensure that fire safety can be reliably achieved within circular material flows.

In this chapter, an inorganic flame-retardant system based on magnesium hydroxide ($Mg(OH)_2$) is investigated in both virgin polypropylene (vPP) and recycled polypropylene (rPP). Magnesium hydroxide was selected due to its well-established flame-retardant mechanism, which relies on an endothermic dehydration reaction accompanied by the release of water vapor [176].

The recycled polypropylene (rPP) employed in this study was obtained by subjecting virgin polypropylene (vPP) to eight consecutive extrusion cycles within a twin-screw extruder. This approach was intentionally adopted to simulate an accelerated end-of-life condition, ensuring a controlled and reproducible degradation state of the polymer. The resulting rPP exhibits a reduced molecular weight and altered rheological behavior compared to the virgin material, thus providing a suitable benchmark for evaluating the robustness of the flame-retardant system.

60 wt.% of $Mg(OH)_2$ was introduced inside both virgin (vPP+MH) and recycled PP (rPP+MH) through a step of melt compounding performed by using a twin-screw extruder.

3.1.1 Microstructure assessment

As widely reported, the rheological behavior and the processability of a polymeric system is strongly affected by both the thermo-mechanical degradation occurring during mechanical recycling processes [51] and the introduction of fillers [177]. Dynamic rheological measurements were herein employed to evaluate the possible microstructural modification of the PP chains induced by the reprocessing and to gain some useful information about the morphology of the FR-containing materials.

In Figure 26a, the complex viscosity curves as a function of the frequency for all investigated materials are reported. Unfilled virgin PP (vPP) exhibits the typical Newtonian plateau at low frequencies, followed by a mild shear thinning, thus a decrease of the complex viscosity as the frequency increased. As a consequence of thermo-mechanical degradation underwent during the reprocessing cycles, the complex viscosity of unfilled rPP decreases over the entire frequency range. Furthermore, an amplification of the Newtonian behavior can be clearly observed. Both these features can be ascribed to the decrease in the PP molecular weight resulting from the chain-scission reactions occurring during the reprocessing steps [113].

As observable in Figure 26a, the addition of $Mg(OH)_2$ at a high loading (namely, 60 wt%) dramatically alters the rheological response of both matrices. In fact, in both vPP+MH and rPP+MH, the Newtonian plateau disappears completely, and a strong shear-thinning behavior is observed. This behavior is typical of highly filled systems, where the presence of rigid inorganic particles restricts macromolecular mobility and leads to longer relaxation times. Despite the substantial viscosity increase induced by the filler, the relative difference between the two composites remains consistent with that observed for the neat matrices, with rPP+MH exhibiting a lower viscosity than vPP+MH.

The storage modulus (G′) reported in Figure 26b further highlights the influence of both reprocessing and filler addition. Neat vPP exhibits higher G′ values than rPP, particularly at low frequencies, reflecting a more elastic response associated with higher molecular weight. Upon addition of $Mg(OH)_2$, both composites show a pronounced increase in G′ and a reduced frequency-dependence. The similar behavior of vPP+MH and rPP+MH suggests that the rheological response of both systems in the low frequency region is dominated by the inorganic filler network rather than by the intrinsic properties of the polymer matrix.

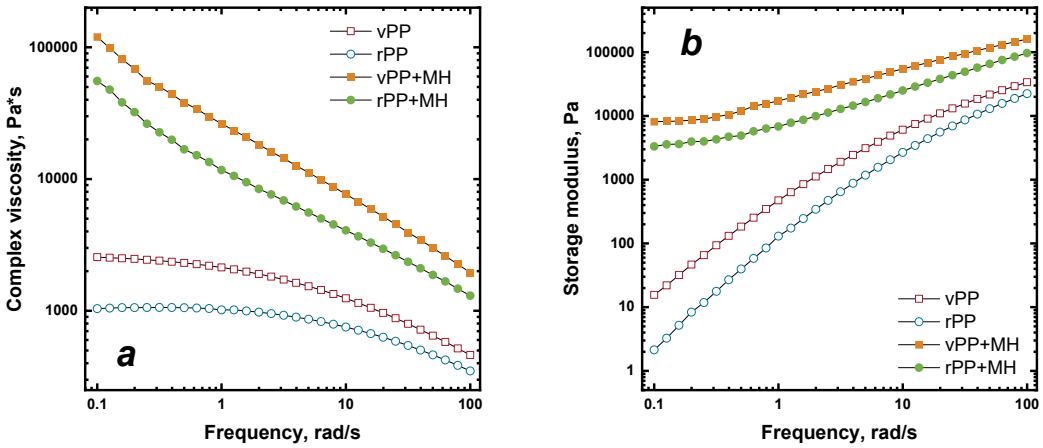

Figure 26. Complex viscosity (a) and storage modulus (b) as a function of frequency collected at 180 °C for unfilled virgin and recycled PP (vPP, rPP) and $Mg(OH)_2$-filled PP systems (vPP+MH, rPP+MH).

Morphological characterization by scanning electron microscopy (SEM) was carried out to investigate the dispersion and distribution of $Mg(OH)_2$ within the polymer matrices. SEM micrographs in Figure 27 a-b reveal a homogeneous distribution of $Mg(OH)_2$ particles in both vPP and rPP matrices. Quantitative image analysis was performed using the Feret diameter as a shape-independent parameter to describe agglomerate size distributions [178], reported in Figure 27 c-d. Both Feret diameter distributions display a similar trend. In vPP+MH, an average Feret diameter of 1.54 μm is determined, whereas the average Feret diameter in rPP+MH is equal to 1.27 μm. Despite a slight lower average diameter for recycled PP-based system, the close similarity between these values and the diameter distribution indicates that the lower viscosity of the recycled matrix does not significantly modify the dispersion of $Mg(OH)_2$.

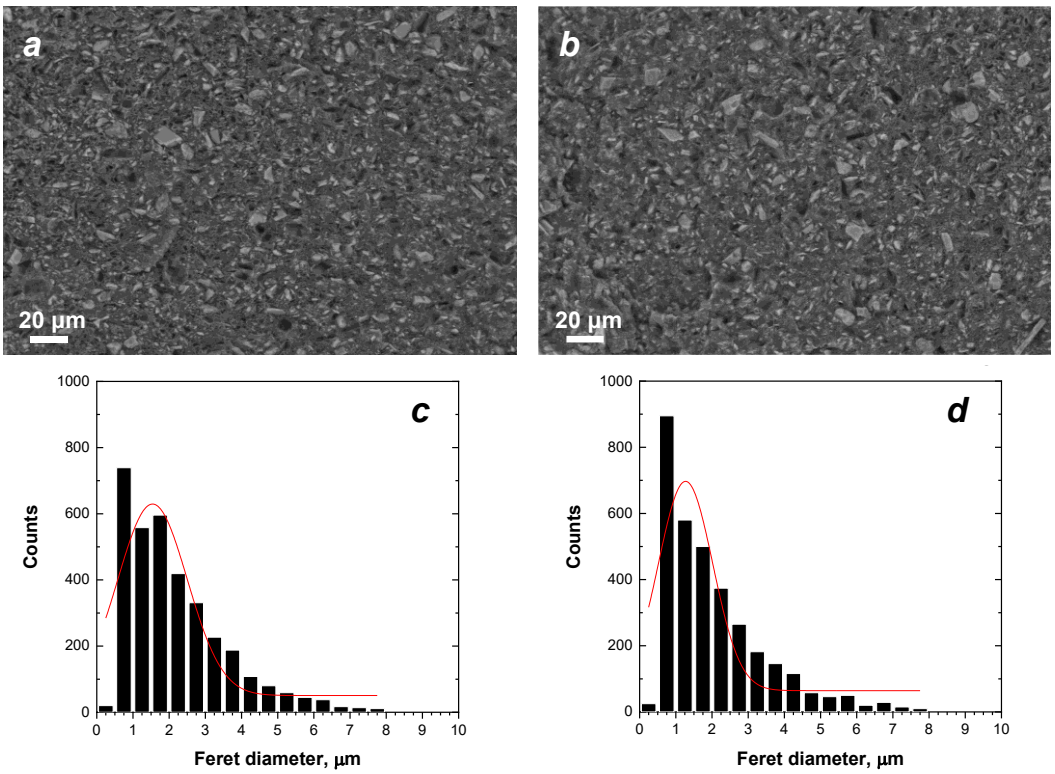

Figure 27. SEM micrographs of vPP+MH (a) and rPP+MH (b); distribution of $Mg(OH)_2$ particles' Feret diameter of vPP+MH (c) and rPP+MH (d).

3.1.2 Thermo-oxidative degradation

Thermogravimetric analysis (TGA) in air atmosphere was employed to investigate the thermo-oxidative stability of all investigated materials, and the obtained results are reported in Figure 28 and Table 9. From TGA tests, the following data were evaluated: T_{onset} (temperature at which 2% of weight loss occurs), T_{max} (temperature at which maximum weight loss rate is observed in dTG - derivative - curves), and the residue at 600°C.

As observed in Figure 28, both unfilled virgin and recycled PP display a single degradation step, with no char residue remaining at the end of the analysis. Furthermore, the temperatures of degradation onset and of maximum degradation for the two materials are practically coincident, indicating that the thermo-mechanical degradation occurring during the reprocessing cycles did not affect the thermo-oxidative stability of PP.

The introduction of magnesium hydroxide to both vPP and rPP results in a delayed onset temperature of degradation, likely because the absence of degradation of magnesium hydroxide before 300 °C could cover the degradation of the polymer matrix [179], and higher temperature of maximum degradation compared to the pure polypropylene matrices, according to the literature [180,181]. The final residues measured at 600 °C are approximately 42 wt% for vPP+MH and 43 wt% for rPP+MH, which agree with stoichiometric predictions based on filler content.

The similarity between virgin and recycled composites confirms that the flame-retardant action of $Mg(OH)_2$ is largely insensitive to the recycling-induced modification of the PP microstructure.

Table 9. Thermo-oxidative degradation data for unfilled virgin and recycled PP (vPP, rPP) and $Mg(OH)_2$-filled PP systems (vPP+MH, rPP+MH).

	T_{onset} [°C]	T_{max} [°C]	Residue @600°C [%]
vPP	250	316	0.2
rPP	249	314	0.1
vPP+MH	274	344	42
rPP+MH	272	353	43

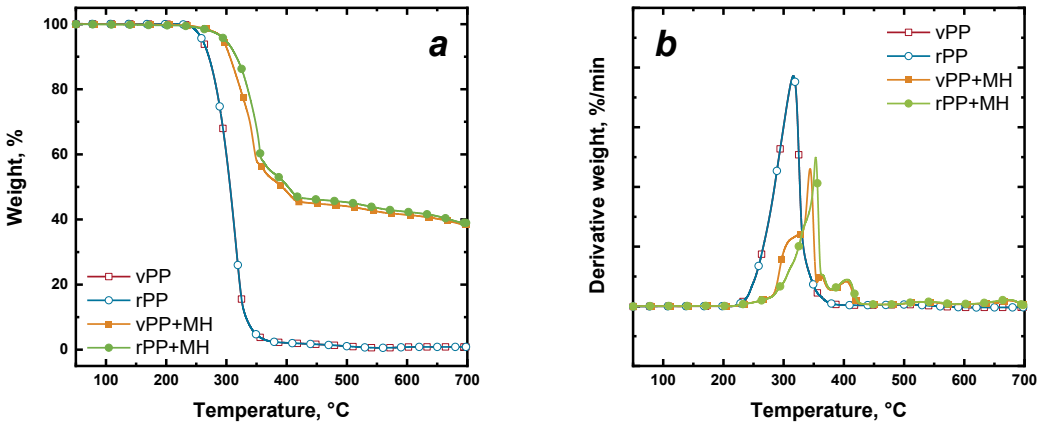

Figure 28. TGA (a) and dTG (b) curves of unfilled virgin and recycled PP (vPP, rPP) and $Mg(OH)_2$-filled PP systems (vPP+MH, rPP+MH).

3.1.3 Flame-retardant performances

3.1.3.1 Flammability evaluation

The UL-94 test evaluates ignition on a small scale and vertical flame propagation, assigning an increasing flammability classification ranging from V-2 to V-0, where V-0 is the most stringent, as it requires rapid flame extinction and the absence of dripping capable of igniting the cotton.

The results reported in Table 10 for vPP and rPP confirm the intrinsically flammable behavior of unfilled polypropylene. All specimens ignited easily, exhibited dripping with cotton ignition, and the flame reached the clamps. After the first flame application, the extinction times (t_1) were on the order of a few seconds, whereas after the second application the extinction time (t_2) systematically exceeded 30 s. Consequently, for both vPP and rPP no rating (NR) was achieved in UL-94, in agreement with findings reported in the literature

[182]. Moreover, the differences between virgin and recycled materials are marginal, and the overall results clearly justify the introduction of flame-retardant additives to reduce the flammability of these polymers.

The addition of $Mg(OH)_2$ reduces flame intensity and slows down combustion, but does not fully suppress dripping after the first flame application. Consequently, both vPP+MH and rPP+MH remain non-classifiable in the UL-94 test, with no substantial differences observed between virgin and recycled matrices.

Table 10. UL-94 vertical burning results for unfilled virgin and recycled PP (vPP, rPP) and $Mg(OH)_2$-filled PP systems (vPP+MH, rPP+MH).

	Rating	**t_1 [s]**	**t_2 [s]**	**Dripping**
vPP	NR	5.4 ± 2.7	> 30	Yes
rPP	NR	4.6 ± 2.1	> 30	Yes
vPP+MH	NR	> 30	-	Yes
rPP+MH	NR	> 30	-	Yes

3.1.3.2 Combustion behavior

Cone calorimeter tests provide a more comprehensive assessment of combustion behavior under well-defined heat flux conditions. The results of the cone calorimeter tests are summarized in Table 11 and Figure 29. As shown in Figure 29a, the heat release rate (HRR) curves indicate that both virgin and recycled PP exhibit essentially the same combustion behavior. In particular, the two materials display comparable times to ignition (TTI), after which the HRR rapidly increases and then sharply decreases, with flame extinction occurring at approximately 200 s. Moreover, during combustion the samples are completely consumed, as evidenced by the almost immediate reduction in specimen mass (Figure 29d).

An examination of the cone calorimeter data reported in Table 11 reveals no substantial differences between the two materials, suggesting that the thermo-mechanical degradation of PP and the associated microstructural modifications do not significantly influence its combustion behavior.

By contrast, the incorporation of magnesium hydroxide leads to a marked reduction in heat release for both vPP- and rPP-based samples. The heat release rate curve of both composites no longer shows a sharp maximum. Instead, after reaching the highest values of HRR, both curves progressively decrease until the extinction after about 800 s. The combustion process of $Mg(OH)_2$-filled systems is, thus, characterized by prolonged burning times and delayed extinction. This behavior arises from the combined effects of flame dilution and gas-phase flame inhibition of the FR additive studied. The mechanism of action of magnesium hydroxide as flame retardant is already well established [180]. Upon heating above approximately 300 °C, magnesium hydroxide decomposes and releases

water vapor, which dilutes the combustible gases and lowers the local oxygen concentration in the flame zone. At the same time, the endothermic nature of this decomposition absorbs a substantial amount of heat, leading to flame cooling and a further attenuation of combustion. The decomposition also produces magnesium oxide, which forms a protective, thermally insulating layer on the polymer surface. This barrier hinders heat transfer into the material, slows the pyrolysis process, and ultimately reduces the combustion rate, resulting in lower heat release rate and total heat release values.

The reduction of HRR and THR for both $Mg(OH)_2$-filled systems is approximately equal to 80 % and 33 %, respectively, if compared to unfilled matrices. Therefore, irrespective of the level of degradation of the matrix, magnesium hydroxide is able to ensure flame retardancy properties in both PP-based systems.

If compared to unfilled vPP and rPP, also the smoke production is markedly reduced due to the release of water vapor, which dilutes combustible gases and lowers flame temperature. In fact, lower values of total smoke production (TSP) and total smoke release (TSR) are obtained in the FR systems. As far as the time to ignition (TTI) is concerned, the values of both systems do not change with the addition of magnesium hydroxide.

The residual mass after the test, approximately 46 wt% for vPP+MH and about 44 wt% for rPP+MH, assumes values that are slightly higher than those observed in TGA, possibly because of a re-hydration of magnesium oxide after the total decomposition of magnesium hydroxide [183].

All the above considerations confirm the effectiveness of this type of inorganic flame-retardant system also in recycled polypropylene. No differences in combustion behavior are observed between the virgin- and recycled-based systems, confirming that magnesium hydroxide provides the same level of fire protection in recycled polypropylene as in the virgin material.

Table 11. Cone calorimeter tests results for unfilled virgin and recycled PP (vPP, rPP) and $Mg(OH)_2$-filled PP systems (vPP+MH, rPP+MH).

	vPP	***rPP***	***vPP+MH***	***rPP+MH***
TTI [s]	32 ± 2	28 ± 1	34 ± 1	33 ± 1
Ignition to flameout [s]	188 ± 9	202 ± 10	718 ± 25	744 ± 3
peak-HRR [kW/m^2]	1172 ± 59	1147 ± 57	219 ± 7	223 ± 2
t peak-HRR [s]	136 ± 7	140 ± 7	62 ± 1	60 ± 6
THR [MJ/m^2]	109 ± 6	107 ± 5	72 ± 6	72 ± 1
peak-SPR [m^2/s]	0.220 ± 0.010	0.200 ± 0.020	0.046 ± 0.005	0.049 ± 0.007
t peak-SPR [s]	152 ± 8	152 ± 7	65 ± 5	56 ± 1
TSP [m^2]	24.3 ± 0.5	23.6 ± 0.8	9.6 ± 0.4	9.8 ± 0.7
TSR [m^2/m^2]	2433 ± 122	2356 ± 118	977 ± 80	967 ± 100
Residue [wt.%]	0	0	46.1 ± 0.3	44.4 ± 0.1
SEA [m^2/kg]	921 ± 30	905 ± 27	425 ± 26	417 ± 36
EHC [MJ/kg]	41 ± 1	42 ± 1	31 ± 2	32 ± 1
MARHE [kW/m^2]	593 ± 23	591 ± 27	144 ± 2	146 ± 5

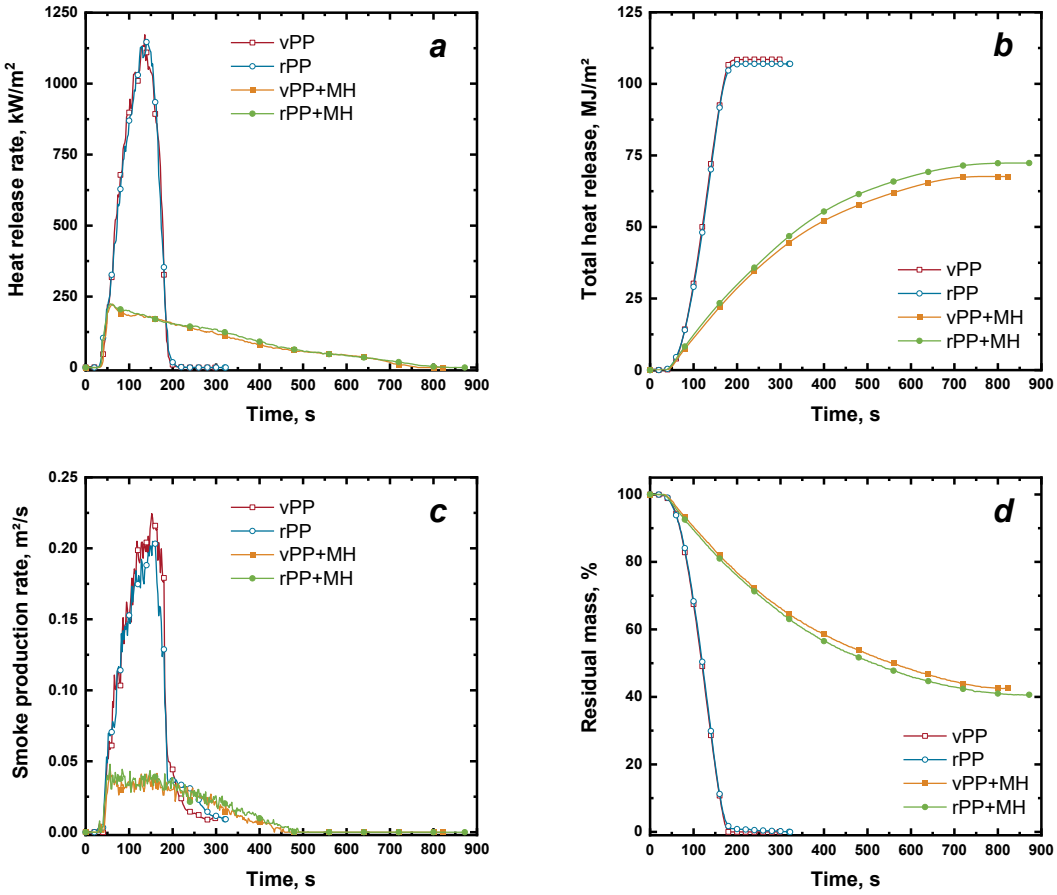

Figure 29. Cone calorimeter graphs for unfilled virgin and recycled PP (vPP, rPP) and $Mg(OH)_2$-filled PP systems (vPP+MH, rPP+MH): heat release rate (a), total heat release (b), smoke production rate (c) and residual mass (d).

For assessing the fire safety performance, two indices were employed: the Fire Performance Index (FPI= TTI/pkHRR) and the Fire Growth Rate Index (FIGRA=pkHRR/t_{pk}HRR). The former increases when ignition is delayed and/or when the HRR peak is reduced; therefore, the higher the FPI value, the lower the fire risk (also referred to as fire hazard) [184]. The latter index increases as the HRR peak becomes higher and is reached more rapidly. According to the literature, polymer systems characterized by high FPI and low FIGRA values are considered safer from a fire protection perspective [185]. To complete the analysis, the Flame Retardancy Index (FRI) was also considered [186]. This dimensionless index quantifies the effectiveness of the flame-retardant additive by taking the neat polymer (vPP and rPP) as the reference; values between 10^0 and 10^1 represents good flame retardancy performances. These indices were calculated and are reported in Table 12.

Concerning the performance of the matrices (vPP and rPP), they exhibit very low FPI and high FIGRA values, in agreement with the intrinsic flammability of these materials. In the systems containing $Mg(OH)_2$, the FPI becomes very high due to a strongly reduction in the HRR peak, and the FIGRA value is significantly reduced. The FRI for both systems is about 8.70. All the calculated indexes

clearly indicate that $Mg(OH)_2$ significantly improves fire safety compared to neat polypropylene. Importantly, the results obtained for rPP+MH are comparable to, and in some cases slightly better than, those of vPP+MH. This result further confirms that the inorganic flame-retardant system is suitable for use with recycled polypropylene.

Table 12. FPI, FIGRA and FRI value for unfilled virgin and recycled PP (vPP, rPP) and $Mg(OH)_2$-filled PP systems (vPP+MH, rPP+MH).

	FPI [m^2*s/kW]	**FIGRA [kW/m^2/s]**	**FRI**
vPP	0.027 ± 0.001	8.62 ± 0.43	-
vPP+MH	0.155 ± 0.007	3.53 ± 0.10	8.62
rPP	0.024 ± 0.001	8.19 ± 0.41	-
rPP+MH	0.145 ± 0.007	3.73 ± 0.38	8.85

3.1.4 Conclusions

In this work, the applicability of flame-retardant originally developed for virgin polypropylene to recycled polypropylene was systematically evaluated. An inorganic flame-retardant system based on magnesium hydroxide, incorporated at 60 wt.%, was assessed in both virgin and recycled polypropylene matrices in order to determine its effectiveness and sensitivity to recycling-induced degradation.

Rheological characterization confirmed that mechanical reprocessing significantly reduces the melt viscosity of polypropylene as a result of chain scission reactions. Nevertheless, in the case of $Mg(OH)_2$-filled systems, this difference in matrix viscosity had a limited influence on the overall behavior of the material.

UL-94 vertical burning tests revealed that the incorporation of $Mg(OH)_2$ lowers flame intensity and retards the combustion process, but it does not completely inhibit dripping. As a result, both vPP+MH and rPP+MH remain non-classifiable in the UL-94 test, with no significant differences observed between the virgin and recycled matrices.

Cone calorimeter tests clearly highlighted the contribution of the inorganic system to fire performance in both virgin and recycled PP. Irrespective of the matrix, the $Mg(OH)_2$ formulations proved to be effective in reducing the total heat released during combustion and in limiting smoke production. Importantly, both virgin and recycled $Mg(OH)_2$-filled composites exhibited comparable reductions in heat release, confirming the robustness of the inorganic flame-retardant system when applied to recycled polypropylene.

Overall, the obtained results demonstrate that magnesium hydroxide retains its effectiveness in recycled polypropylene, providing a level of fire safety comparable to that achieved in virgin matrices.

3.2 Ammonium polyphosphate and pentaerythritol as intumescent flame-retardant for recycled polypropylene

Intumescent flame-retardant systems represent one of the most effective approaches for improving the fire behavior of polypropylene, as they act primarily in the condensed phase through the formation of an expanded and insulating char layer. In this chapter, an intumescent system based on ammonium polyphosphate (APP) and pentaerythritol (PER) in a 3:1 weight ratio is investigated in both virgin (vPP) and recycled polypropylene (rPP) matrices. The system was incorporated at 30 wt.% into virgin (vPP+AP) and recycled PP (rPP+AP) through a step of melt compounding using a twin-screw extruder. Following the methodology used for magnesium hydroxide-filled materials, the recycled polypropylene (rPP) was produced by subjecting virgin polypropylene (vPP) to eight consecutive extrusion cycles in a twin-screw extruder.

As discussed in the previous chapters, recycling induces significant changes in polypropylene, particularly in terms of molecular weight and viscosity. These changes are expected to influence not only processing and mechanical behavior, but also the efficiency of intumescent flame-retardant mechanisms, which strongly depend on melt viscosity, char cohesion, and resistance to dripping [187]. For this reason, the comparison between vPP and rPP is integrated throughout the present chapter, with particular attention paid to how matrix degradation affects intumescence, char formation, and combustion dynamics.

3.2.1 Microstructure assessment

Frequency sweep tests were performed on all the samples in order to establish direct comparisons between virgin and recycled matrices and their corresponding IFR-containing systems. As already mentioned in the previous chapter, the complex viscosity curves reported in Figure 30 clearly show that rPP exhibits a significantly lower viscosity than vPP across the entire frequency range, confirming the occurrence of chain scission during recycling and reprocessing.

Upon addition of APP:PER, the rheological response of the materials differs as a function of the matrix (Figure 30a). In virgin PP, the introduction of IFR results in increased complex viscosity in the whole investigated frequency range, causing the appearance of a more pronounced non-Newtonian behavior in the low frequency region. On the other hand, for rPP+AP the complex viscosity curve overlapped almost completely those of unfilled rPP at higher frequencies but a substantial increase in viscosity at low frequencies can be noticed. This increase is associated with the disappearance of the Newtonian plateau and the development of a yield stress behavior, indicative of restricted chain mobility and the formation of a filler-induced network [188]. This suggests that the lower viscosity of the recycled matrix as compared to vPP facilitates a more homogeneous dispersion of the intumescent system.

The effects of the flame retardants particles on polymer chain mobility are also illustrated by the storage modulus G′, whose trends are reported in Figure 30b. The presence of the IFR additive leads, in both systems, to an increase in G′ in the low frequency range, with a less frequency-dependent behavior compared to that of the neat matrices. This result can be ascribed to the modification of the macromolecular dynamics arising from the formation of polymer–particle and particle–particle interactions. However, this feature is more pronounced in the case of recycled PP-based system, thus confirming that a better dispersion of the IFR additive is achieved with the low-viscosity matrix.

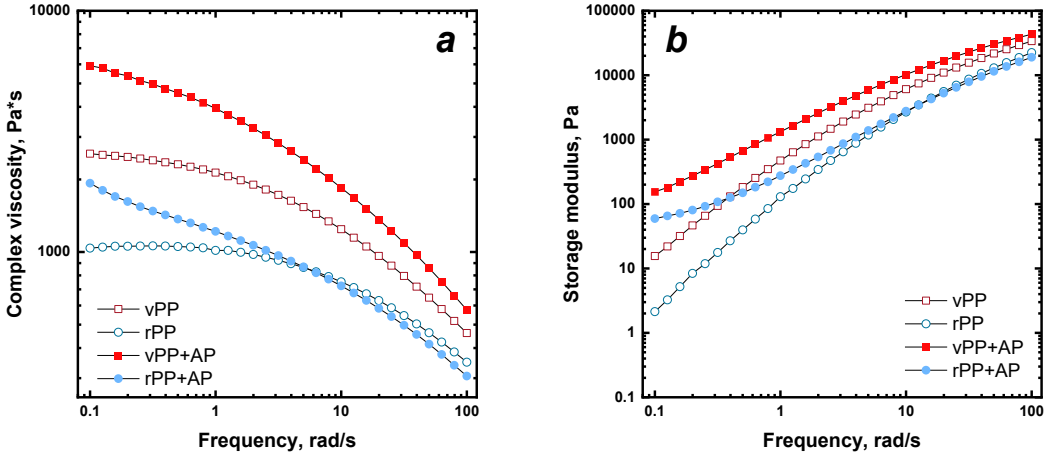

Figure 30. Complex viscosity (a) and storage modulus (b) as a function of frequency collected at 180 °C for unfilled virgin and recycled PP (vPP, rPP) and APP:PER-filled PP systems (vPP+AP, rPP+AP).

Morphological analysis by SEM provides further insight into the dispersion of APP:PER within the polymer matrices. SEM micrographs reported in Figure 31a-b reveal the presence of well distributed additive-rich clusters in both composites, with significant differences in size distribution between vPP+AP and rPP+AP. In fact, quantitative image analysis, supported by the distribution of the particles Feret diameter in Figure 31c-d, shows that vPP+AP contains a higher number of large agglomerates with average diameter equal to 3.91 μm, while rPP+AP exhibits a narrower size distribution shifted toward smaller cluster sizes and an average diameter of 1.23 μm.

The more pronounced yield stress behavior observed from rheological characterization in rPP+AP is consistent with the morphological evidence. In fact, the particles size distribution revealed agglomerates that were on average smaller than those present in vPP+AP, thus suggesting that the system based on the recycled matrix allowed for a more finely dispersion of the flame-retardant due to its lower viscosity, as also demonstrated by other authors [189,190].

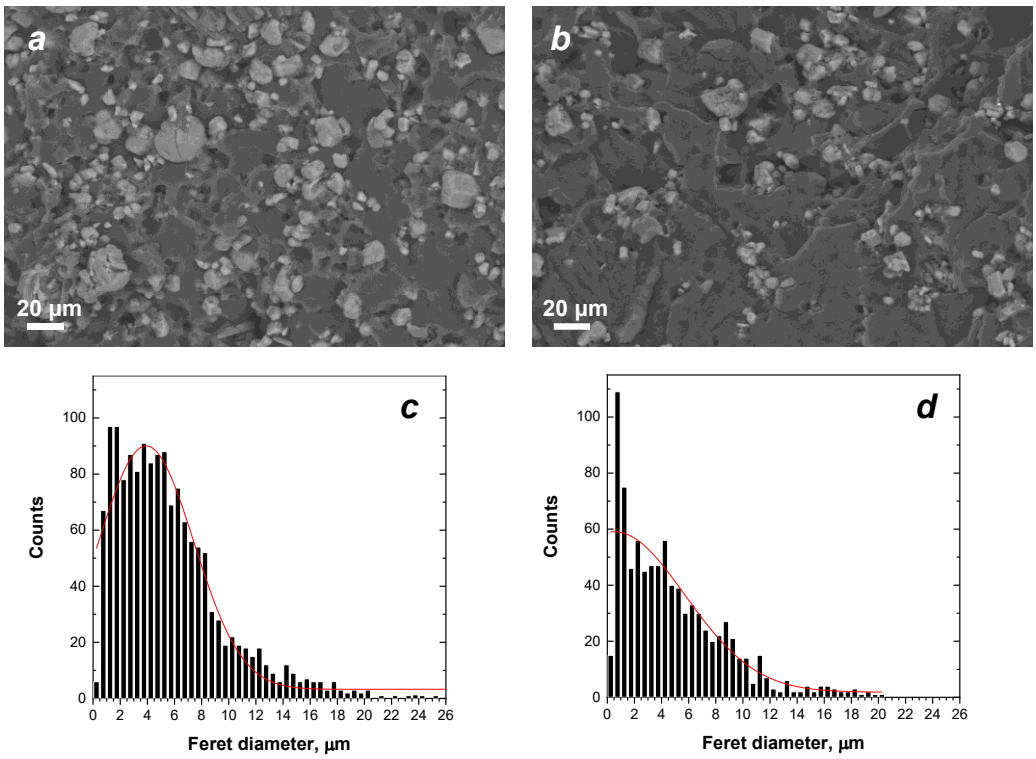

Figure 31. SEM micrographs of vPP+AP (a) and rPP+AP (b); distribution of particles' Feret diameter of vPP+AP (c) and rPP+AP (d).

3.2.2 Thermo-oxidative degradation

Thermogravimetric analysis (TGA) in air was used to assess the thermo-oxidative stability of the virgin and recycled matrices and the IFR-containing materials (Table 13 and Figure 32). As already discussed in the previous chapter, both unfilled virgin and recycled PP exhibit a single degradation step with no residual char, and show nearly coincident degradation onset and maximum degradation temperatures, confirming that reprocessing did not significantly affect the thermo-oxidative stability of PP.

As far as IFR composites is concerned, thermogravimetric analysis reveals that both vPP+AP and rPP+AP exhibit a main degradation step, occurring at lower temperatures, due to additive decomposition. The dTG curves in Figure 32b provide additional insight into the maximum degradation rate: for vPP+AP, the maximum occurs at around 292 °C, whereas rPP+AP shows a shifted maximum toward higher temperatures. The small shoulders observed in the dTG curves can be attributed to the formation of the carbonaceous layer.

Another difference between the two IFR systems concerns the residual mass at 600 °C: vPP+AP shows a residue of about 18 %, while rPP+AP exhibits a lower value of about 15 %, as reported in Table 13. This indicates that the composite based on the recycled matrix leaves a smaller residue, which may be related to a lower stability under oxidative conditions.

Table 13. Thermo-oxidative degradation data for unfilled virgin and recycled PP (vPP, rPP) and APP:PER-filled PP systems (vPP+AP, rPP+AP).

	T_{onset} [°C]	T_{max} [°C]	Residue @600°C [%]
vPP	250	316	0.2
rPP	249	314	0.1
vPP+AP	233	292	18
rPP+AP	226	336	15

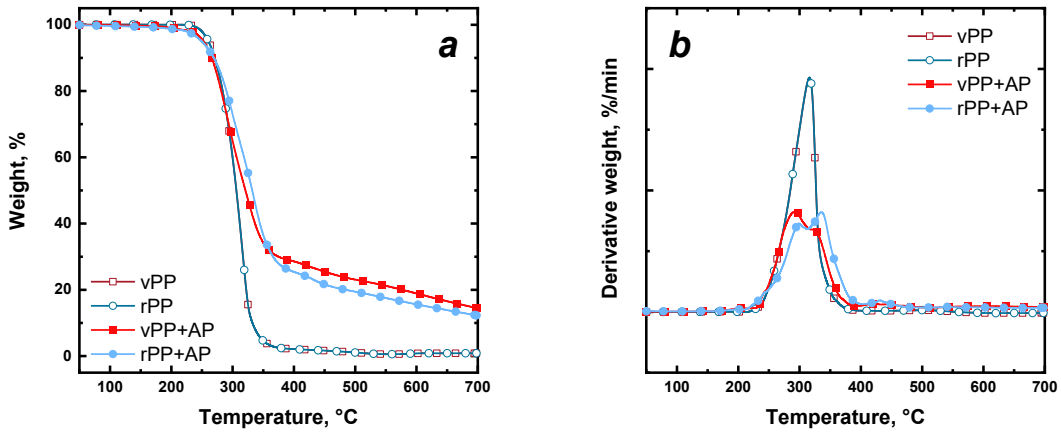

Figure 32. TGA (a) and dTG (b) curves of unfilled virgin and recycled PP (vPP, rPP) and APP:PER-filled PP systems (vPP+AP, rPP+AP).

3.2.3 Flame-retardant performances

3.2.3.1 Flammability evaluation

Flammability was assessed by means of UL-94 vertical burning tests, and the results are reported in Table 14. As already discussed, both unfilled vPP and rPP show intense dripping and fast flame spread, leading to a no rating (NR) classification.

UL-94 vertical burning tests of IFR systems instead clearly demonstrate the influence of matrix viscosity on intumescent performance. All five specimens of vPP+AP achieves a V-0 classification with rapid self-extinction after both the first and second flame applications, without the flame reaching the clamps and without dripping or cotton ignition. For rPP+AP, it was necessary to repeat the test on ten specimens, highlighting a variability among the samples that resulted in classifications ranging from V-0 to V-2. Although effective flame suppression after the first flame application and short extinction times during the second one, dripping accompanied by cotton ignition was observed in 5 out of the 10 total samples tested. This behavior is attributed to the lower viscosity of the recycled

matrix, which promotes droplet detachment before the formation of the compact char layer.

Table 14. UL-94 vertical burning results for unfilled virgin and recycled PP (vPP, rPP) and APP:PER-filled PP systems (vPP+AP, rPP+AP).

	Rating	**t_1 [s]**	**t_2 [s]**	**Dripping**
vPP	NR	5.4 ± 2.7	> 30	Yes
rPP	NR	4.6 ± 2.1	> 30	Yes
vPP+AP	V-0	0	1.8 ± 1.3	No
rPP+AP	V-2	0	3.6 ± 2.5	Yes

3.2.3.2 Combustion behavior

The combustion behavior of the materials was measured using a cone calorimeter and the corresponding results are reported in Table 15 and Figure 33. As previously discussed, virgin and recycled PP exhibit comparable combustion behavior (Figure 33a), with similar TTI, rapid HRR evolution, and complete sample consumption (Figure 33d).

Upon the introduction of the intumescent flame-retardant based on APP:PER into both vPP and rPP, an earlier time to ignition (TTI) and a longer time to flame-out are observed, compared with the curves of the unfilled polymers. As expected, the TTI is lower in the APP:PER-containing system because IFR additives promoted the accelerated decomposition of the polymeric matrix. Moreover, for both materials the curves display the formation of two main peaks with significantly lower intensity than the single HRR peak characteristic of the neat polymers. As already reported [191–193], the initial peak, in this case associated with the first increase of the HRR values, corresponds to ignition and surface flame propagation, followed by a plateau phase related to the development of a protective char layer. The subsequent peak, occurring at longer times, is associated to the breakdown of this char layer as volatile products generated by substrate degradation escape.

Specifically, as already discussed in the literature [194,195], the charring mechanism of APP and PER starts with the reactions between the acidic species generated from APP and its degradation products (orthophosphates and phosphoric acids) and the char-forming agent PER, leading to the formation of phosphorus-containing structures. This stage promotes dehydration and initiates carbonization of the system through free-radical processes. As the temperature increases, the blowing action becomes dominant. The decomposition of APP releases gaseous products, mainly ammonia, which cause the developing char to expand and form an intumescent, foamed structure. This stage involves a combination of gas generation and char swelling. Then at higher temperatures, the intumescent structure progressively degrades and loses its foamed character. Despite this structural collapse, the char exhibits reduced thermal conductivity at

elevated temperatures, thereby maintaining an effective insulating barrier that protects the underlying polymer substrate.

As observable from the results reported in Table 15 and Figure 33, vPP+AP exhibits a 70% and 23% reduction of the peak of HRR and of THR, respectively, and the mass lost rate was significantly reduced (Figure 33d) as compared to unfilled virgin PP.

Considering the rPP-based system, the second HRR peak is on average higher, but it is delayed in time, indicating postponed heat release. The plateau zone reflecting the development of the protective char layer is longer and characterized by lower values of HRR if compared to vPP+AP, suggesting the ability of the intumescent system to create a more stable char if employed in recycled PP. Indeed, in agreement with the literature [196], char cracking is delayed when the protective char layer is more robust, and the formation of a stronger intumescent char is associated with smaller particle sizes. As a consequence, both the total heat release (Figure 33b) and the mass loss (Figure 33d) evolve slower with respect to flame-retardant virgin PP, anyway achieving comparable values at the end of the test.

Consistently, the smoke production rate (SPR, Figure 33c) follows the same trend observed in the HRR and THR curves: the SPR profile of rPP+AP displays a higher and delayed maximum, corresponding to the collapse of the char layer. In contrast, the total smoke production (TSP) during the entire cone calorimeter test is lower for recycled PP-based material.

These results clearly demonstrate that the intumescent flame-retardant system studied remains effective also when applied to recycled PP. The ammonium polyphosphate and pentaerythritol system is able to impart more efficient flame-retardant properties to recycled polypropylene, because of a more pronounced plateau in the HRR curve and delayed main peak, both leading to a lower MARHE if compared to virgin PP-based system, thereby enabling its use even in applications where fire safety is a mandatory requirement.

Table 15. Cone calorimeter tests results for unfilled virgin and recycled PP (vPP, rPP) and APP:PER-filled PP systems (vPP+AP, rPP+AP).

	vPP	***rPP***	***vPP+AP***	***rPP+AP***
TTI [s]	32 ± 2	28 ± 1	18 ± 3	15 ± 1
Ignition to flameout [s]	188 ± 9	202 ± 10	488 ± 37	475 ± 10
peak-HRR [kW/m^2]	1172 ± 59	1147 ± 57	345 ± 37	397 ± 64
t peak-HRR [s]	136 ± 7	140 ± 7	314 ± 8	356 ± 20
THR [MJ/m^2]	109 ± 6	107 ± 5	84 ± 1	84 ± 2
peak-SPR [m^2/s]	0.220 ± 0.010	0.200 ± 0.020	0.120 ± 0.009	0.140 ± 0.007
t peak-SPR [s]	152 ± 8	152 ± 7	327 ± 5	375 ± 10
TSP [m^2]	24.3 ± 0.5	23.6 ± 0.8	28.7 ± 1.1	25.1 ± 0.9
TSR [m^2/m^2]	2433 ± 122	2356 ± 118	2886 ± 205	2579 ± 152
Char residue [wt.%]	0	0	18.4 ± 0.2	18.9 ± 0.3
SEA [m^2/kg]	921 ± 30	905 ± 27	1236 ± 69	1121 ± 75
EHC [MJ/kg]	41 ± 1	42 ± 1	36 ± 2	37 ± 1
MARHE [kW/m^2]	593 ± 23	591 ± 27	203 ± 7	190 ± 5

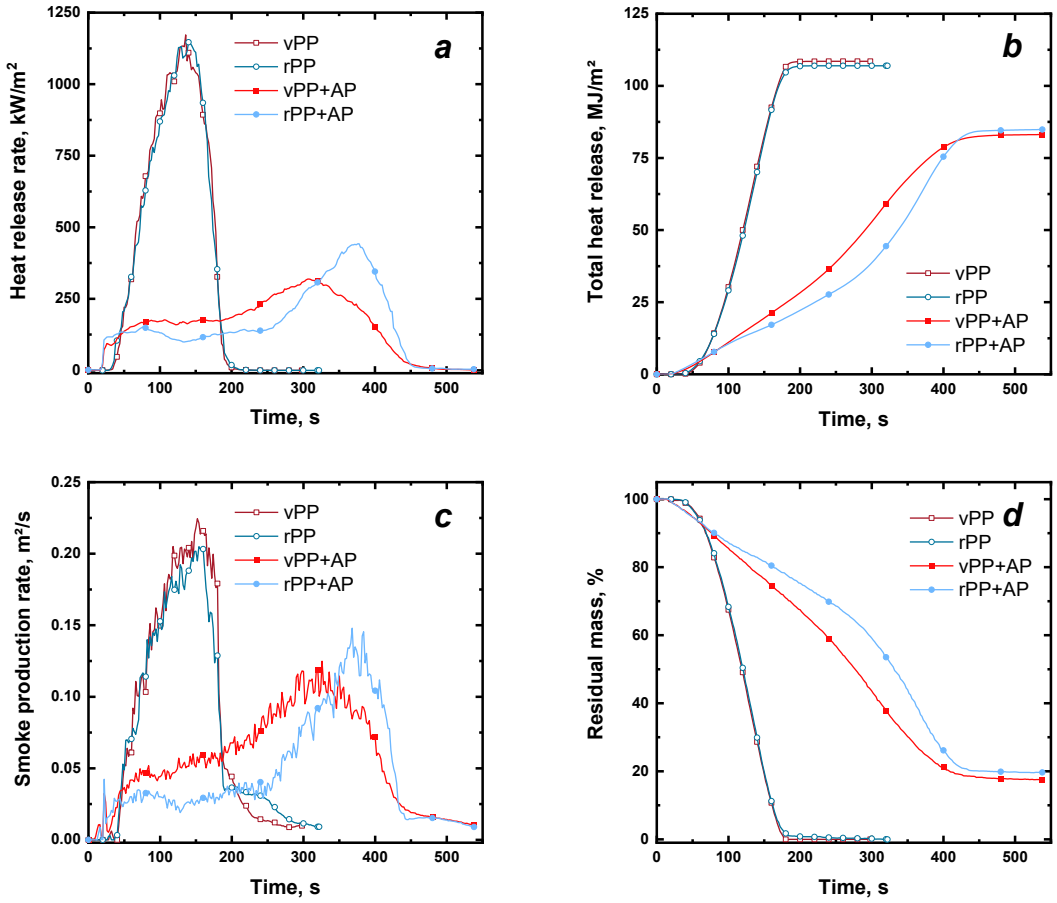

Figure 33. Cone calorimeter graphs for unfilled virgin and recycled PP (vPP, rPP) and APP:PER-filled PP systems (vPP+AP, rPP+AP): heat release rate (a), total heat release (b), smoke production rate (c) and residual mass (d).

Fire safety indices (FPI, FIGRA and FRI reported in Table 16) further confirm the effectiveness of the intumescent system. The incorporation of APP:PER particles leads to a marked change in fire dynamics compared with the neat matrices: FIGRA drops sharply, indicating a strong reduction in fire growth rate due to the formation of an expanded char layer that insulates the material and limits heat transfer. At the same time, FPI increases with respect to the unfilled polymers as a consequence of a reduced HRR peak, although the ignition time is shortened because APP:PER starts to decompose at lower temperatures. The Flame Retardancy Index reaches values of about 2.46 for vPP+AP and 1.97 for rPP+AP, indicating an overall "good" improvement in flame-retardant performance induced by the intumescent system, notwithstanding lower FRI values for rPP+AP highlight the influence of matrix degradation on intumescent efficiency.

Table 16. FPI, FIGRA and FRI values of for unfilled virgin and recycled PP (vPP, rPP) and APP:PER-filled PP systems (vPP+AP, rPP+AP).

	FPI [m^2*s/kW]	FIGRA [kW/m^2/s]	FRI
vPP	0.027 ± 0.001	8.62 ± 0.43	-
vPP+AP	0.052 ± 0.003	1.10 ± 0.08	2.46
rPP	0.024 ± 0.001	8.19 ± 0.41	-
rPP+AP	0.038 ± 0.003	1.12 ± 0.09	1.97

3.2.3.3 Char analysis

The char structure is a key factor in evaluating the barrier properties of an intumescent system; therefore, SEM micrographs of both the external and internal regions of the residues of the APP:PER-containing materials at the end of the cone calorimeter tests were acquired (Figure 34).

The micrographs reported in Figure 34 show that, for both matrices, a compact microstructure with few holes is formed on the external surface, whereas the internal char exhibits a more porous structure. The combination of these two morphologies increases the tortuosity of diffusion pathways, thereby reducing oxygen and heat transport and shielding the polymer matrix from heat exposure. A comparison between the external char layers of the two composites reveals that the outer layer of vPP+AP (b) appears more compact, with a closed-cell morphology, while that of rPP+AP (e) shows a higher density of pores and discontinuities. Moreover, the internal char of vPP+AP (c) exhibits smaller pores than those observed in rPP+AP (f).

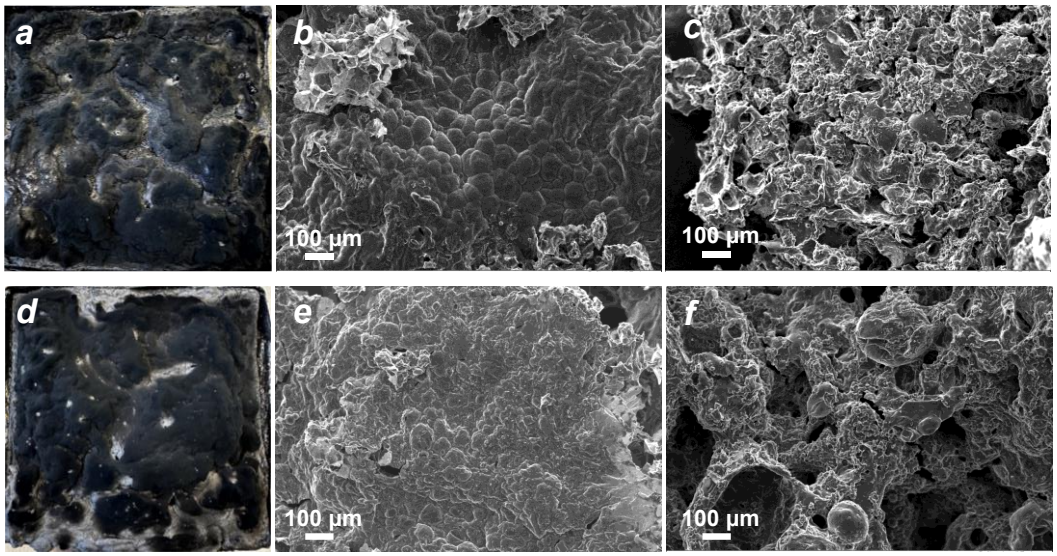

Figure 34. Photos and SEM images of residual char: (a,b,c) vPP+AP; (d,e,f) rPP+AP.

To complement the morphological analysis with a chemical evaluation, elemental mapping was performed on both the internal and external char layers. Figure 35 shows the elemental maps of phosphorus, nitrogen and carbon of the internal and external char of vPP+AP and rPP+AP. As observable, EDX analysis show a homogeneous distribution of phosphorus and nitrogen in all the samples analyzed. Moreover, the comparison of the carbon and phosphorus contents in the internal and external char layers provides insight into the organization of the intumescent structure during combustion. Based on the calculated weight percentages (Table 17), in the case of vPP+AP, the external char surface exhibits a lower C/P ratio (≈0.6) than the internal residue (≈1.8), suggesting a greater formation of phosphorus oxides at the outer surface. Conversely, for the composite with the recycled matrix, the C/P ratio remains nearly constant between the inner (≈1.1) and outer (≈1.2) regions, indicating a more uniform distribution of the phosphorus phase throughout the char thickness.

Overall, the elemental maps confirm the presence of phosphorus oxides in all cases, while the nitrogen content remains low, consistent with the release of ammonia during the decomposition reactions of APP.

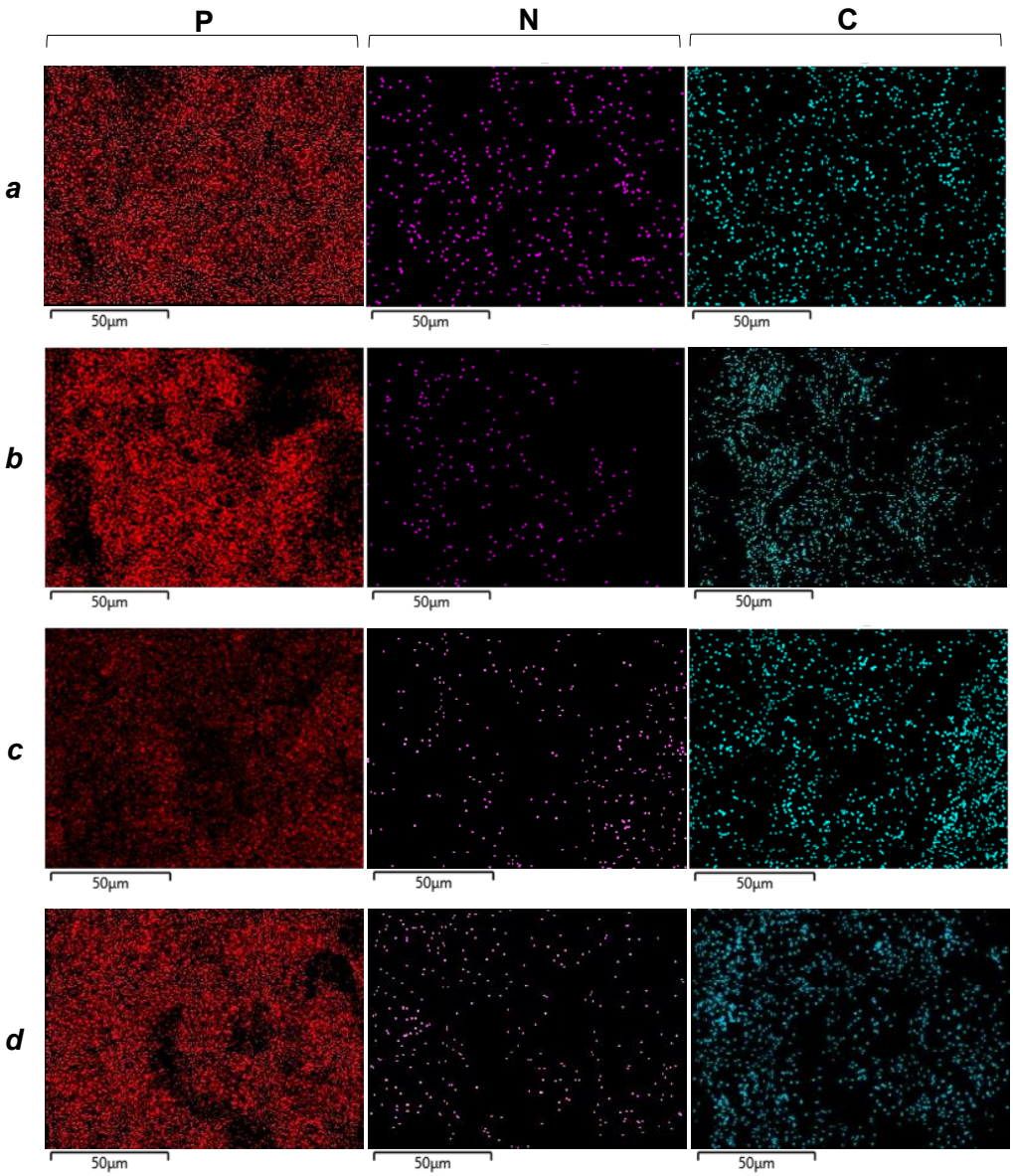

Figure 35. EDX analysis of P, N and C of the char structure: outer layer of vPP+AP (a), inner layer of vPP+AP (b), outer layer of rPP+AP (c), and inner layer of rPP+AP (d).

Table 17. Amount of P, C, N, and O in weight percentages derived from EDX analysis for outer and inner char of vPP+AP and rPP+AP.

	P [%]	**C [%]**	**N [%]**	**O [%]**
vPP+AP outer char	23.0	14.0	2.6	60.3
vPP+AP inner char	18.7	32.8	3.4	44.6
rPP+AP outer char	20.2	25.0	3.5	46.7
rPP+AP inner char	20.5	23.1	3.7	52.2

3.1.4 Conclusions

An intumescent flame-retardant system based on ammonium polyphosphate and pentaerythritol (APP:PER), incorporated at 30 wt.%, was investigated in virgin and recycled polypropylene to assess the effectiveness also in recyclates and evaluate the influence of matrix degradation on intumescent efficiency.

The reduction in viscosity of recycled PP because of thermo-mechanical degradation had a dual effect on the FR system with APP:PER. On one hand, the lower viscosity of the recycled matrix facilitated improved dispersion of the FR additive during compounding, as confirmed by the reduced size of APP:PER clusters observed in SEM micrographs of rPP+AP fracture surfaces. On the other hand, the reduced viscosity promoted increased dripping under flame exposure. This behavior strongly affected the UL-94 performance of the intumescent system. While the APP:PER formulation achieved a V-0 classification in virgin polypropylene through the rapid formation of a coherent intumescent char and the suppression of dripping, the recycled composite exhibited pronounced dripping, leading to cotton ignition and a V-2 classification.

Cone calorimeter tests showed the effectiveness of the APP:PER intumescent system in improving the fire performance of both virgin and recycled PP. In both matrices, the addition of the IFR additive leads to a significant reduction in the heat release rate. In particular, while both composites exhibit a two-peak HRR profile typical of char-forming systems, the HRR peak is delayed in the recycled PP composite, following a longer plateau phase associated with the formation of a more stable and protective char layer. These results confirm that the APP:PER system effectively impart flame retardancy properties in both virgin and recycled matrices, while also promoting enhanced char stability in recycled polypropylene.

In conclusion, the APP:PER intumescent system can be successfully applied to recycled polypropylene, although its performance is strongly influenced by recycling-induced viscosity reduction. These findings emphasize the need to consider dripping mitigation strategies when designing this kind of intumescent flame-retardant formulations for recycled polyolefin matrices.

3.3 Enhanced flame retardancy for recycled polypropylene with piperazine pyrophosphate and melamine pyrophosphate

The final intumescent flame-retardant (IFR) system evaluated for its effectiveness in recycled polypropylene (rPP) is based on a mixture of piperazine pyrophosphate (PAPP) and melamine polyphosphate (MPP). The used IFR has been proved to be very effective for the flame retardancy of PP-based materials [185,191,197–200]; however its effectiveness in recycled PP has yet to be systematically elucidated. Also in this case, rPP was obtained by melt processing eight times virgin PP (vPP) in a twin-screw extruder and was used as a suitable benchmark for a thermo-mechanically degraded polymer. Then, flame retarded vPP- and rPP-based materials were prepared by melt compounding the two polymers with 21 wt.% of IFR (vPP+PM and rPP+PM).

3.3.1 Microstructure assessment

Dynamic rheological measurements were employed to evaluate the possible structural modification of the PP chains induced by the recycling and to gain some information about the morphology of the IFR-containing materials.

In Figure 36a, the complex viscosity curves as a function of the frequency are reported. Unfilled virgin PP (vPP) exhibits the typical Newtonian plateau at low frequencies, followed by a slight shear thinning, thus a decrease of the complex viscosity as the frequency increased. As a consequence of thermo-mechanical degradation underwent during the reprocessing cycles, the complex viscosity of unfilled rPP decreases over the entire frequency range.

Concerning the rheological response of the materials containing IFRs, the addition of the additive results in an increase of the complex viscosity in the whole investigated frequency range. Furthermore, the Newtonian plateau almost disappeared for both systems, resulting in a sharp increase of viscosity at low frequencies and the appearance of a yield stress behavior. The embedded solid particles, in fact, are able to restrict the mobility of the polymer chains, thereby hampering their complete relaxation. The effects of the IFR on the mobility of polymeric chains can also be recognized in the trend of the storage modulus as a function of the frequency depicted in Figure 36b. In fact, for both filled systems, the storage modulus increases in the low frequency region, tending to become frequency independent; once again, this behavior can be related to the alteration of the macromolecular dynamics resulting from the establishment of polymer/particles and particle/particle interactions.

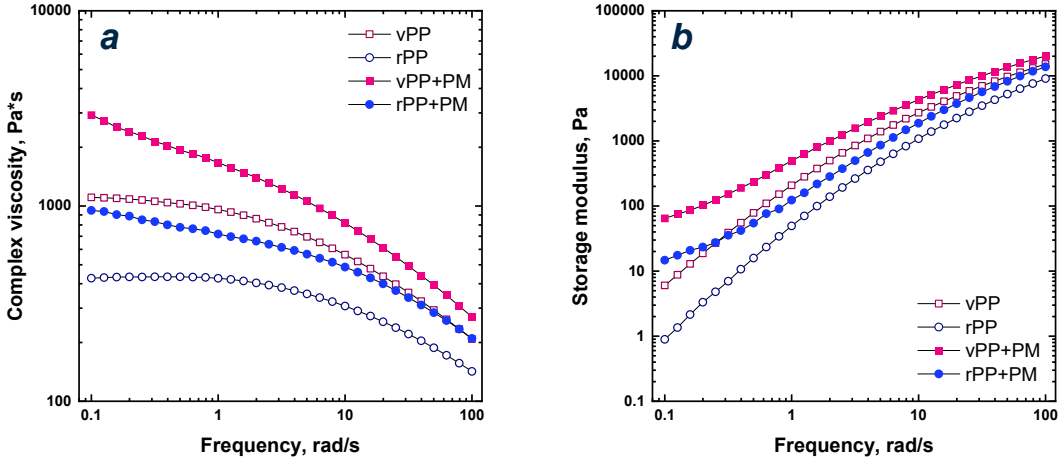

Figure 36. Complex viscosity (a) and storage modulus (b) as a function of frequency collected at 180 °C for unfilled virgin and recycled PP (vPP, rPP) and PAPP:MPP-filled PP systems (vPP+PM, rPP+PM).

The SEM micrographs of the IFR-containing materials are displayed in Figure 37 (a-b). From a general point of view, the IFR particles appear homogeneously distributed in both virgin and reprocessed polymers. In order to gain more information about the morphology of the two samples, the distribution of the particles' diameter was evaluated considering the Feret diameter, which is extensively employed to measure particles with irregular shape and micrometric dimensions [178]. Comparing Figure 37c with Figure 37d, reporting the distribution of the diameters in vPP- and rPP-based materials, respectively, different trends can be noticed. In particular, in rPP+PM the distribution of particles' diameter is shifted towards lower values and a lower average diameter is obtained: 1.85 μm and 1.34 μm for vPP+PM and rPP+PM, respectively. This result, in agreement with the literature [189,190], can be ascribed to the lower viscosity of rPP as compared to the virgin matrix, which allows a finer and more homogeneous distribution of the embedded IFR particles.

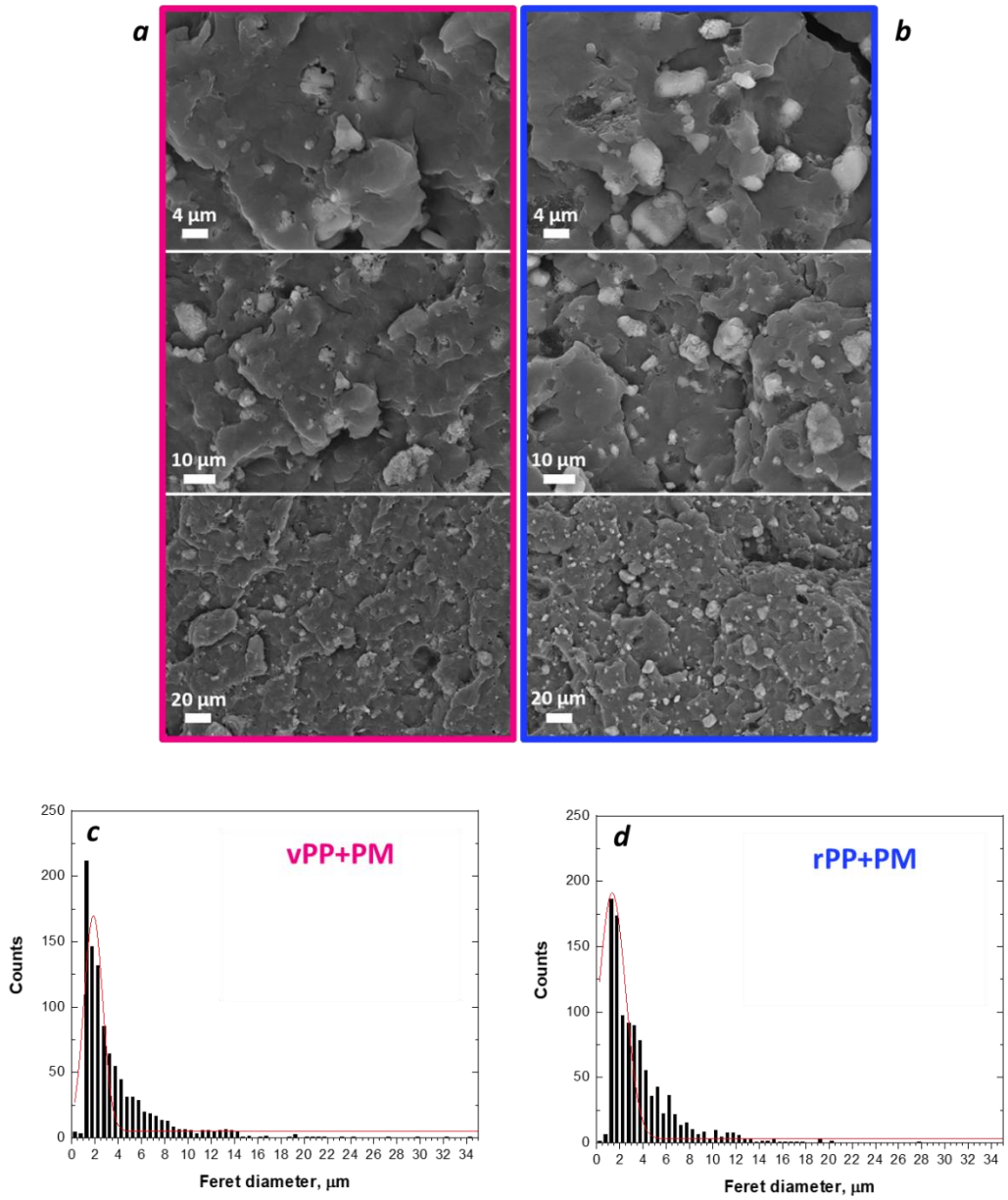

Figure 37. SEM micrographs of vPP+PM (a) and rPP+PM (b); distribution of IFR particles' Feret diameter of vPP+PM (c) and rPP+PM (d).

From FTIR spectra reported in Figure 38, no variations in the chemical structure and no appearance of signals associable with oxygen-containing groups were found when comparing virgin and recycled PP. According with the literature [51], for thermo-mechanically degraded PP the structural degradation (involving the decrease of the molecular weight) is prevailing with respect to the functional degradation, which is almost negligible. When IFR is introduced in both virgin and recycled PP, different peaks associable with the chemical structure of the mixture PAPP:MPP appear, and in particular: P-N-C at 763 cm^{-1}, P-O-P stretching at 885 cm^{-1}, P-O-P at 1072 cm^{-1}, C-N at 1086 cm^{-1}, P=O stretching at 1164 cm^{-1}, NH_{3+} at 1514 cm^{-1} and C=N at 1681 cm^{-1} [191,197,199].

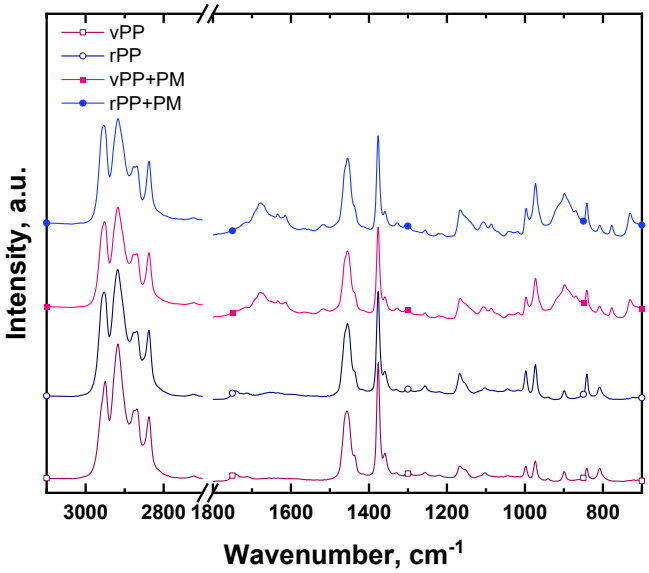

Figure 38. FTIR spectra of unfilled virgin and recycled PP (vPP, rPP) and PAPP:MPP-filled PP systems (vPP+PM, rPP+PM).

3.3.2 Thermo-oxidative degradation

The thermo-oxidative degradation of unfilled and IFR-containing virgin and recycled PP was investigated through TGA tests in air atmosphere, and the obtained results are reported in Figure 39 and Table 18. As observable from Figure 39 a-b, both unfilled virgin and recycled PP show one degradation step with no char residue at the end of the analysis. Additionally, despite recycled PP exhibits slightly early degradation onset as compared to the virgin polymer, the temperatures of maximum degradation of the two materials are practically coincident, indicating that the thermo-mechanical degradation occurred during the reprocessing cycles did not affect the PP thermo-oxidative stability. The IFR-containing materials, irrespective of the degradation level of the matrix, show the same main degradation step of unfilled PP, indicating that the introduction of IFR did not influence the main decomposition mechanism of PP, notwithstanding the occurrence of a second degradation step at higher temperatures, due to the IFR reactions [185,197–199]. Furthermore, it should be noticed that the onset temperatures are practically unaffected by the introduction of IFR, while, as expected, T_{max} is slightly lower for the flame-retardant systems.

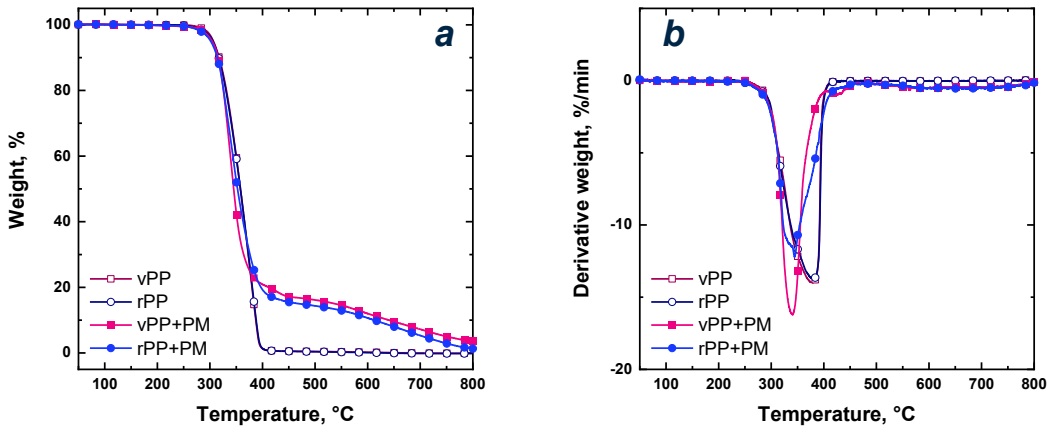

Figure 39. TGA (a) and dTG (b) curves of unfilled virgin and recycled PP (vPP, rPP) and PAPP:MPP-filled PP systems (vPP+PM, rPP+PM).

Table 18. Thermo-oxidative degradation data for unfilled virgin and recycled PP (vPP, rPP) and PAPP:MPP-filled PP systems (vPP+PM, rPP+PM).

	T_{onset} [°C]	T_{max} [°C]	Residue @600°C [%]
vPP	294	379	0.2
rPP	289	381	0.1
vPP+PM	287	340	12
rPP+PM	283	344	11

3.3.3 Flame-retardant performances

3.3.3.1 Flammability evaluation

In order to estimate the flame-retardant performances of IFR-containing materials and their flammability, limiting oxygen index (LOI) and vertical burning (UL-94) tests were carried out. The obtained results for all investigated materials are reported in Table 19. For unfilled PP, whether virgin or recycled, no rating (NR) was achieved during vertical burning tests; besides, similar LOI values were achieved for both samples. As expected, both the IFR-containing materials achieved a V-0 classification and increased values of LOI are observed as compared to unfilled PPs. During vertical burning tests, both materials stopped burning after the first ignition, and during the second application of the flame they burned for a limited time without any dripping. No significant differences were observed for FR vPP or rPP, suggesting that the used IFR system was effective in improving the fire performances also of recycled PP.

Table 19. UL-94 vertical burning and LOI results for unfilled virgin and recycled PP (vPP, rPP) and PAPP:MPP-filled PP systems (vPP+PM, rPP+PM).

	Rating	t_1 [s]	t_2 [s]	Dripping	LOI [%]
vPP	NR	5.4 ± 2.7	> 30	Yes	21
rPP	NR	4.6 ± 2.1	> 30	Yes	20.5
vPP+PM	V-0	0	3.5 ± 1.0	No	32.5
rPP+PM	V-0	0	3.9 ± 1.5	No	33.4

3.3.3.2 Combustion behavior

The results obtained from cone calorimeter tests are reported in Table 20 and Figure 40. As observable in Figure 40a from the curves of heat release rate (HRR), both virgin and recycled PP exhibit the same combustion behavior. As already mentioned, both samples are characterized by similar time to ignition (TTI), after which the HRR curves show a sharp increase followed by a fast decrease with the flame being out in about 190 s and a complete consumption of the entire sample, with a decrease of the specimen mass almost immediate (Figure 40d).

Looking at the results of the cone calorimeter tests reported in Table 20, no substantial differences are observed, suggesting that the thermo-mechanical degradation of PP, and the consequent microstructural modifications, did not affect its combustion behavior.

Due to the incorporation of IFR, for both vPP- and rPP-based samples the heat release significantly decreases. Additionally, the HRR curves display two main peaks, attributable to the typical behavior of char-forming material [191,192]. In particular, the first peak can be attributed to ignition and flame spread on the surface. After this, a plateau effect occurs due to the formation of a protective char layer. The second peak, which appears at a longer time, is associated with rupture of the char layer caused by volatile gases escaping from the degradation of the substrate.

Specifically, the charring mechanism of PAPP and MPP, as already described in the literature [199], involves the initial decomposition of P–OH groups and –NH^+_2–OP– moieties in PAPP and the consequent release of H_2O and generation of P–O–P and P–N–C structures. As the temperature increases, MPP starts to react with the remaining P–OH groups in PAPP to form melamine salts featuring branched or cross-linked architectures. Subsequently, both the previously formed P–N–C structures and the melamine salts undergo further decomposition, resulting in a dense, intumescent, and thermally stable char layer, along with the evolution of non-flammable gases and phosphorus-containing species.

As clearly observable from the results reported in Table 20 and Figure 40a, vPP+PM exhibits an 87% reduction of the peak of HRR (pkHRR) as compared to the unfilled matrix, with an expected decrease of the TTI, due to the accelerated decomposition of the polymeric matrix promoted by IFR. However, a dramatic

increase of the time from ignition to flameout as compared to vPP can be clearly observed. Furthermore, the incorporation of IFR in vPP induced a reduction of about 24% (roughly corresponding to the amount of embedded IFR) of THR (Figure 40b), and the mass loss rate (Figure 40d) for this sample was significantly reduced as compared to the unfilled matrix.

Notably, the incorporation of IFR into rPP induces a markedly different combustion behavior. Specifically, the HRR of the rPP+PM formulation decreases by approximately 90% as compared to that of neat rPP. Although ignition occurs earlier than in the unfilled polymer, the TTI remains higher than that observed for the vPP+PM sample. More importantly, while the first HRR peak appears at nearly the same time as in vPP+PM, the onset of the second peak is substantially delayed in rPP+PM (Figure 40a). This result indicates that the char layer formed after ignition in the rPP-based system remains stable up to approximately 800 s, effectively suppressing flame propagation. Additional evidence of the enhanced stability of the char formed in this sample is provided by the much slower increase in THR (Figure 40b) and the reduced mass loss rate compared to the vPP-based counterpart. In addition, regarding THR, it should be noted that a reduction of approximately 31% was achieved for rPP+PM in comparison with neat rPP. This result indicates that, in this case, approximately 10% of the polymer underwent charring during the tests, thereby preventing it from contributing to the combustion process.

Besides, as observable from the results reported in Table 20, lower values of SEA, EHC and MARHE were obtained for rPP+PM. Thus, when introducing the PAPP:MPP mixture in recycled PP, lower amount of smoke was generated (lower SEA), lower energy was released from the material when it burned owing to an improved flame inhibition (lower EHC), and the fire safety was enhanced since the fire growth potential is reduced (lower MARHE).

All the previous considerations ensure the effectiveness of such kind of intumescent flame-retardant also into recycled PP and, even more importantly, it appears that the used IFR system is able to provide enhanced effectiveness when employed in recycled PP as compared to its use in virgin polymer.

This surprising result can be explained considering two different phenomena. On one hand, the initial melt viscosity of the material can influence the evolution of melt rheology during fire exposure. In fact, melt viscosity is known to strongly affect polymer combustion behavior and flame retardancy [201]. The recycled PP-based system exhibits lower viscosity and shorter polymer chains if compared to its virgin counterpart due to chain scission reactions occurring during the mechanical recycling. Therefore, a lower initial viscosity, typically associated with reduced molecular weight and increased chain mobility, may facilitate radical recombination reactions during thermal degradation, promoting a better reactivity with the IFR system. This could promote condensed-phase stabilization and char formation, contributing to improved flame retardancy [95].

On the other hand, the results could be also explained considering the different extent of distribution of the IFR particles in virgin or recycled PP. More specifically, as assessed from the morphological characterization, IFR is better

dispersed in rPP, owing to its lower viscosity as compared to vPP, thus leading to improved fire performances. In fact, according with literature [189,196,202–204], a more uniform dispersion of the flame retardant additive, resulting in particles of smaller dimensions embedded in the polymeric matrix, promotes a faster formation of a continuous intumescent charred layer, thereby resulting in enhanced fire performances.

Table 20. Cone calorimeter tests results for unfilled virgin and recycled PP (vPP, rPP) and PAPP:MPP-filled PP systems (vPP+PM, rPP+PM)

	vPP	**rPP**	**vPP+PM**	**rPP+PM**
TTI [s]	34 ± 5	32 ± 3	13 ± 2	20 ± 1
Ignition to flameout [s]	189 ± 10	187 ± 23	933 ± 153	1738 ± 60
peak$_1$-HRR [kW/m^2]	3406 ± 194	3445 ± 151	338 ± 35	349 ± 45
t peak$_1$-HRR [s]	178 ± 9	180 ± 2	308 ± 8	246 ± 22
peak$_2$-HRR [kW/m^2]	-	-	451 ± 17	279 ± 46
t peak$_2$-HRR [s]	-	-	819 ± 126	1514 ± 161
THR [MJ/m^2]	263 ± 6	265 ± 1	200 ± 2	183 ± 10
peak$_1$-SPR [m^2/s]	0.191 ± 0.011	0.198 ± 0.028	0.023 ± 0.005	0.025 ± 0.007
t peak$_1$-SPR [s]	167 ± 6	182 ± 2	297 ± 25	232 ± 15
peak$_2$-SPR [m^2/s]	-	-	0.067 ± 0.013	0.045 ± 0.013
t peak$_2$-SPR [s]	-	-	801 ± 137	1495 ± 223
TSP [m^2]	17.1 ± 0.5	18.5 ± 1.6	19.2 ± 2.8	17.7 ± 2.8
TSR [m^2/m^2]	2108 ± 58	2276 ± 208	2352 ± 334	2188 ± 351
Char residue [wt.%]	1.2 ± 0.5	1.6 ± 0.4	11.3 ± 0.4	10.8 ± 0.8
SEA [m^2/kg]	651 ± 8	758 ± 42	604 ± 27	433 ± 53
EHC [MJ/kg]	55.1 ± 3.2	55.9 ± 1.8	48.1 ± 3.2	34.1 ± 3.0
MARHE [kW/m^2]	1264 ± 73	1255 ± 30	220 ± 32	155 ± 20
MLR [g/s]	0.140 ± 0.007	0.139 ± 0.017	0.030 ± 0.005	0.015 ± 0.001

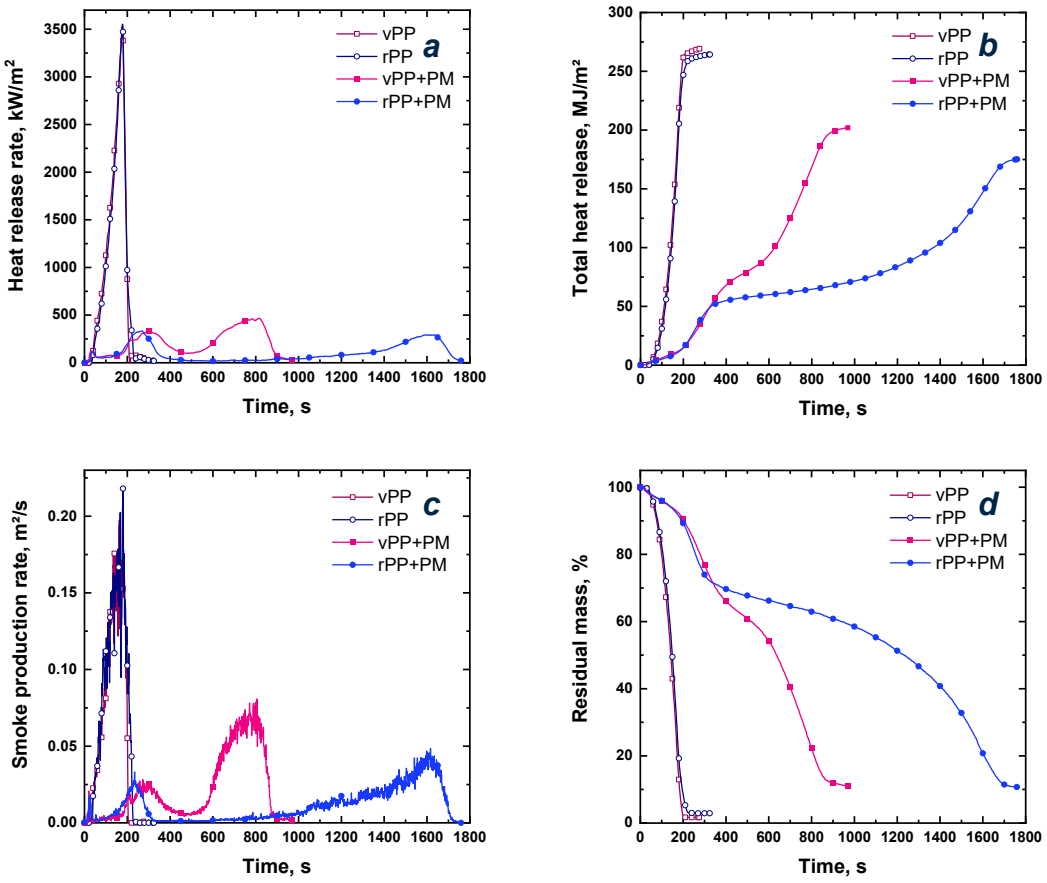

Figure 40. Cone calorimeter graphs for unfilled virgin and recycled PP (vPP, rPP) and PAPP:MPP-filled PP systems (vPP+PM, rPP+PM): heat release rate (a), total heat release (b), smoke production rate (c) and residual mass (d).

In order to assess the fire safety performances, thus the fire intensity and the fire hazard, two parameters are evaluated, namely fire performance index (FPI=TTI/pkHRR) and fire growth rate index (FIGRA=pkHRR/t_{pk}HRR). These indexes have been calculated for both unfilled and FR/PPs and the obtained values are reported in Table 21. As expected, neat virgin and recycled PP showed very low values of FPI and very high values of FIGRA. With the introduction of IFR, both vPP+PM and rPP+PM exhibited an increase in the FPI and a decrease in FIGRA, revealing the achievement of increased fire safety performances as compared to the unfilled matrices.

The Flame Retardancy Index (FRI) is also reported in Table 21. FRI is a dimensionless index which quantify the flame retardancy ability of polymeric systems, taking the neat polymer as a reference sample [186]. An FRI value between 10^0 and 10^1 represents good flame retardancy performances and, as shown in Table 21, the FRI values of both IFR-containing materials lie in that range. However, the FRI of rPP+PM was higher than that of vPP+PM suggesting, once again, better flame retardancy performances for the rPP-based system.

Table 21. FPI, FIGRA and FRI values of unfilled virgin and recycled PP (vPP, rPP) and PAPP:MPP-filled PP systems (vPP+PM, rPP+PM).

	FPI [m^2*s/kW]	FIGRA [kW/m^2/s]	FRI
vPP	0.010 ± 0.003	19.2 ± 2.0	-
vPP+PM	0.040 ± 0.005	1.10 ± 0.13	5.1
rPP	0.009 ± 0.001	19.2 ± 1.1	-
rPP+PM	0.058 ± 0.009	1.43 ± 0.28	8.9

3.3.3.2 Char analysis

The char layer collected at the end of the cone calorimeter tests was also characterized. It should be pointed out that, due to the different time of flame-out of the IFR-containing materials, the condensed phase analyses have been carried out after about 900 s in the case of vPP+PM and after about 1700 s for rPP+PM. The evolution of the char during the tests was comparable for the two samples; however, the longer time elapsed from the ignition to the flame-out for recycled PP-based materials affected the final morphology of the char residues.

The pictures of the residual char of virgin and recycled PP-based materials are shown in Figure 41. It can be clearly observed that vPP+PM formed a relatively high intumescent char layer with few holes on the outer surface. On the other hand, the height of the residue collected for rPP+PM was about half that than of its virgin PP-based counterpart. In both samples the presence of holes could be ascribed to the decomposition reaction of MPP that, producing inert gases, causes the breakage of the char layer [205]. The differences in the height of the char residues can be attributed to the remarkably different time interval in which the combustion takes place for the two samples (about 13 minutes longer for rPP+PM). However, as demonstrated in the literature [98], the noticed difference in the char height should not affect the fire performances. The evaluation of the char morphology through SEM characterization (see micrographs reported in Figure 41e-f) highlights that for vPP-IFR the outer layer has a dense structure with few holes, while the inner layer is characterized by a porous structure with some micro-sized channels. On the other hand, these differences between the outer and the inner surface were not observed for rPP+PM. In particular, in this last case, a less dense structure for the outer layer and a more closed and compact structure for the inner one can be recognized.

The more compact structure of the char in rPP+PM can be invoked to explain the reduced fire growth during the cone calorimeter test noticed for this sample. In fact, the compact char can hinder the diffusion of heat and volatiles in a more efficiently way as compared to the porous structure of vPP+PM, which instead provide a more rapid mass (oxygen and pyrolysis products) and heat transport.

The observed different morphology of the char can be correlated with the distribution and the dimension of the IFR particles: in fact, as already mentioned

by other authors, a more compact and dense structure of char usually results from materials containing low viscosity polymers and better distributed smaller FR particles [189,196].

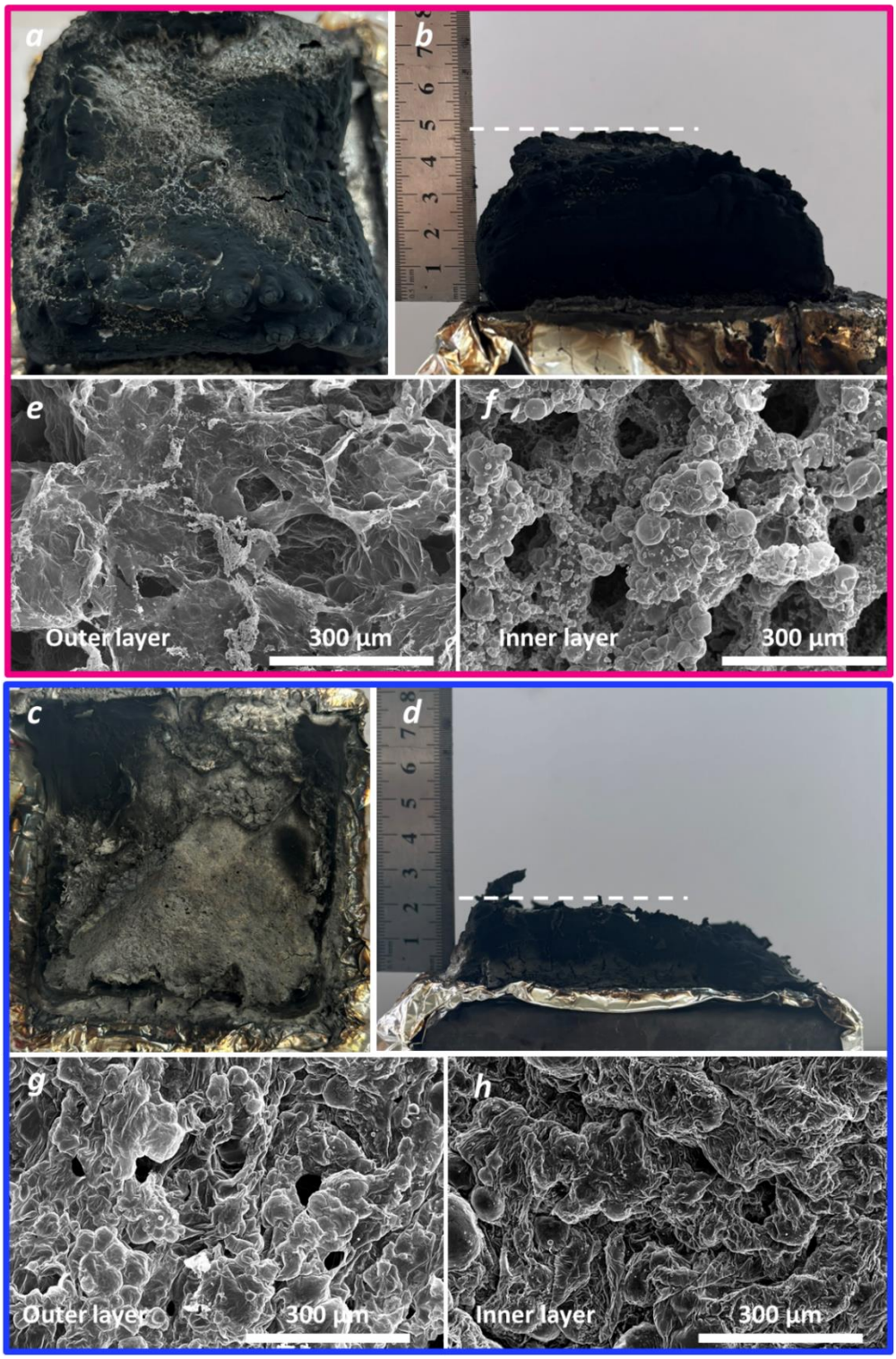

Figure 41. Photos and SEM images of residual char: (a,b,e,f) vPP+PM; (c,d,g,h) rPP+PM.

The elemental maps obtained through EDX analysis of phosphorus, nitrogen and carbon of the internal and external char of vPP+PM and rPP+PM are shown in Figure 42 and the amount of each element in weight percentage is reported in Table 22. A homogeneous distribution of phosphorus and nitrogen can be observed in both samples. Moreover, the ratio between the carbon and phosphorus content was calculated, based on the values reported in Table 22. The outer char layer exhibits comparable value among vPP+PM (≈2.1) and rPP+PM (≈2.0), while the internal char layer of rPP+PM displays slightly higher value (≈1.3) if compared to vPP+PM (≈0.7).

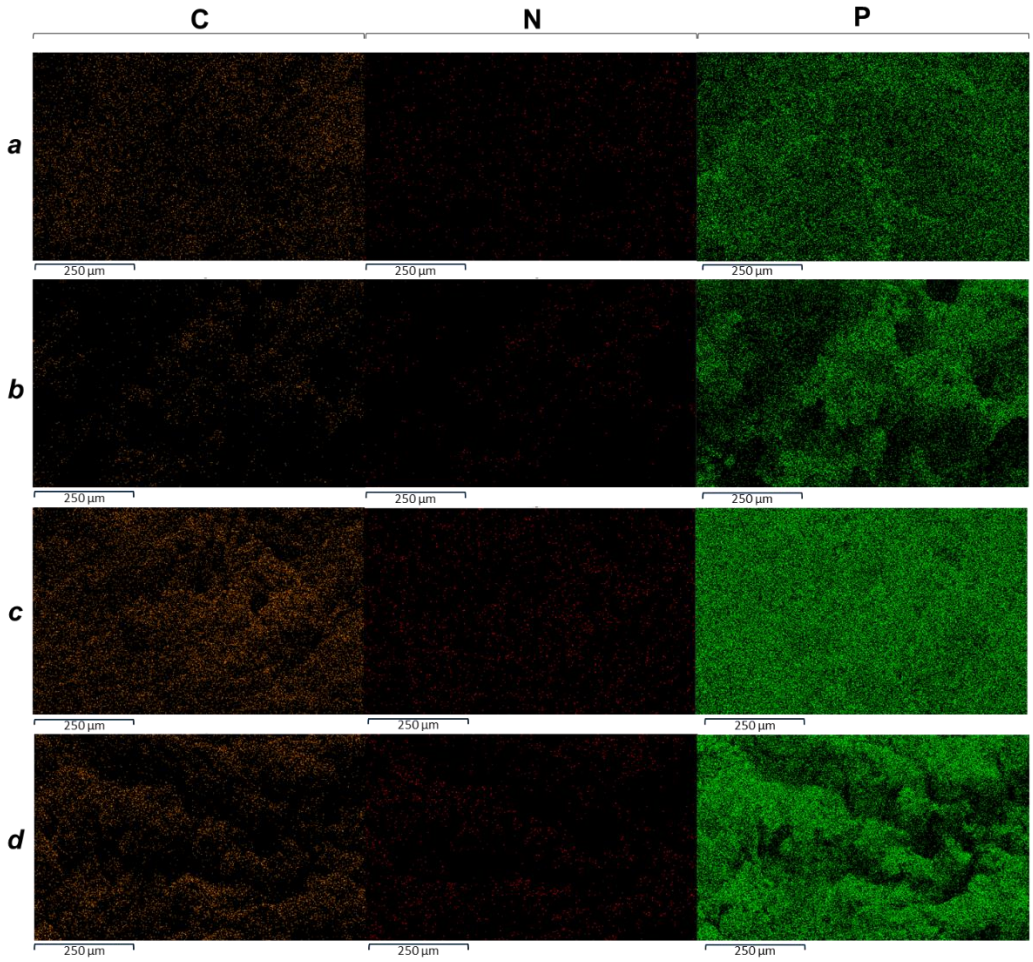

Figure 42. EDX analysis of C, N and P of the char structure: outer layer of vPP+PM (a), inner layer of vPP+PM (b), outer layer of rPP+PM (c), and inner layer of rPP+PM (d).

Table 22. Amount of P, C, N, and O in weight percentages derived from EDX analysis for outer and inner char of vPP+PM and rPP+PM.

	P [%]	C [%]	N [%]	O [%]
vPP+PM outer char	16.3	34.9	4.8	44.0
vPP+PM inner char	31.9	21.9	3.5	42.7
rPP+PM outer char	20.6	41.6	4.0	33.8
rPP+PM inner char	23.8	30.9	4.3	41.0

Finally, the graphitized structure of the residual char was analyzed by Raman spectroscopy. In particular, the degree of graphitization was quantitatively determined by calculating the ratio between the peak areas of the defect and graphite bands (I_D/I_G), located in the range 1350-1380 cm^{-1} and 1580-1600 cm^{-1}, respectively. In general, a high degree of graphitization of the residues (i.e., lower values of the ratio I_D/I_G) is associated with better fire performances [187,205,206]. A lower I_D/I_G (namely, 0.7) was obtained for rPP+PM when compared to vPP+PM (I_D/I_G = 1.2), confirming that the char layer formed in the materials based on recycled PP was denser, and more able to inhibit the heat emission and the release of gases. Therefore, the results indicated that the intumescent carbon layer of rPP+PM exhibited an enhanced degree of graphitization, which contributed to increased structural strength of the char. Such enhancement of the char strength significantly improved its barrier functionality, effectively attenuating the transmission of heat from the combustion zone to the underlying polymer matrix.

3.3.4 Mechanical properties

Lastly, in order to assess the actual structural usability of flame-retardant materials, the mechanical behavior of the samples was characterized through bending, tensile, and impact tests. In fact, it is well known that the introduction of FR additives usually induces a worsening of the mechanical properties of the material, particularly affecting its deformability [105,189,207,208]. Additionally, this issue is even more important for recycled polymers, considering that the degradation underwent from the material during the reprocessing usually results in a severe worsening of the mechanical performance as compared to its virgin counterpart [114].

As reported in Figure 43, vPP+PM and rPP+PM show practically comparable values of tensile strength and flexural strength. Conversely, the impact strength and the elongation at break decreases when rPP is used as matrix, likely due to the typical embrittlement showed by recycled polymers [40]. Nonetheless, the results indicate that, despite the presence of the IFR and the use of a recycled polymer, the rPP+PM system exhibits adequate mechanical properties for a broad spectrum of potential applications.

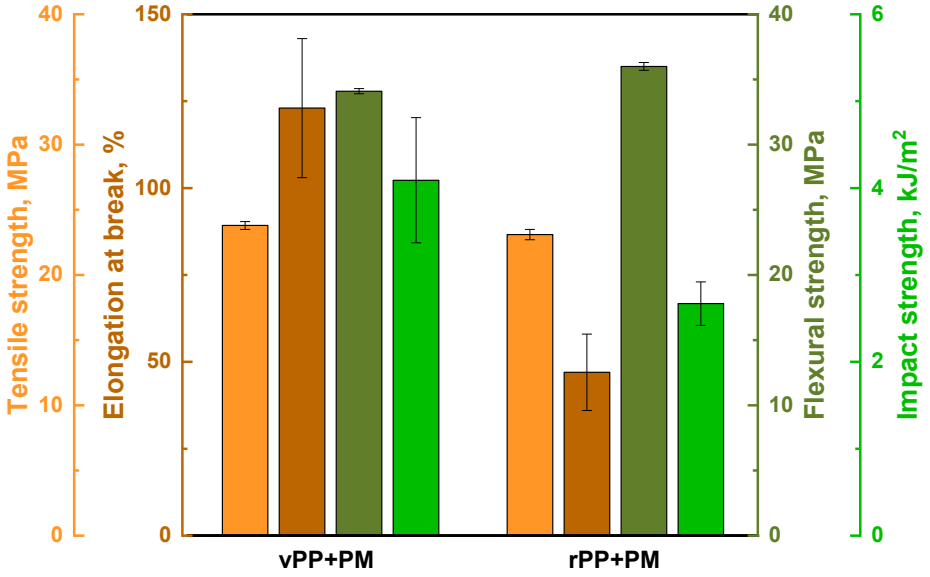

Figure 43. Mechanical properties of PAPP:MPP-filled virgin and recycled PP systems (vPP+PM, rPP+PM).

3.3.5 Conclusions

The effectiveness of an intumescent flame-retardant system based on piperazine pyrophosphate (PAPP) and melamine pyrophosphate (MPP) for recycled PP-based materials was evaluated and compared with that of its virgin PP-based counterpart. Both materials were melt-compounded with 21 wt.% of a PAPP/MPP mixture (2:1) and characterized for rheological, morphological, mechanical, and fire-performance properties. Owing to the lower viscosity of the recycled polymer, rPP+PM sample showed a more finely and uniformly dispersion of the IFR particles, which contributed to the improved combustion behavior observed in cone calorimeter tests. Despite the comparable decrease in heat release rate observed for vPP+PM and rPP+PM, the system based on rPP demonstrated a higher time to ignition and especially a more stable char layer, which resulted in a substantial delay in the occurrence of the second HRR peak. Lower SEA, EHC, and MARHE values further indicated enhanced fire safety for rPP+PM. Furthermore, both systems achieved a V-0 rating in UL-94 and comparable LOI values.

Additionally, the evaluation of the mechanical behavior of the samples demonstrated that the utilization of rPP as matrix did not compromise the tensile and the flexural strength of the material, despite a slight decrease in ductility and impact strength.

Overall, this study demonstrates that recycled PP can effectively support intumescent flame-retardant systems, thereby enabling high-performance, flame-retarded materials while promoting circular-economy strategies and reducing reliance on virgin PP.

3.4 Reprocessing of flame-retardant polypropylene

By simulating the thermo-mechanical conditions encountered in industrial mechanical recycling, this last chapter provides a comprehensive assessment of the rheological, morphological, combustion and mechanical properties of the flame-retardant reprocessed material. The results aim to clarify whether the intumescent FR system considered in Chapter 3.3, composed of piperazine pyrophosphate (PPAP) and melamine pyrophosphate (MPP), can withstand repeated processing steps without compromising fire performance or mechanical integrity, thereby supporting the development of recycling-compatible FR formulations suitable for circular plastic streams.

Virgin PP (vPP) was melt compounded with 21 wt.% of PAPP:MPP in a ratio equal to 2:1 (vPP+IFR) and five subsequent extrusions have been conducted in order to simulate the conditions to which the plastics are subjected during a typical mechanical recycling process. Therefore vPP+IFR has been melt compounded, collected, characterized and then reprocessed again, aiming at evaluate the variations in the properties when this kind of material reaches its end-of-life and need to be recycled. The so obtained materials have been named denoting the number of reprocessing cycle (Table 23).

Table 23. Sample coding for IFR-containing virgin and reprocessed PP-based systems.

	Processing step	**Number of reprocessing cycles**
vPP+IFR	Melt compounding	0
r(PP+IFR) n1	1st recycling	1
r(PP+IFR) n2	2nd recycling	2
r(PP+IFR) n3	3rd recycling	3
r(PP+IFR) n4	4th recycling	4
r(PP+IFR) n5	5th recycling	5

3.4.1 Thermal stability upon reprocessing

TGA tests were employed to study the thermo-oxidative stability upon the introduction of IFR filler and reprocessing. The corresponding results are reported in Figure 44 and Table 24. Virgin unfilled PP started to decompose at about 294 °C with a single degradation peak at about 379 °C and zero residue at the end of the test. With the introduction of the IFR, the main thermal degradation mechanism of PP did not change. In fact, vPP+IFR started to decompose at

approximately 287 °C exhibiting a one-step degradation with a final residue of roughly 12 % at 600 °C, due to the charring ability of the mixture PAPP:MPP.

After analyzing the thermo-oxidative mechanism of the virgin PP/IFR system, evaluating its stability during reprocessing is crucial to determine whether mechanical recycling may lead to flame-retardant deterioration, and consequently, to assess whether this approach for recycling is suitable for this type of system. First of all, the stability of IFR filler was verified by performing a TGA analysis under isothermal conditions. More specifically, IFR powders were heated to 180 °C at 10 °C/min and then kept at this temperature for 10 minutes. As depicted in Figure 45, IFR filler lost less than 1.2 % of its initial weight after 10 minutes. Therefore, IFR could be considered thermally stable during the 5 reprocessing steps, each lasting approximately 1 minute and carried out at a maximum temperature of 180 °C.

Concerning the reprocessed materials, they showed one-step thermal decomposition, exhibiting the same behavior as their virgin counterpart. In fact, all the TGA curves of the reprocessed samples overlapped. If compared to vPP+IFR, the one-time reprocessed composite r(PP+IFR) n1 displayed a slight decrease of the onset temperature, a small increase in the temperature of maximum degradation and a lower residue at 600 °C. Notwithstanding very negligible differences in the onset degradation temperature, the temperature of the maximum degradation rate and the char residue at 600 °C remained unchanged moving from the first reprocessing step to the fifth. Therefore, the mechanical recycling did not affect the thermo-oxidative stability of PP/IFR systems, nor the charring ability of the IFR fillers at least up to 5 reprocessing cycles.

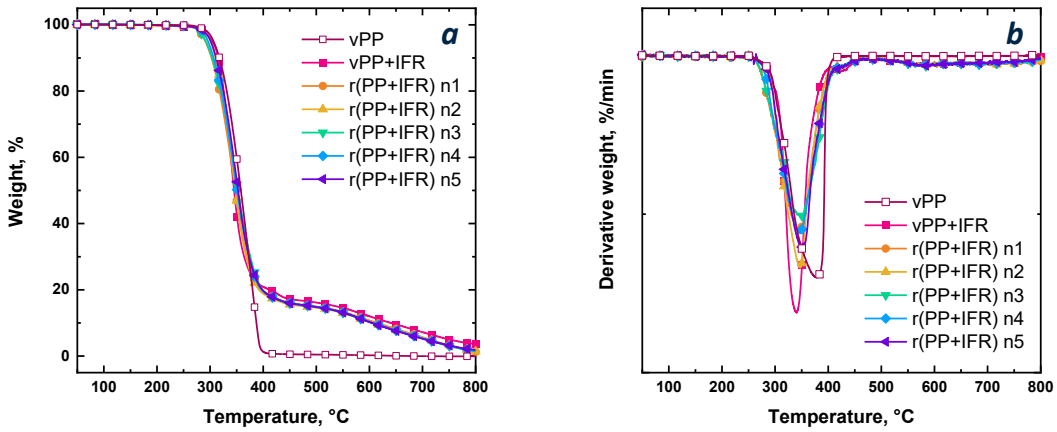

Figure 44. TGA (a) and dTG (b) curves of unfilled and IFR-containing virgin and reprocessed PP-based systems.

Table 24. Thermo-oxidative degradation data for unfilled and IFR-containing virgin and reprocessed PP-based systems.

	T_{onset} [°C]	T_{max} [°C]	Residue @600°C [%]
vPP	294	379	0.2
vPP+IFR	287	340	12.0
r(PP+IFR) n1	280	347	10.7
r(PP+IFR) n2	287	347	10.3
r(PP+IFR) n3	280	348	10.3
r(PP+IFR) n4	286	347	10.3
r(PP+IFR) n5	288	351	10.3

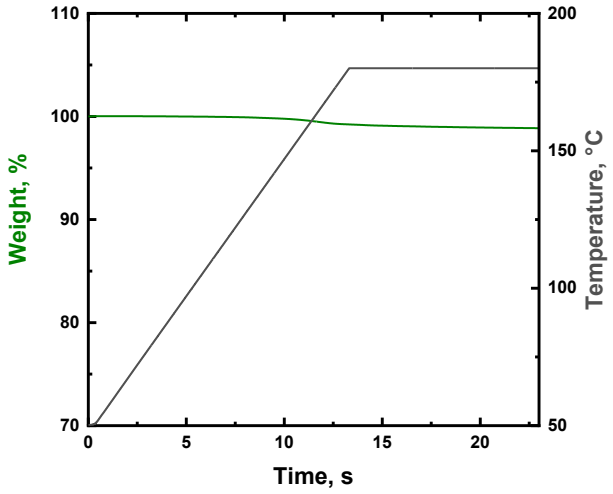

Figure 45. Isothermal TGA at 180°C of IFR (PAPP:MPP).

3.4.2 Effect of reprocessing on PP/IFR microstructure

Assessing the evolution of the rheological behavior of a polymeric system when subjected to reprocessing and several consecutive extrusions is of paramount importance when dealing with mechanical recycling process. In fact, variations in the processability of recycled materials can pose some problems in the further reprocessing since some adjustments in the processing parameters could be required. The complex viscosity curves of unfilled vPP, vPP+IFR and the five reprocessed samples are reported in Figure 46. Virgin unfilled PP showed the typical Newtonian plateau at low and intermediate frequencies followed by a mild shear thinning as the frequencies increased. The incorporation of IFR within vPP resulted in increased complex viscosity over all the investigated frequency

range. More specifically, the Newtonian plateau was no longer fully visible, and a yield stress behavior appeared at low frequencies. Both these features can be ascribed to the embedded solid fillers able to hamper the mobility of the macromolecules, causing a retardation of the chain relaxation [188].

Regarding the rheological behavior of reprocessed PP/IFR systems, all the curves almost overlapped at intermediate and high frequencies, irrespective of the number of reprocessing cycles. As already reported by other authors [209,210], the reprocessing, thus the mechanical recycling, had a less marked influence on the rheological behavior of polymeric composites than on unfilled polymers.

Furthermore, it should be pointed out that no adjustments of the processing parameters were required during the extrusions, meaning that the processability was not affected by the consecutive extrusions and all materials, starting from the virgin PP-based systems to its counterpart reprocessed five times, could be melt-compounded under the same identical conditions.

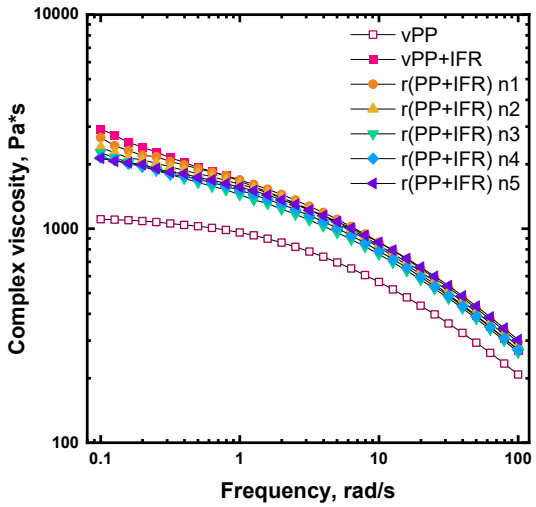

Figure 46. Complex viscosity curves as a function of the frequency collected at 180 °C of unfilled and IFR-containing virgin and reprocessed PP-based systems.

In order to evaluate the extent of dispersion and distribution of IFR within the host matrix, SEM characterization was performed, and some representative micrographs are reported in Figure 47. Additionally, the distribution of the Feret diameter was evaluated for each flame-retarded system and the obtained results are depicted in Figure 48. It is clearly observable that the reprocessing caused significant variations in particle size and dispersion. Moving from vPP+IFR (Figure 47a) to the sample reprocessed up to 2 times (Figure 47b and 47c), no significant differences could be detected in the distribution of the diameter of the particles, notwithstanding a small decrease in the mean size, suggesting that the first two reprocessing cycles slightly affected the dispersion of IFR. A decrease in the particles size has been already observed for the reprocessing of PP-talc composite [211]. Conversely, increasing the number of reprocessing steps from 3 to 5 (Figure 47d-47f) resulted in a progressive variation of the distribution of the

particles' diameter: in particular, the distribution shifted towards higher values and the number of bigger particles was continuously increasing. The mean size of the particles in the samples reprocessed 3, 4 and 5 times was higher if compared to previous extrusion cycles, suggesting that the further reprocessing had a negative impact on the dispersion of IFR fillers and led to some re-agglomeration phenomena of the particles. Also the formation of agglomerates has been already reported in the literature for reprocessed PP-talc composite [212].

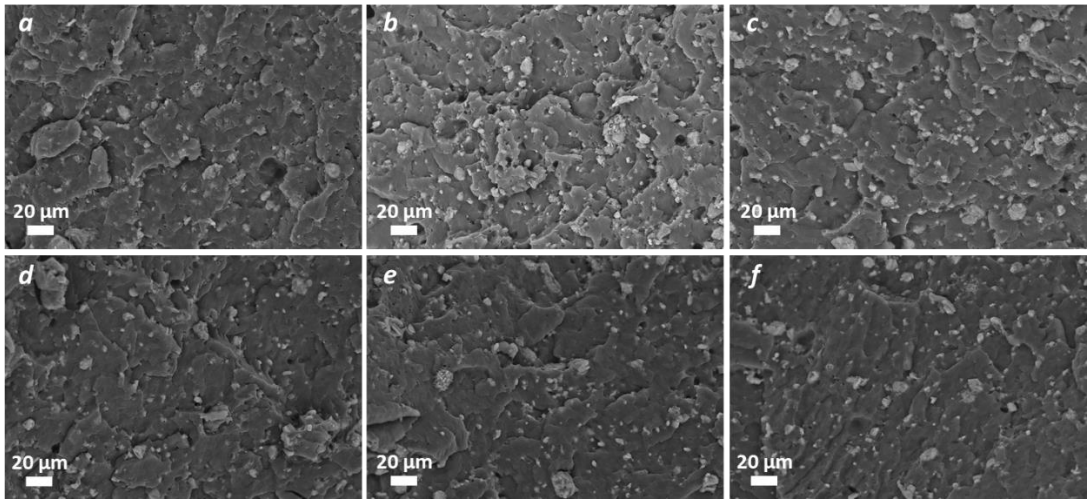

Figure 47. SEM micrographs of vPP+IFR (a) and reprocessed samples: n1 (b), n2 (c), n3 (d), n4 (e) and n5 (f).

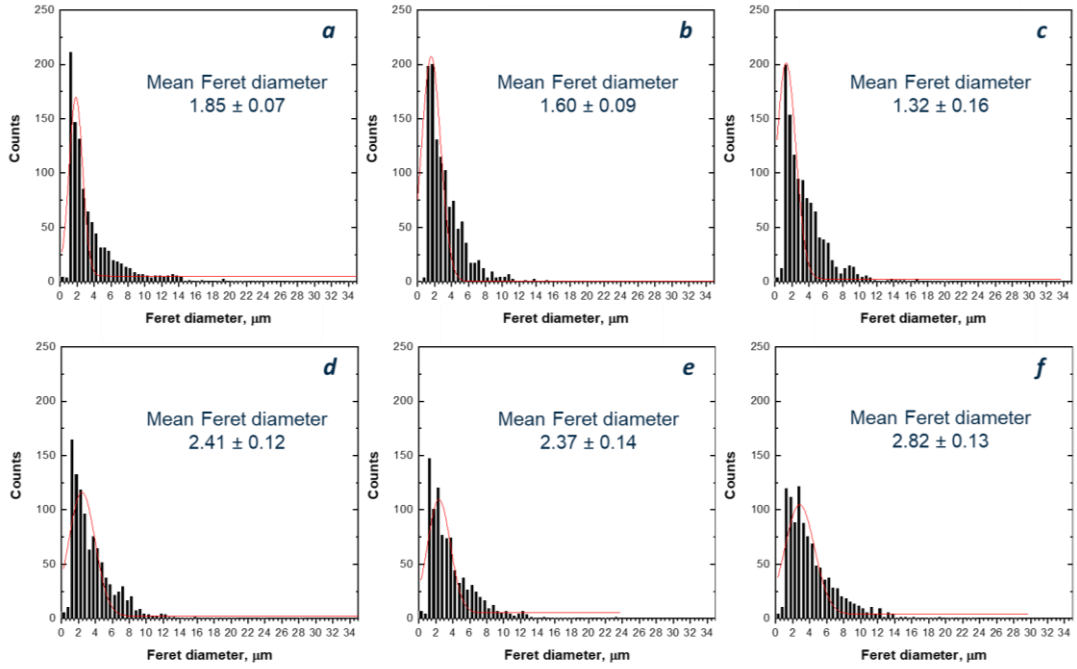

Figure 48. Distribution of IFR particles' Feret diameter and mean values for vPP+IFR (a) and reprocessed samples: n1 (b), n2 (c), n3 (d), n4 (e) and n5 (f).

3.4.3 Effects of reprocessing on flame retardancy

The flammability of the IFR-containing systems was evaluated through UL-94 vertical burning and LOI tests and the corresponding results for virgin and reprocessed PP/IFR materials are reported in Table 25. For virgin unfilled PP no-rating could be achieved in the UL-94 test because of dripping phenomena and burning time higher than 30 seconds. Upon the introduction of IFR, the so-obtained material was able to achieve a V-0 classification: the samples stopped burning both after the first and the second flame application without any drops able to ignite the cotton. As expected, also LOI value increased when IFR was introduced in vPP.

Interestingly all the other investigated materials, irrespective of the reprocessing cycle, displayed a V-0 classification. Despite a slight increase of the burning time after the second flame application, each reprocessed sample was able to stop burning and to avoid dripping. On the other hand, LOI values remained basically unchanged passing from the virgin FR system to the five-time reprocessed material. Therefore, the reprocessing did not affect the flammability of the system. The intumescent flame-retardant used in this study did not lose its protective properties and its ability to create a char capable of extinguishing the flame, unlike other studies in which the UL-94 classification of the materials changed from V-0 to no rating after the second reprocessing cycle [106,109] or LOI values decreased [106,109,110].

Table 25. UL-94 vertical burning and LOI results for unfilled and IFR-containing virgin and reprocessed PP-based systems.

	Rating	**t1 [s]**	**t2 [s]**	**Dripping**	**LOI [%]**
vPP	NR	5.4 ± 2.7	> 30	Yes	21
vPP+IFR	V-0	0	3.5 ± 1.0	No	32.5
r(PP+IFR) n1	V-0	0	5.1 ± 1.6	No	33.4
r(PP+IFR) n2	V-0	0	4.6 ± 1.4	No	33.2
r(PP+IFR) n3	V-0	0	5.0 ± 2.1	No	33.8
r(PP+IFR) n4	V-0	0	5.2 ± 2.4	No	32.8
r(PP+IFR) n5	V-0	0	7.4 ± 2.2	No	32.5

Regarding the combustion behavior, the results obtained from cone calorimeter tests are reported in Table 26 and Figure 49. Without incorporating any flame-retardant, virgin PP ignited after about 34 seconds and burned very quickly, reaching almost immediately the heat release rate (HRR) peak and then, after consuming completely the sample, stopped burning in about 190 seconds.

As already mentioned, the introduction of the mixture PAPP:MPP into virgin PP led to the development of an intumescent structure under cone calorimeter

conditions. In fact, the typical HRR curve of char-forming material with two main peaks can be recognized [109,192]. The charring mechanism of PAPP and MPP has been already explained in the previous chapter.

Besides the charring ability of IFR into vPP, the heat release rate decreased of about 87 % for the FR system whereas the time to ignition (TTI) was anticipated, because the addition of IFR caused early degradation phenomena of the polymeric matrix [205]. Concerning the total heat release (THR), the presence of IFR resulted in a slow increase over time and the maximum THR value decreased of about 24 % if compared to unfilled virgin PP.

As expected, the addition of the mixture PAPP:MPP into virgin PP resulted in enhanced fire retardancy, but then the effects that mechanical recycling has on the flame retardancy of the reprocessed materials need to be discussed. What immediately emerged from the cone calorimeter graphs shown in Figure 49 was that the variations caused by reprocessing are truly minimal. In fact, irrespective of the reprocessing cycle, all the HRR curves displayed the same two main peaks as virgin PP-based composite, indicating that all the reprocessed samples are able to form the intumescent protective layer approximately at the same time of vPP+IFR after the ignition without any significant changes in the peak values of HRR. Then, just like their virgin counterpart, for all the reprocessed samples the second peak was ascribed to the degradation and breaking of the char layer, also in this case without any shift in the time at which the phenomena occurs and very few differences in the values of HRR peaks. There were also no significant variations in the final residual weight of the char obtained from combustion and in the time between ignition and flameout. Each cone calorimeter test performed on FR virgin and reprocessed materials proceeded in the same manner. In fact, even the weight loss of the sample proceeded in stages, and the mass loss rate (MLR) was comparable regardless of the reprocessing cycle. The time to ignition (TTI) was slightly increased as the number of recycling cycle increased, without, however, reaching the value of virgin unfilled PP.

Finally, SEA, EHC and MARHE determined on the basis of the cone calorimeter tests are also reported in Table 26. Since SEA remained unchanged during the reprocessing if compared to vPP+IFR, there was no increase in smoke production for the reprocessed samples, therefore the safety related to the smoke release was not compromised. No variations of the inhibition effects in gas phase combustion process were observed, indeed EHC values remained constant between virgin PP-based material and the five-time reprocessed sample. In conclusion, also MARHE values remained unchanged as reprocessing occurred, meaning that the recycling did not affect the fire safety and the fire growth.

From the fire retardancy point of view, the composite based on virgin PP filled with 21 wt.% of the mixture PAPP:MPP could be mechanically recycled up to five times not losing the ability to be a safe material in a fire-risk scenario.

Table 26. Cone calorimeter tests results of unfilled and IFR-containing virgin and reprocessed PP-based systems.

	vPP	vPP +IFR	n1	n2	n3	n4	n5
TTI [s]	34 ± 5	13 ± 2	14 ± 3	16 ± 3	19 ± 1	21 ± 5	18 ± 7
Ignition to flameout [s]	189 ± 10	933 ± 153	958 ± 63	847 ± 97	1111 ± 166	989 ± 125	939 ± 39
peak$_1$-HRR [kW/m^2]	3406 ± 194	338 ± 35	428 ± 60	346 ± 56	344 ± 64	338 ± 37	372 ± 28
t peak$_1$-HRR [s]	178 ± 9	308 ± 8	267 ± 22	303 ± 25	259 ± 15	261 ± 28	284 ± 17
peak$_2$-HRR [kW/m^2]	-	451 ± 17	431 ± 113	526 ± 71	315 ± 11	404 ± 60	450 ± 1
t peak$_2$-HRR [s]	-	819 ± 126	654 ± 63	697 ± 128	618 ± 73	843 ± 127	630 ± 31
THR [MJ/m^2]	263 ± 6	200 ± 2	206 ± 10	203 ± 13	204 ± 10	194 ± 13	197 ± 12
peak$_1$-SPR [m^2/s]	0.191 ± 0.011	0.023 ± 0.005	0.034 ± 0.07	0.026 ± 0.003	0.028 ± 0.001	0.028 ± 0.010	0.033 ± 0.014
t peak$_1$-SPR [s]	167 ± 6	297 ± 25	228 ± 34	267 ± 24	266 ± 23	261 ± 38	260 ± 45
peak$_2$-SPR [m^2/s]	-	0.067 ± 0.013	0.069 ± 0.025	0.079 ± 0.015	0.050 ± 0.004	0.058 ± 0.010	0.077 ± 0.001
t peak$_2$-SPR [s]	-	801 ± 137	662 ± 48	688 ± 109	599 ± 63	824 ± 117	619 ± 38
TSP [m^2]	17.1 ± 0.5	19.2 ± 2.8	18.9 ± 1.7	18.8 ± 3.6	18.7 ± 1.6	18.0 ± 0.5	19.1 ± 0.6
TSR [m^2/m^2]	2108 ± 58	2352 ± 334	2338 ± 210	2315 ± 341	2296 ± 190	2218 ± 63	2349 ± 57
Char residue [wt.%]	1.2 ± 0.5	11.3 ± 0.4	9.9 ± 1.3	13.3 ± 3.5	11.1 ± 1.8	8.1 ± 0.7	9.7 ± 0.8
SEA [m^2/kg]	651 ± 8	604 ± 27	554 ± 74	607 ± 92	620 ± 14	548 ± 36	577 ± 86
EHC [MJ/kg]	55.1 ± 3.2	48.1 ± 3.2	44.5 ± 5.8	45.4 ± 4.1	44.9 ± 5.8	48.1 ± 1.8	49.3 ± 0.7
MARHE [kW/m^2]	1264 ± 73	220 ± 32	252 ± 27	242 ± 13	203 ± 26	201 ± 23	232 ± 10
MLR [g/s]	0.140 ± 0.007	0.030 ± 0.005	0.029 ± 0.002	0.032 ± 0.002	0.025 ± 0.004	0.030 ± 0.007	0.030 ± 0.001

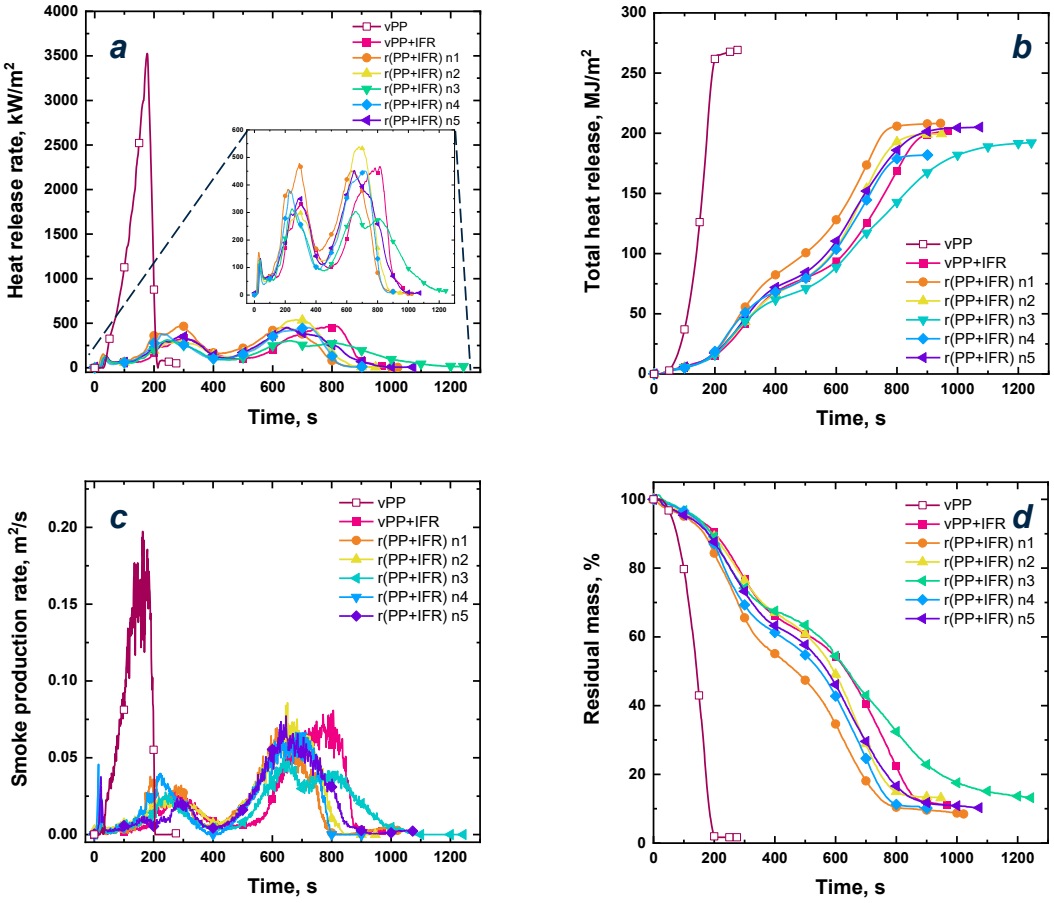

Figure 49. Cone calorimeter graphs for unfilled and IFR-containing virgin and reprocessed PP-based systems: heat release rate (a), total heat release (b), smoke production rate (c) and residual mass (d).

In order to conclude the considerations about the combustion behavior after reprocessing and to effectively consider safe in fire-risk scenario such materials even after mechanical recycling, the three main parameters describing the fire intensity, the fire hazard and the fire retardancy ability are reported in Table 27. More specifically, the fire performance index (FPI=TTI/pkHRR), the fire growth rate index (FIGRA=pkHRR/t_{pk}HRR) and the flame retardancy index (FRI) [186] have been calculated. Usually polymer-based systems exhibiting a high FPI and a low FIGRA implies great fire safety [185]. In fact, virgin PP without any flame-retardant fillers displayed very high values of FIGRA and low values of FPI. As expected, the introduction of IFR resulted in increased FPI and decreased FIGRA. Despite very small variations, none of the five reprocessing cycles changed these values. Therefore, the mechanical recycling did not worsen the fire intensity or the fire hazard, indeed neither FPI or FIGRA reached the original value of unfilled PP. Regarding FRI, which is a dimensionless index able to quantify the flame retardancy ability of the FR system, all the values from the virgin PP-based composite to the material reprocessed five times lied in a range between 10^0 and 10^1. This was a very interesting result since the values remaining in this range meant good flame retardancy performances [186].

The studied PP/IFR could be then considered safe after five reprocessing steps, thus after five rounds of mechanical recycling, also from the point of view of fire intensity and hazard.

Table 27. FPI, FIGRA and FRI values of unfilled and IFR-containing virgin and reprocessed PP-based systems.

	FPI [m^2*s/kW]	**FIGRA [kW/m^2/s]**	**FRI**
vPP	0.010 ± 0.003	19.2 ± 2.0	-
vPP+IFR	0.040 ± 0.005	1.10 ± 0.13	5.1
r(PP+IFR) n1	0.033 ± 0.012	1.60 ± 0.13	4.0
r(PP+IFR) n2	0.045 ± 0.003	1.15 ± 0.25	5.8
r(PP+IFR) n3	0.056 ± 0.011	1.32 ± 0.16	6.9
r(PP+IFR) n4	0.062 ± 0.020	1.32 ± 0.29	8.2
r(PP+IFR) n5	0.048 ± 0.028	1.31 ± 0.18	6.2

The protective char layer formed after the combustion of the tested FR systems was also characterized in order to evaluate the charring ability and its morphology during reprocessing.

From the digital pictures of the char residue at the end of the cone calorimeter tests shown in Figure 50, the charring ability of the mixture PAPP:MPP into PP could be clearly observable. The external surface of the char of vPP+IFR (Figure 50a) was very compact with few holes, associable to the gases formed after decomposition reactions of MPP [205], and the final height of char reached almost 5 cm. As the number of reprocessing increased (from Figure 50b representing the sample reprocessed one time to Figure 50f related to the sample reprocessed five times), there was an increased amount of holes and the final height of the char residue decreased slightly, remaining between 3 and 5 cm irrespective of the reprocessing cycle. Therefore, the charring ability of these flame-retardant fillers into PP was not affected by the reprocessing, as already stated from cone calorimeter tests.

The morphologies of the outer and inner layers of char residue analyzed with SEM were also reported in Figure 50 from the virgin PP/IFR system to the five-times reprocessed sample. SEM observations of the vPP+IFR char indicated a distinctly layered morphology: the outer surface appeared dense and relatively intact, containing only limited voids, while the inner region was characterized by a highly porous network with well-defined micro-channels. The first reprocessing cycle of PP/IFR seemed to affect the morphology of the protective char layer. While the outer part was very similar to that of virgin PP/IFR, characterized by a compact and dense structure, the inner layer instead showed smaller pores and channels if compared to virgin PP/IFR. The same considerations could be made also for the material reprocessed up to two times, which morphology did not differ

from that of the previous discussed sample. Moving from the third reprocessing cycle to the fifth, instead, led to some variations in the morphology of the char. More specifically, the char outer layers from Figure 50d to Figure 50f lost their compactness, approaching to the typical morphology of the inner layers. Nevertheless, EDX analysis performed on inner layers (Figure 51) showed a homogeneous distribution of phosphorus and nitrogen in all the samples analyzed.

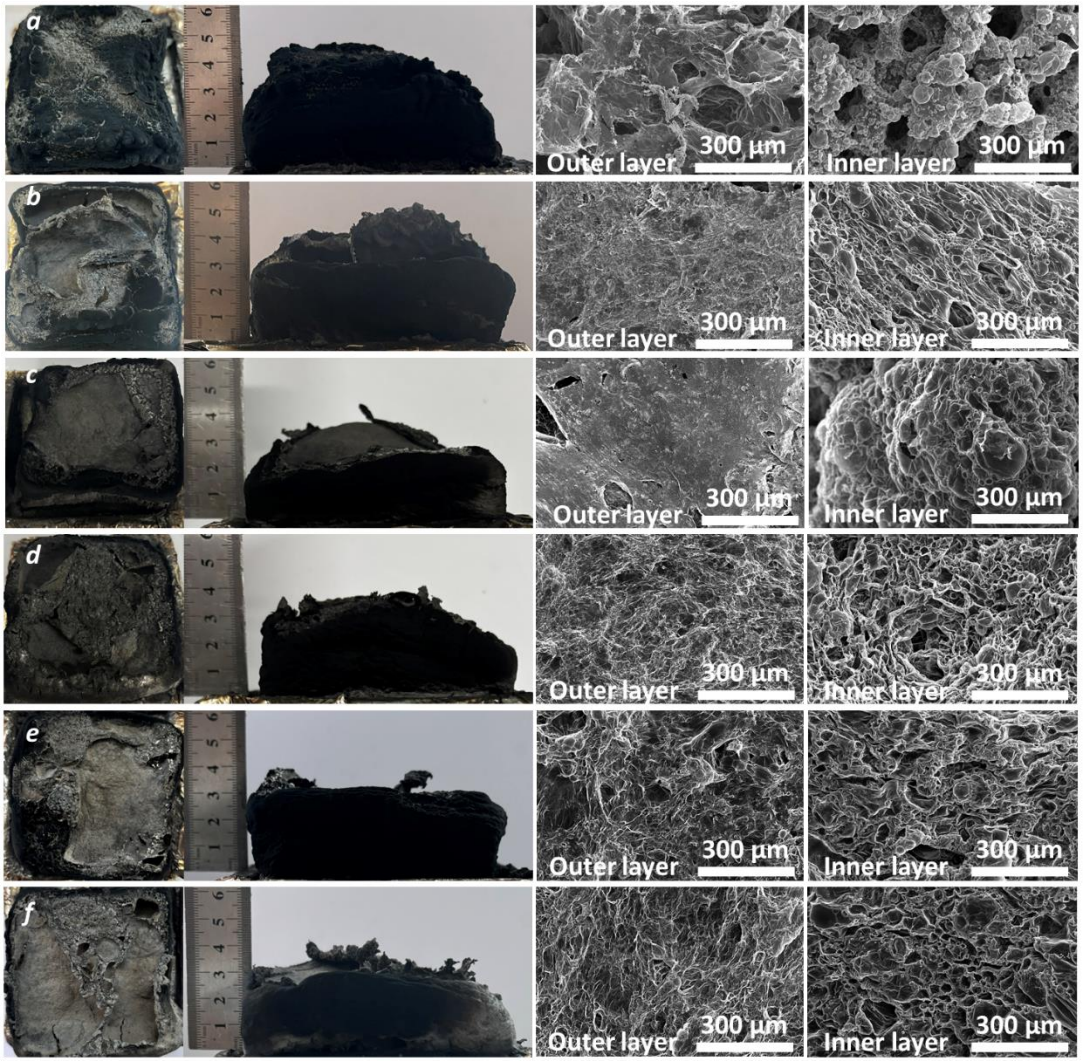

Figure 50. Photos and SEM images of residual char of vPP+IFR (a) and reprocessed samples: n1 (b), n2 (c), n3 (d), n4 (e) and n5 (f).

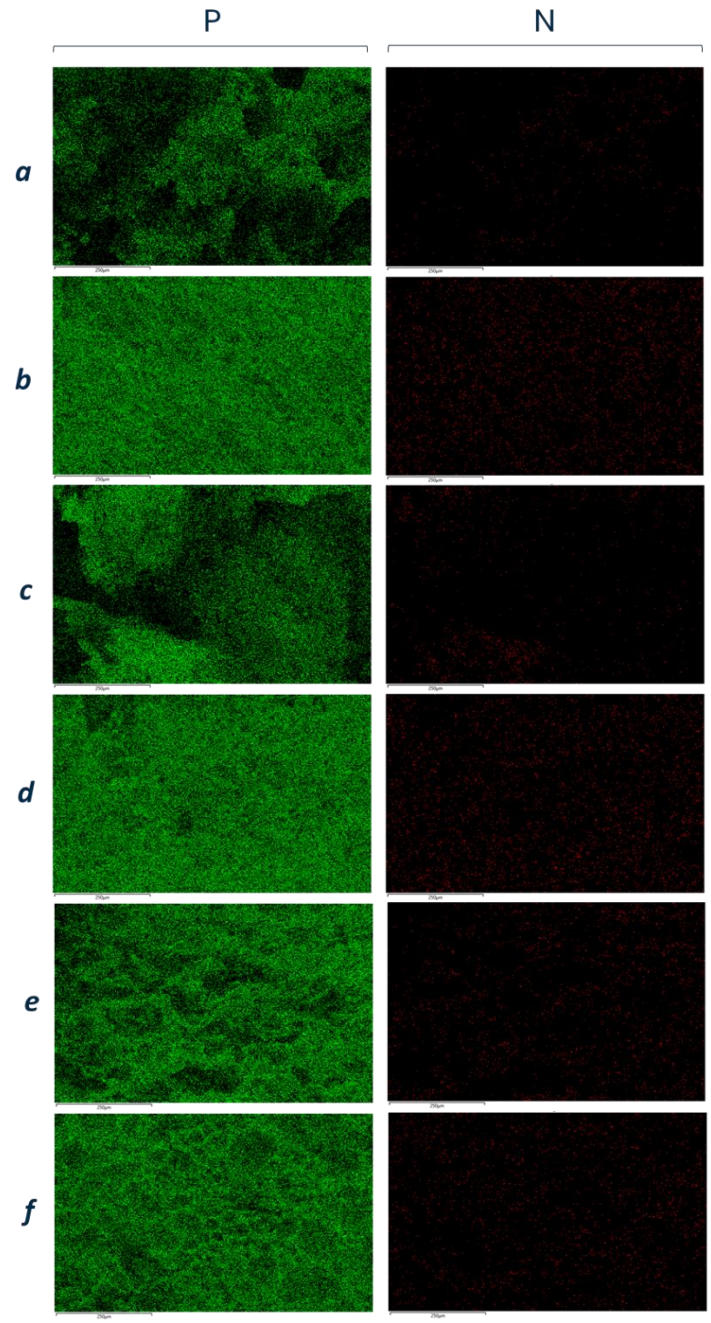

Figure 51. Phosphorus (left column) and nitrogen (right column) EDX analysis of inner char layer of vPP+IFR (a) and reprocessed samples: n1 (b), n2 (c), n3 (d), n4 (e) and n5 (f).

The microstructure of the residual chars was further investigated through Raman analyses, and the collected spectra show overlapped D and G peaks [213,214]. In Table 28 the ratio between the area of the two peaks (I_D/I_G) is listed, along with the calculated crystalline size (L_a) [215].

The char collected from vPP+IFR exhibits a high I_D/I_G up to 1.2 with a small L_a up to 15.9 nm, and these characteristics remain almost unchanged for the samples obtained from the first and the second reprocessing cycles. However, from the third to the fifth cycles, the I_D/I_G values tend to remarkably decrease,

with a significant increment in L_a, indicating a more efficient graphitization of the material.

Table 28. I_D/I_G and L_a of vPP+IFR and reprocessed samples: n1-n5.

	I_D/I_G	L_a [mm]
vPP+IFR	1.2	15.9
r(PP+IFR) n1	1.1	17.5
r(PP+IFR) n2	1.1	17.5
r(PP+IFR) n3	0.9	21.4
r(PP+IFR) n4	0.8	24.0
r(PP+IFR) n5	0.7	27.9

3.4.4 Mechanical properties

Finally, having verified that PP/IFR system was able to maintain its flammability and combustion properties from the virgin sample to its five-times reprocessed counterpart, tensile, flexural and impact tests have been performed in order to assess the effect of reprocessing also on the mechanical properties. The obtained results are depicted in Figure 52. First of all, the addition of IFR resulted in decreased tensile strength, elongation at break and impact strength, as compared to unfilled PP. These changes were in agreement with the literature [105,198], which already reported the poor compatibility between flame-retardants and PP as one of the main issues related to the dramatic decrease of the mechanical properties and resulting in a more brittle behavior of the FR materials. However, despite the noticeable decrease of the elongation at break with the introduction of IFR particles, the obtained values of approximately 120% were quite higher than those typically reported for PP-based composites [105,106,198,216]. Regarding the flexural strength, the mean values increased in vPP+IFR if compared to unfilled virgin PP, as already observed by other authors [217].

Very interesting results have been obtained when analyzing the mechanical response upon reprocessing. Overall, tensile strength, flexural strength and impact strength were not affected by the reprocessing, keeping constant values from the virgin material to the sample reprocessed up to five times. As already shown in other works [106,109,110,218], the mechanical recycling of FR polymers did not induce noteworthy variations in the mechanical properties. On the other hand, the ductility was little affected by the reprocessing: elongation at break values increased slightly until the second recycling cycle likely because of the smaller IFR particles diameter, and then gradually decreased. At the end of the fifth cycle, elongation at break decreased of about 40% if compared to the virgin PP-based system. However, all the obtained values for reprocessed samples remained higher

if compared to those reported in the literature for FR virgin PP-based systems confirming the potential of the studied materials even after mechanical recycling [105,106,198].

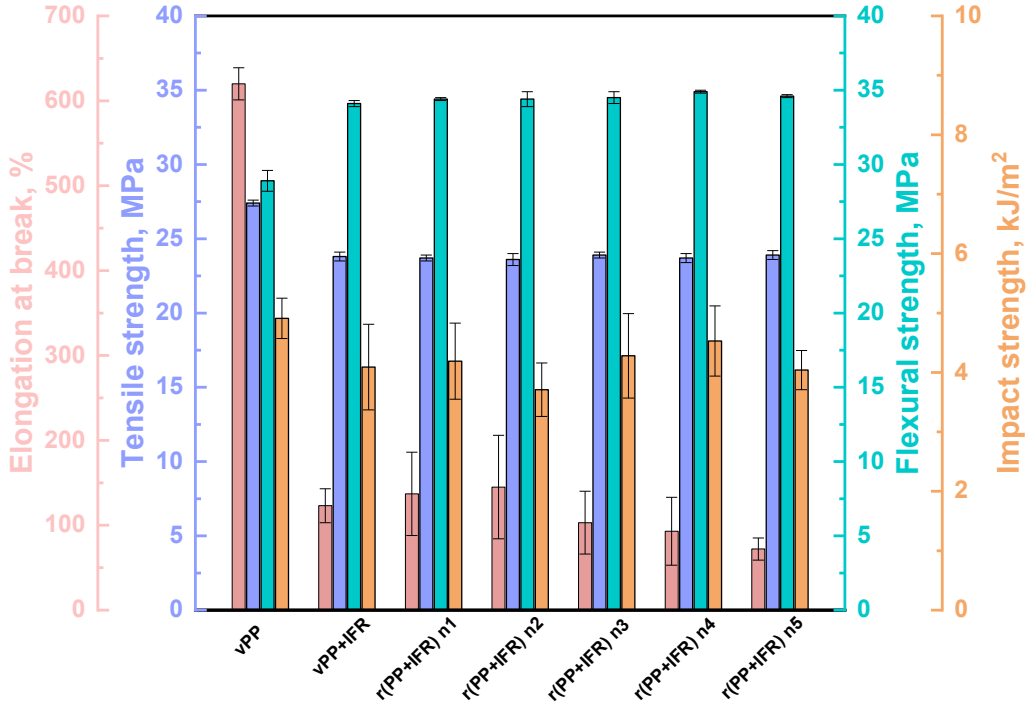

Figure 52. Mechanical properties of unfilled and IFR-containing virgin and reprocessed PP-based systems.

3.4.5 Conclusions

The design of plastic products frequently fails to consider their potential for reuse, repair or recycling, but this approach is no longer viable in the context of the required transition toward a plastic circular economy. This work demonstrated that flame-retardant PP-based composite with 21 wt.% of piperazine pyrophosphate and melamine pyrophosphate mixture (in a ratio 2:1) exhibited a remarkable stability under repeated mechanical recycling conditions. Despite minor morphological changes, such as the progressive agglomeration of IFR particles, neither the thermal stability nor the charring ability of the intumescent formulation was significantly affected by up to five reprocessing cycles. As a consequence, both flammability and combustion performance remained essentially unchanged, with all samples maintaining V-0 classification in UL 94 tests and comparable LOI values as compared to the virgin material. Mechanical properties were also largely preserved, aside from a slight decrease of elongation at break at higher reprocessing cycles due to cumulative thermo-mechanical degradation.

Nevertheless, the studied IFR system composed of PPAP and MPP seems to be more effective when incorporated into a degraded PP derived from mechanical recycling processes, as demonstrated in the previous chapter, than when introduced into a virgin system and subsequently recycled.

Overall, these findings indicated anyway that mechanical recycling can be considered a viable end-of-life strategy for this PP/IFR composites, supporting their potential integration into circular plastic streams without compromising fire safety requirements.

Chapter 4

Concluding remarks

The results presented in this thesis provide a clear and comprehensive contribution to the understanding and advancement of mechanical recycling of polyolefins. By addressing degradation phenomena, microstructural evolution, functional upgrading, and end-of-life behavior, this work demonstrates that the limitations traditionally associated with recycled polypropylene and high-density polyethylene are not intrinsic, but largely the result of uncontrolled degradation and insufficient material design strategies.

The first outcome of this thesis is the detailed clarification of the degradation mechanisms governing mechanically recycled polypropylene. The experimental evidence shows that thermo-mechanical recycling of PP is dominated by random chain scission, leading to a progressive and irreversible reduction in molecular weight and viscosity, without significant oxidative functionalization. This finding confirms that the loss of processability and performance observed in recycled PP is primarily structural. Importantly, the work demonstrates that this degradation pathway can be effectively mitigated through reactive extrusion strategies. The introduction of a repair additive, evaluated under conditions representative of both pre-consumer and post-consumer recycling, enables partial rebuilding of molecular weight and induces melt structuring phenomena in the macromolecular architecture. This dual effect, i.e. molecular weight stabilization combined with topology modification, represents a significant advancement, as it transforms degradation from a purely detrimental phenomenon into a tool for tailoring processability of recycled PP.

A further important contribution of this thesis concerns the analysis of the photo-oxidative aging behavior of recycled polypropylene films under humid conditions. The introduction of the repair additive, able to rebuild recycled PP molecular weight, is also effective in maintaining adequate mechanical properties over prolonged exposure to photo-oxidative degradation. In this way, the service life of films made from recycled plastics can be prolonged, significantly limiting the deterioration of elongation at break and tensile strength, even under exposure

to solar UV radiation and repeated condensation cycles. These results demonstrate that appropriate stabilization can significantly delay mechanical embrittlement of recycled PP during outdoor exposure, thereby improving its suitability for applications requiring long-term durability.

The thesis further delivers a contribution to the understanding and valorization of recycled high-density polyethylene. Unlike polypropylene, HDPE exhibits a complex degradation behavior in which chain scission, branching, and crosslinking coexist. This work demonstrates that, rather than attempting to suppress these mechanisms, they can be exploited to generate long-chain branched architectures. The resulting enhancement in melt strength and ductility enables the production of high melt strength recycled HDPE suitable for elongational flow-dominated processing technologies. This represents a concrete step toward the upcycling of recycled HDPE into higher value-added applications that are typically inaccessible to conventional recyclates.

A further contribution of this thesis is the investigation of functional upgrading of recycled polypropylene through flame-retardant formulations. The results demonstrate that recycled PP can achieve effective flame retardancy, with fire performance comparable to, and in some cases better than, that of virgin-based systems. At the same time, the work highlights how polymer degradation influences the efficiency, stability, and distribution of flame-retardant additives. These findings provide critical insight into the interaction between recycling-induced degradation and functional performance and demonstrate that recycled polypropylene can be securely used even in applications where fire safety is a concern.

Importantly, this thesis addresses one of the most neglected challenges in plastic circularity: the mechanical recycling of flame-retarded polymers at end of life. By subjecting intumescent flame-retarded polypropylene to multiple reprocessing cycles, the work demonstrates how thermo-mechanical degradation and additive redistribution affect rheological behavior, mechanical properties, and fire performance. These results show that functional performances can be preserved across multiple life cycles by selecting a suitable intumescent flame-retardant, underlining the necessity of designing flame-retardant systems with end-of-life recyclability in mind.

From an industrial perspective, the strategies investigated in this thesis present the potential for scalability, as they rely on processing techniques that are already well established in the plastics industry, such as extrusion-based reactive processing and conventional compounding. The possibility of integrating the proposed strategies directly within existing recycling lines suggests that they could be implemented without major modifications to current infrastructures.

The economic implications of these findings are equally significant. By enabling the recovery of mechanical performance, processability, and functional properties, the strategies presented in this work contribute to increasing the market value and application range of recycled polyolefins. Improving the quality and reliability of recyclates can reduce the dependence on virgin polymers and enhance the competitiveness of mechanically recycled materials. In this context,

the ability to maintain functionality, such as flame retardancy or enhanced melt strength, across multiple recycling cycles represents an important step toward more economically viable circular material flows.

Overall, the central contribution of this thesis lies in establishing a unified and experimentally validated framework that links degradation mechanisms, microstructure control, functional performance, and end-of-life behavior of recycled polyolefins. The work moves beyond the traditional downcycling paradigm and demonstrates that mechanical recycling, when guided by specific strategies, can deliver recycled materials with tailored properties, enhanced performance, and increased application potential. In this perspective, the thesis provides practical strategies that can support the transition of mechanical recycling from a low-value recovery route to a key technological pillar of a truly circular plastics economy.

References

[1] Plastics Europe, Plastics Europe - The Facts 2025, 2025. https://plasticseurope.org/wp-content/uploads/2025/09/PE_TheFacts_25_digital-1pager-scrollable.pdf (accessed December 9, 2025).

[2] Y. Gao, A. Cabrera Serrenho, Evaluating the potential to reduce the global demand for polymers, Resources, Conservation and Recycling 223 (2025) 108518. https://doi.org/10.1016/j.resconrec.2025.108518.

[3] R. Geyer, J.R. Jambeck, K.L. Law, Production, use, and fate of all plastics ever made, Science Advances 3 (2017) e1700782. https://doi.org/10.1126/sciadv.1700782.

[4] J.N. Hahladakis, E. Iacovidou, An overview of the challenges and trade-offs in closing the loop of post-consumer plastic waste (PCPW): Focus on recycling, Journal of Hazardous Materials 380 (2019) 120887. https://doi.org/10.1016/j.jhazmat.2019.120887.

[5] A. Ghosh, Performance modifying techniques for recycled thermoplastics, Resources, Conservation and Recycling 175 (2021) 105887. https://doi.org/10.1016/j.resconrec.2021.105887.

[6] D. Hassanian-Moghaddam, N. Asghari, M. Ahmadi, Circular Polyolefins: Advances toward a Sustainable Future, Macromolecules 56 (2023) 5679–5697. https://doi.org/10.1021/acs.macromol.3c00872.

[7] V.S. Cecon, P.F. Da Silva, G.W. Curtzwiler, K.L. Vorst, The challenges in recycling post-consumer polyolefins for food contact applications: A review, Resources, Conservation and Recycling 167 (2021) 105422. https://doi.org/10.1016/j.resconrec.2021.105422.

[8] D. Civancik-Uslu, T.T. Nhu, B. Van Gorp, U. Kresovic, M. Larrain, P. Billen, K. Ragaert, S. De Meester, J. Dewulf, S. Huysveld, Moving from linear to circular household plastic packaging in Belgium: Prospective life cycle assessment of mechanical and thermochemical recycling, Resources, Conservation and Recycling 171 (2021) 105633. https://doi.org/10.1016/j.resconrec.2021.105633.

[9] A. Rahimi, J.M. García, Chemical recycling of waste plastics for new materials production, Nature Reviews Chemistry 1 (2017) 0046. https://doi.org/10.1038/s41570-017-0046.

[10] V. Titone, L. Botta, F.P. La Mantia, Mechanical Recycling of New and Challenging Polymer Systems: A Brief Overview, Macromolecular Materials and Engineering 310 (2025) 2400275. https://doi.org/10.1002/mame.202400275.

[11] A.H. Westlie, E.Y. -X. Chen, C.M. Holland, S.S. Stahl, M. Doyle, S.R. Trenor, K.M. Knauer, Polyolefin Innovations toward Circularity and Sustainable Alternatives, Macromolecular Rapid Communications 43 (2022) 2200492. https://doi.org/10.1002/marc.202200492.

[12] Z.O.G. Schyns, M.P. Shaver, Mechanical Recycling of Packaging Plastics: A Review, Macromolecular Rapid Communications 42 (2021) 2000415. https://doi.org/10.1002/marc.202000415.

[13] J.R. Jambeck, R. Geyer, C. Wilcox, T.R. Siegler, M. Perryman, A. Andrady, R. Narayan, K.L. Law, Plastic waste inputs from land into the ocean, Science 347 (2015) 768–771. https://doi.org/10.1126/science.1260352.
[14] G. Suzuki, N. Uchida, K. Tanaka, O. Higashi, Y. Takahashi, H. Kuramochi, N. Yamaguchi, M. Osako, Global discharge of microplastics from mechanical recycling of plastic waste, Environmental Pollution 348 (2024) 123855. https://doi.org/10.1016/j.envpol.2024.123855.
[15] Plastics Europe, The Circular Economy for Plastics – A European Analysis 2024, 2024. https://plasticseurope.org/knowledge-hub/the-circular-economy-for-plastics-a-european-analysis-2024/ (accessed December 11, 2025).
[16] Plastics Europe, The Plastics Transition, 2024. https://plasticseurope.org/changingplasticsforgood/the-plastics-transition/ (accessed December 11, 2025).
[17] Plastics Europe, Plastics recycling industry figures 2024, 2024. https://www.plasticsrecyclers.eu/wp-content/uploads/2025/11/Statistics_2025_Final.pdf (accessed December 11, 2025).
[18] S. Hemachandra, M. Hadjikakou, S. Pettigrew, A scoping review of food packaging life cycle assessments that account for packaging-related food waste, Int J Life Cycle Assess 29 (2024) 1899–1915. https://doi.org/10.1007/s11367-024-02349-z.
[19] F. Meng, M. Brandão, J.M. Cullen, Replacing Plastics with Alternatives Is Worse for Greenhouse Gas Emissions in Most Cases, Environ. Sci. Technol. 58 (2024) 2716–2727. https://doi.org/10.1021/acs.est.3c05191.
[20] D. Carullo, A. Casson, C. Rovera, M. Ghaani, T. Bellesia, R. Guidetti, S. Farris, Testing a coated PE-based mono-material for food packaging applications: an in-depth performance comparison with conventional multi-layer configurations, Food Packaging and Shelf Life 39 (2023) 101143. https://doi.org/10.1016/j.fpsl.2023.101143.
[21] A. Mengozzi, D. Carullo, F. Bot, S. Farris, E. Chiavaro, Functional properties of food packaging solutions alternative to conventional multilayer systems, J Food Sci Technol 62 (2025) 483–491. https://doi.org/10.1007/s13197-024-06038-5.
[22] M.M. Gutierrez, M. Meleddu, A. Piga, Food losses, shelf life extension and environmental impact of a packaged cheesecake: A life cycle assessment, Food Res Int 91 (2017) 124–132. https://doi.org/10.1016/j.foodres.2016.11.031.
[23] M.C. Heller, S.E.M. Selke, G.A. Keoleian, Mapping the Influence of Food Waste in Food Packaging Environmental Performance Assessments, Journal of Industrial Ecology 23 (2019) 480–495. https://doi.org/10.1111/jiec.12743.
[24] The State of Food and Agriculture 2019. Moving forward on food loss and waste reduction., Food and Agriculture Organization of the United Nations, Rome, 2019.
[25] H. Tetteh, M. Balcells, I. Sazdovski, P. Fullana-i-Palmer, M. Margallo, R. Aldaco, R. Puig, Environmental comparison of food-packaging systems: The significance of shelf-life extension, Cleaner Environmental Systems 13 (2024) 100197. https://doi.org/10.1016/j.cesys.2024.100197.
[26] Y. Saleh, Comparative life cycle assessment of beverages packages in Palestine, Journal of Cleaner Production 131 (2016) 28–42. https://doi.org/10.1016/j.jclepro.2016.05.080.

[27] H.C. Kim, T.J. Wallington, Life Cycle Assessment of Vehicle Lightweighting: A Physics-Based Model To Estimate Use-Phase Fuel Consumption of Electrified Vehicles, Environ. Sci. Technol. 50 (2016) 11226–11233. https://doi.org/10.1021/acs.est.6b02059.
[28] S.S. Muthu, Assessing the Environmental Impact of Textiles and the Clothing Supply Chain, Woodhead Publishing, 2014.
[29] L. Shen, E. Worrell, M.K. Patel, Environmental impact assessment of man-made cellulose fibres, Resources, Conservation and Recycling 55 (2010) 260–274. https://doi.org/10.1016/j.resconrec.2010.10.001.
[30] N.M. van der Velden, M.K. Patel, J.G. Vogtländer, LCA benchmarking study on textiles made of cotton, polyester, nylon, acryl, or elastane, Int J Life Cycle Assess 19 (2014) 331–356. https://doi.org/10.1007/s11367-013-0626-9.
[31] R. Auras, B. Harte, S. Selke, An Overview of Polylactides as Packaging Materials, Macromolecular Bioscience 4 (2004) 835–864. https://doi.org/10.1002/mabi.200400043.
[32] K.S. Anderson, K.M. Schreck, M.A. Hillmyer, Toughening Polylactide, Polymer Reviews 48 (2008) 85–108. https://doi.org/10.1080/15583720701834216.
[33] N. Grassie, E.J. Murray, The Thermal Degradation of Poly(-(D)-fl-Hydroxybutyric Acid): Part 2 Changes in Molecular Weight, Polymer Degradation and Stability 6 (1984) 95–103. https://doi.org/10.1016/0141-3910(84)90075-2.
[34] M. Larsson, O. Markbo, P. Jannasch, Melt processability and thermomechanical properties of blends based on polyhydroxyalkanoates and poly(butylene adipate- co -terephthalate), RSC Advances 6 (2016) 44354–44363. https://doi.org/10.1039/C6RA06282B.
[35] T.P. Haider, C. Völker, J. Kramm, K. Landfester, F.R. Wurm, Plastics of the Future? The Impact of Biodegradable Polymers on the Environment and on Society, Angewandte Chemie International Edition 58 (2019) 50–62. https://doi.org/10.1002/anie.201805766.
[36] M. Karamanlioglu, R. Preziosi, G.D. Robson, Abiotic and biotic environmental degradation of the bioplastic polymer poly(lactic acid): A review, Polymer Degradation and Stability 137 (2017) 122–130. https://doi.org/10.1016/j.polymdegradstab.2017.01.009.
[37] M. Islam, T. Xayachak, N. Haque, D. Lau, M. Bhuiyan, B.K. Pramanik, Impact of bioplastics on environment from its production to end-of-life, Process Safety and Environmental Protection 188 (2024) 151–166. https://doi.org/10.1016/j.psep.2024.05.113.
[38] S. Ishimwe, Bioplastics market development update 2023, 2023. https://www.european-bioplastics.org/bioplastics-market-development-update-2023-2/ (accessed December 28, 2025).
[39] B. Manjula, A.B. Reddy, E.R. Sadiku, V. Sivanjineyulu, G.F. Molelekwa, J. Jayaramudu, K. Raj Kumar, Use of polyolefins in hygienic applications, in: Polyolefin Fibres, Elsevier, 2017: pp. 539–560.
[40] D. Jubinville, E. Esmizadeh, S. Saikrishnan, C. Tzoganakis, T. Mekonnen, A comprehensive review of global production and recycling methods of polyolefin (PO) based products and their post-recycling applications, Sustainable Materials and Technologies 25 (2020) e00188. https://doi.org/10.1016/j.susmat.2020.e00188.
[41] F. Awaja, D. Pavel, Recycling of PET, European Polymer Journal 41 (2005) 1453–1477. https://doi.org/10.1016/j.eurpolymj.2005.02.005.

[42] F.P. La Mantia, V. Titone, L. Botta, P. Glerean, Mechanical Recycling Processes of Polyethylene Terephthalate (PET) in the Framework of Circular Bottle-To-Bottle Manufacturing, Journal of Applied Polymer Science 143 (2026) e57954. https://doi.org/10.1002/app.57954.
[43] F. Welle, Twenty years of PET bottle to bottle recycling—An overview, Resources, Conservation and Recycling 55 (2011) 865–875. https://doi.org/10.1016/j.resconrec.2011.04.009.
[44] G. Grause, M.-F. Chien, C. Inoue, Changes during the weathering of polyolefins, Polymer Degradation and Stability 181 (2020) 109364. https://doi.org/10.1016/j.polymdegradstab.2020.109364.
[45] J. Aurrekoetxea, M.A. Sarrionandia, I. Urrutibeascoa, M.Ll. Maspoch, Effects of recycling on the microstructure and the mechanical properties of isotactic polypropylene, Journal of Materials Science 36 (2001) 2607–2613. https://doi.org/10.1023/A:1017983907260.
[46] A. Jansson, K. Möller, T. Gevert, Degradation of post-consumer polypropylene materials exposed to simulated recycling—mechanical properties, Polymer Degradation and Stability 82 (2003) 37–46. https://doi.org/10.1016/S0141-3910(03)00160-5.
[47] S.K. Najafi, M. Mostafazadeh-Marznaki, M. Chaharmahali, M. Tajvidi, Effect of Thermomechanical Degradation of Polypropylene on Mechanical Properties of Wood-Polypropylene Composites, Journal of Composite Materials 43 (2009) 2543–2554. https://doi.org/10.1177/0021998309345349.
[48] S.V. Canevarolo, Chain scission distribution function for polypropylene degradation during multiple extrusions, Polymer Degradation and Stability 70 (2000) 71–76. https://doi.org/10.1016/S0141-3910(00)00090-2.
[49] H. Hinsken, S. Moss, J.-R. Pauquet, H. Zweifel, Degradation of polyolefins during melt processing, Polymer Degradation and Stability 34 (1991) 279–293. https://doi.org/10.1016/0141-3910(91)90123-9.
[50] V.A. González-González, G. Neira-Velázquez, J.L. Angulo-Sánchez, Polypropylene chain scissions and molecular weight changes in multiple extrusion, Polymer Degradation and Stability 60 (1998) 33–42. https://doi.org/10.1016/S0141-3910(96)00233-9.
[51] C. Spicker, N. Rudolph, I. Kühnert, C. Aumnate, The use of rheological behavior to monitor the processing and service life properties of recycled polypropylene, Food Packaging and Shelf Life 19 (2019) 174–183. https://doi.org/10.1016/j.fpsl.2019.01.002.
[52] H.M. da Costa, V.D. Ramos, M.C.G. Rocha, Rheological properties of polypropylene during multiple extrusion, Polymer Testing 24 (2005) 86–93. https://doi.org/10.1016/j.polymertesting.2004.06.006.
[53] L. Incarnato, P. Scarfato, D. Acierno, Rheological and mechanical properties of recycled polypropylene, Polymer Engineering & Science 39 (1999) 749–755. https://doi.org/10.1002/pen.11463.
[54] L. Delva, K. Ragaert, J. Degrieck, L. Cardon, The Effect of Multiple Extrusions on the Properties of Montmorillonite Filled Polypropylene, Polymers 6 (2014) 2912–2927. https://doi.org/10.3390/polym6122912.
[55] T. Andersson, B. Stålbom, B. Wesslén, Degradation of polyethylene during extrusion. II. Degradation of low-density polyethylene, linear low-density polyethylene, and high-density polyethylene in film extrusion, Journal of Applied Polymer Science 91 (2004) 1525–1537. https://doi.org/10.1002/app.13024.

[56] A. Felgel-Farnholz, A. Schweighuber, C.W. Klampfl, J. Fischer, Comparative study on the degradation of HDPE, LLDPE and LDPE during multiple extrusions, Polymer Degradation and Stability 216 (2023) 110486. https://doi.org/10.1016/j.polymdegradstab.2023.110486.

[57] C.N. Kartalis, C.D. Papaspyrides, R. Pfaendner, K. Hoffmann, H. Herbst, Mechanical recycling of postused high-density polyethylene crates using the restabilization technique. I. Influence of reprocessing, Journal of Applied Polymer Science 73 (1999) 1775–1785. https://doi.org/10.1002/(SICI)1097-4628(19990829)73:9<1775::AID-APP20>3.0.CO;2-G.

[58] M.K. Loultcheva, M. Proietto, N. Jilov, F.P. La Mantia, Recycling of high density polyethylene containers, Polymer Degradation and Stability 57 (1997) 77–81. https://doi.org/10.1016/S0141-3910(96)00230-3.

[59] L.A. Pinheiro, M.A. Chinelatto, S.V. Canevarolo, The role of chain scission and chain branching in high density polyethylene during thermo-mechanical degradation, Polymer Degradation and Stability 86 (2004) 445–453. https://doi.org/10.1016/j.polymdegradstab.2004.05.016.

[60] R. Scaffaro, F.P. La Mantia, L. Botta, M. Morreale, N. Tz. Dintcheva, P. Mariani, Competition between chain scission and branching formation in the processing of high-density polyethylene: Effect of processing parameters and of stabilizers, Polymer Engineering & Science 49 (2009) 1316–1325. https://doi.org/10.1002/pen.21317.

[61] F. Gugumus, Thermooxidative degradation of polyolefins in the solid state: Part 1. Experimental kinetics of functional group formation, Polymer Degradation and Stability 52 (1996) 131–144. https://doi.org/10.1016/0141-3910(95)00229-4.

[62] S.A. Cruz, M. Zanin, Evaluation and identification of degradative processes in post-consumer recycled high-density polyethylene, Polymer Degradation and Stability 80 (2003) 31–37. https://doi.org/10.1016/S0141-3910(02)00379-8.

[63] L. Douiri, H. Jdidi, S. Kordoghli, G. El Hajj Sleiman, Y. Béreaux, Degradation indicators in multiple recycling processing loops of impact polypropylene and high density polyethylene, Polymer Degradation and Stability 219 (2024) 110617. https://doi.org/10.1016/j.polymdegradstab.2023.110617.

[64] E. Epacher, J. Tolvéth, K. Stoll, B. Pukánszky, Two-step degradation of high-density polyethylene during multiple extrusion, Journal of Applied Polymer Science 74 (1999) 1596–1605. https://doi.org/10.1002/(SICI)1097-4628(19991107)74:6<1596::AID-APP35>3.0.CO;2-D.

[65] P. Oblak, J. Gonzalez-Gutierrez, B. Zupančič, A. Aulova, I. Emri, Processability and mechanical properties of extensively recycled high density polyethylene, Polymer Degradation and Stability 114 (2015) 133–145. https://doi.org/10.1016/j.polymdegradstab.2015.01.012.

[66] A.T.P. Zahavich, B. Latto, E. Takacs, J. Vlachopoulos, The effect of multiple extrusion passes during recycling of high density polyethylene, Advances in Polymer Technology 16 (1997) 11–24. https://doi.org/10.1002/(SICI)1098-2329(199721)16:1<11::AID-ADV2>3.0.CO;2-M.

[67] J. Zhang, V. Hirschberg, A. Goecke, M. Wilhelm, W. Yu, M. Orfgen, D. Rodrigue, Effect of mechanical recycling on molecular structure and rheological properties of high-density polyethylene (HDPE), Polymer 297 (2024) 126866. https://doi.org/10.1016/j.polymer.2024.126866.

[68] J. Zhang, V. Hirschberg, D. Rodrigue, Mechanical fatigue of recycled and virgin high-/low-density polyethylene, Journal of Applied Polymer Science 140 (2023) e53312. https://doi.org/10.1002/app.53312.
[69] D.S. Gabriel, A.N. Tiana, Mechanical Properties Improvement of Recycled Polypropylene with Material Value Conservation Schemes Using Virgin Plastic Blends, Materials Science Forum 1015 (2020) 76–81. https://doi.org/10.4028/www.scientific.net/MSF.1015.76.
[70] R. Arrigo, D. Battegazzore, G. Bernagozzi, F. Cravero, D.N. Ribero Pedraza, A. Frache, Recycled PP for 3D Printing: Material and Processing Optimization through Design of Experiment, Applied Sciences 12 (2022) 10840. https://doi.org/10.3390/app122110840.
[71] S. Stanic, T. Koch, K. Schmid, S. Knaus, V.-M. Archodoulaki, Improving Rheological and Mechanical Properties of Various Virgin and Recycled Polypropylenes by Blending with Long-Chain Branched Polypropylene, Polymers 13 (2021) 1137. https://doi.org/10.3390/polym13071137.
[72] F. Kamleitner, B. Duscher, T. Koch, S. Knaus, V.-M. Archodoulaki, Long chain branching as an innovative up-cycling process of polypropylene post-consumer waste – Possibilities and limitations, Waste Management 68 (2017) 32–37. https://doi.org/10.1016/j.wasman.2017.07.022.
[73] P.K. Fearon, N. Marshall, N.C. Billingham, S.W. Bigger, Evaluation of the oxidative stability of multiextruded polypropylene as assessed by physicomechanical testing and simultaneous differential scanning calorimetry-chemiluminescence, Journal of Applied Polymer Science 79 (2001) 733–741. https://doi.org/10.1002/1097-4628(20010124)79:4<733::AID-APP180>3.0.CO;2-I.
[74] D. Battegazzore, F. Cravero, G. Bernagozzi, A. Frache, Designing a 3D printable polypropylene-based material from after use recycled disposable masks, Materials Today Communications 32 (2022) 103997. https://doi.org/10.1016/j.mtcomm.2022.103997.
[75] F. Kamleitner, B. Duscher, T. Koch, S. Knaus, V.M. Archodoulaki, Upcycling of polypropylene—the influence of polyethylene impurities, Polymer Engineering & Science 57 (2017) 1374–1381. https://doi.org/10.1002/pen.24522.
[76] Y. Li, S. Jia, S. Du, Y. Wang, L. Lv, J. Zhang, Improved properties of recycled polypropylene by introducing the long chain branched structure through reactive extrusion, Waste Management 76 (2018) 172–179. https://doi.org/10.1016/j.wasman.2018.03.040.
[77] H. Jiang, S. Wang, Y. Wang, Y. Wang, L. Li, L. Ma, D. Cui, T. Tang, Synthesis of Long-Subchain Hyperbranched Polypropylene Using Thermally Degraded Products as Precursor, Macromolecules 54 (2021) 5567–5576. https://doi.org/10.1021/acs.macromol.1c00724.
[78] S. Stanic, T. Koch, K. Schmid, S. Knaus, V. Archodoulaki, Upcycling of polypropylene with various concentrations of peroxydicarbonate and dilauroyl peroxide and two processing steps, Journal of Applied Polymer Science 138 (2021) e50659. https://doi.org/10.1002/app.50659.
[79] S. Stanic, G. Gottlieb, T. Koch, L. Göpperl, K. Schmid, S. Knaus, V.-M. Archodoulaki, Influence of Different Types of Peroxides on the Long-Chain Branching of PP via Reactive Extrusion, Polymers 12 (2020) 886. https://doi.org/10.3390/polym12040886.
[80] C. González-Sánchez, A. Martínez-Aguirre, B. Pérez-García, J. Acosta, C. Fonseca-Valero, M.U. de la Orden, C. Sánchez, J. Martínez Urreaga,

Enhancement of mechanical properties of waste-sourced biocomposites through peroxide induced crosslinking, Composites Part A: Applied Science and Manufacturing 80 (2016) 285–291. https://doi.org/10.1016/j.compositesa.2015.10.032.
[81] R. Pfaendner, Restabilization – 30 years of research for quality improvement of recycled plastics review, Polymer Degradation and Stability 203 (2022) 110082. https://doi.org/10.1016/j.polymdegradstab.2022.110082.
[82] J. Zhang, V. Hirschberg, D. Rodrigue, Blending Recycled High-Density Polyethylene HDPE (rHDPE) with Virgin (vHDPE) as an Effective Approach to Improve the Mechanical Properties, Recycling 8 (2023) 2. https://doi.org/10.3390/recycling8010002.
[83] F. Vilaplana, S. Karlsson, Quality Concepts for the Improved Use of Recycled Polymeric Materials: A Review, Macromolecular Materials and Engineering 293 (2008) 274–297. https://doi.org/10.1002/mame.200700393.
[84] A. Khaki, C. Gerlach, K. Ragaert, R. Fiorio, Root causes of post-consumer high-density polyethylene failing in new bottles, Resources, Conservation and Recycling 209 (2024) 107776. https://doi.org/10.1016/j.resconrec.2024.107776.
[85] R. Juan, C. Domínguez, N. Robledo, B. Paredes, R.A. García-Muñoz, Incorporation of recycled high-density polyethylene to polyethylene pipe grade resins to increase close-loop recycling and Underpin the circular economy, Journal of Cleaner Production 276 (2020) 124081. https://doi.org/10.1016/j.jclepro.2020.124081.
[86] S. Yin, R. Tuladhar, F. Shi, R.A. Shanks, M. Combe, T. Collister, Mechanical reprocessing of polyolefin waste: A review, Polymer Engineering & Science 55 (2015) 2899–2909. https://doi.org/10.1002/pen.24182.
[87] R. Arrigo, G. Malucelli, F.P.L. Mantia, Effect of the Elongational Flow on the Morphology and Properties of Polymer Systems: A Brief Review, Polymers 13 (2021) 3529. https://doi.org/10.3390/polym13203529.
[88] X. Liang, Z. Luo, L. Yang, J. Wei, X. Yuan, Q. Zheng, Rheological properties and crystallization behaviors of long chain branched polyethylene prepared by melt branching reaction, Journal of Polymer Engineering 38 (2018) 7–17. https://doi.org/10.1515/polyeng-2016-0221.
[89] H.B. Parmar, R.K. Gupta, S.N. Bhattacharya, Rheological and molecular properties of organic peroxide induced long chain branching of recycled and virgin high density polyethylene resin, Polymer Engineering & Science 49 (2009) 1806–1813. https://doi.org/10.1002/pen.21401.
[90] H.B. Parmar, R.K. Gupta, S.N. Bhattacharya, Melt Strength and Thermal Properties of Organic Peroxide Modified Virgin and Recycled HDPE, International Polymer Processing 23 (2008) 200–207. https://doi.org/10.3139/217.2126.
[91] A.D. Gotsis, B.L.F. Zeevenhoven, A.H. Hogt, The effect of long chain branching on the processability of polypropylene in thermoforming, Polymer Engineering & Science 44 (2004) 973–982. https://doi.org/10.1002/pen.20089.
[92] F.P. La Mantia, A. Valenza, D. Acierno, Elongational behavior of low density/linear low density polyethylenes, Polymer Engineering & Science 28 (1988) 90–95. https://doi.org/10.1002/pen.760280205.
[93] J. Stange, H. Münstedt, Effect of Long-chain Branching on the Foaming of Polypropylene with Azodicarbonamide, Journal of Cellular Plastics 42 (2006) 445–467. https://doi.org/10.1177/0021955X06063520.

[94] A. Bifulco, J. Chen, A. Sekar, W.W. Klingler, A. Gooneie, S. Gaan, Recycling of flame retardant polymers: Current technologies and future perspectives, Journal of Materials Science & Technology 199 (2024) 156–183. https://doi.org/10.1016/j.jmst.2024.02.039.
[95] G. Camino, L. Costa, Performance and mechanisms of fire retardants in polymers—A review, Polymer Degradation and Stability 20 (1988) 271–294. https://doi.org/10.1016/0141-3910(88)90073-0.
[96] A. Dasari, Z.-Z. Yu, G.-P. Cai, Y.-W. Mai, Recent developments in the fire retardancy of polymeric materials, Progress in Polymer Science 38 (2013) 1357–1387. https://doi.org/10.1016/j.progpolymsci.2013.06.006.
[97] P.R. Hornsby, Fire retardant fillers for polymers, International Materials Reviews 46 (2001) 199–210. https://doi.org/10.1179/095066001771048763.
[98] M. Casetta, D. Delaval, M. Traisnel, S. Bourbigot, Influence of the Recycling Process on the Fire-Retardant Properties of PP/EPR Blends, Macromolecular Materials and Engineering 296 (2011) 494–505. https://doi.org/10.1002/mame.201000334.
[99] B. Bodzay, M. Fejos, K. Bocz, A. Toldy, F. Ronkay, Gy. Marosi, Upgrading of recycled polypropylene by preparing flame retarded layered composite, Express Polym. Lett. 6 (2012) 895–902. https://doi.org/10.3144/expresspolymlett.2012.95.
[100] Y. Ren, Y. Wang, L. Wang, T. Liu, Evaluation of intumescent fire retardants and synergistic agents for use in wood flour/recycled polypropylene composites, Construction and Building Materials 76 (2015) 273–278. https://doi.org/10.1016/j.conbuildmat.2014.12.004.
[101] M. Combeau, M. Batistella, A. Breuillac, M.K. Naess, D. Perrin, J.-M. Lopez-Cuesta, POSS in intumescent flame-retardant systems to improve fire behaviour of virgin and recycled high density polyethylene, Polymer Degradation and Stability 233 (2025) 111177. https://doi.org/10.1016/j.polymdegradstab.2025.111177.
[102] L. Delva, S. Hubo, L. Cardon, K. Ragaert, On the role of flame retardants in mechanical recycling of solid plastic waste, Waste Management 82 (2018) 198–206. https://doi.org/10.1016/j.wasman.2018.10.030.
[103] C. Ma, J. Yu, B. Wang, Z. Song, J. Xiang, S. Hu, S. Su, L. Sun, Chemical recycling of brominated flame retarded plastics from e-waste for clean fuels production: A review, Renewable and Sustainable Energy Reviews 61 (2016) 433–450. https://doi.org/10.1016/j.rser.2016.04.020.
[104] I.S. Lase, K. Ragaert, J. Dewulf, S. De Meester, Multivariate input-output and material flow analysis of current and future plastic recycling rates from waste electrical and electronic equipment:The case of small household appliances, Resources, Conservation and Recycling 174 (2021) 105772. https://doi.org/10.1016/j.resconrec.2021.105772.
[105] Y. Li, B. Xue, S. Wang, J. Sun, H. Li, X. Gu, H. Wang, S. Zhang, Photoaging and Fire Performance of Polypropylene Containing Melamine Phosphate, ACS Appl. Polym. Mater. 2 (2020) 4455–4463. https://doi.org/10.1021/acsapm.0c00578.
[106] X. Almeras, M.L. Bras, P. Hornsby, S. Bourbigot, G. Marosi, P. Anna, R. Delobel, Artificial Weathering and Recycling Effect on Intumescent Polypropylenebased Blends, Journal of Fire Sciences 22 (2004) 143–161. https://doi.org/10.1177/0734904104039609.
[107] R. Baron, L. Geoffroy, N. Gay, G. Fontaine, B. Fayolle, S. Bourbigot, Thermal ageing of flame-retardant high-density polyethylene designed for

railway application, Polymer Degradation and Stability 234 (2025) 111202. https://doi.org/10.1016/j.polymdegradstab.2025.111202.
[108] R. Baron, L. Geoffroy, N. Gay, G. Fontaine, B. Fayolle, S. Bourbigot, Investigating the effect of flame-retardants on the thermal ageing of a high-density polyethylene, Polymer Degradation and Stability 240 (2025) 111510. https://doi.org/10.1016/j.polymdegradstab.2025.111510.
[109] X. Almeras, M. Le Bras, P. Hornsby, S. Bourbigot, G. Marosi, P. Anna, R. Delobel, Effect of Recycling on Fire Retardancy of Intumescent Polypropylene Based Blends, Progress in Rubber, Plastics and Recycling Technology 20 (2004) 25–45. https://doi.org/10.1177/147776060402000103.
[110] A. El-sabbagh, L. Steuernagel, G. Ziegmann, Low combustible polypropylene/flax/magnesium hydroxide composites: mechanical, flame retardation characterization and recycling effect, Journal of Reinforced Plastics and Composites 32 (2013) 1030–1043. https://doi.org/10.1177/0731684413480993.
[111] K. Ragaert, L. Delva, K. Van Geem, Mechanical and chemical recycling of solid plastic waste, Waste Management 69 (2017) 24–58. https://doi.org/10.1016/j.wasman.2017.07.044.
[112] V. Beghetto, R. Sole, C. Buranello, M. Al-Abkal, M. Facchin, Recent Advancements in Plastic Packaging Recycling: A Mini-Review, Materials 14 (2021) 4782. https://doi.org/10.3390/ma14174782.
[113] G. Bernagozzi, R. Arrigo, G. Ponzielli, A. Frache, Towards effective recycling routes for polypropylene: Influence of a repair additive on flow characteristics and processability, Polymer Degradation and Stability 223 (2024) 110714. https://doi.org/10.1016/j.polymdegradstab.2024.110714.
[114] G. Bernagozzi, R. Arrigo, A. Frache, High Melt Strength Recycled High-Density Polyethylene: Evaluation of a Novel Route for Targeting the Polymer Microstructure, Polymers 17 (2025) 382. https://doi.org/10.3390/polym17030382.
[115] D. Auhl, J. Stange, H. Münstedt, B. Krause, D. Voigt, A. Lederer, U. Lappan, K. Lunkwitz, Long-Chain Branched Polypropylenes by Electron Beam Irradiation and Their Rheological Properties, Macromolecules 37 (2004) 9465–9472. https://doi.org/10.1021/ma030579w.
[116] Y. Amintowlieh, C. Tzoganakis, S.G. Hatzikiriakos, A. Penlidis, Effects of processing variables on polypropylene degradation and long chain branching with UV irradiation, Polymer Degradation and Stability 104 (2014) 1–10. https://doi.org/10.1016/j.polymdegradstab.2014.03.016.
[117] F. Kamleitner, B. Duscher, T. Koch, S. Knaus, K. Schmid, V.-M. Archodoulaki, Influence of the Molar Mass on Long-Chain Branching of Polypropylene, Polymers 9 (2017) 442. https://doi.org/10.3390/polym9090442.
[118] S. Kurzbeck, F. Oster, H. Münstedt, T.Q. Nguyen, R. Gensler, Rheological properties of two polypropylenes with different molecular structure, Journal of Rheology 43 (1999) 359–374. https://doi.org/10.1122/1.551040.
[119] J.A. Langston, R.H. Colby, T.C.M. Chung, F. Shimizu, T. Suzuki, M. Aoki, Synthesis and Characterization of Long Chain Branched Isotactic Polypropylene via Metallocene Catalyst and T-Reagent, (2007). https://doi.org/10.1021/ma062111.
[120] W. Zhao, Y. Huang, X. Liao, Q. Yang, The molecular structure characteristics of long chain branched polypropylene and its effects on non-

isothermal crystallization and mechanical properties, Polymer 54 (2013) 1455–1462. https://doi.org/10.1016/j.polymer.2012.12.073.
[121] C. Gabriel, D. Lilge, Molecular mass dependence of the zero shear-rate viscosity of LDPE melts: evidence of an exponential behaviour, Rheologica Acta 45 (2006) 995–1002. https://doi.org/10.1007/s00397-005-0047-1.
[122] Y. Zhu, S. Wei, C. Guo, X. Cao, X. Yin, G. He, Preparation and characterization of long-chain branched HDPE by UV-induced reactive extrusion at mild temperature, Polymer 282 (2023) 126193. https://doi.org/10.1016/j.polymer.2023.126193.
[123] C. Gabriel, H. Münstedt, Strain hardening of various polyolefins in uniaxial elongational flow, Journal of Rheology 47 (2003) 619–630. https://doi.org/10.1122/1.1567752.
[124] Z. Yuan, X. Chen, D. Yu, Recent Advances in Elongational Flow Dominated Polymer Processing Technologies, Polymers 13 (2021) 1792. https://doi.org/10.3390/polym13111792.
[125] G. Basseri, M. Mehrabi Mazidi, F. Hosseini, M.K. Razavi Aghjeh, Relationship among microstructure, linear viscoelastic behavior and mechanical properties of SBS triblock copolymer-compatibilized PP/SAN blend, Polymer Bulletin 71 (2014) 465–486. https://doi.org/10.1007/s00289-013-1071-4.
[126] F. Ardakani, Y. Jahani, J. Morshedian, Dynamic viscoelastic behavior of polypropylene/polybutene-1 blends and its correlation with morphology, Journal of Applied Polymer Science 125 (2012) 640–648. https://doi.org/10.1002/app.36324.
[127] V. García-Masabet, O. Santana Pérez, J. Cailloux, T. Abt, M. Sánchez-Soto, F. Carrasco, M.L. Maspoch, PLA/PA Bio-Blends: Induced Morphology by Extrusion, Polymers 12 (2019) 10. https://doi.org/10.3390/polym12010010.
[128] O. Vernáez, A.J. Müller, Relaxation time spectra from short frequency range small-angle dynamic rheometry, Rheologica Acta 53 (2014) 385–399. https://doi.org/10.1007/s00397-014-0766-2.
[129] H.M. da Costa, V.D. Ramos, M.G. de Oliveira, Degradation of polypropylene (PP) during multiple extrusions: Thermal analysis, mechanical properties and analysis of variance, Polymer Testing 26 (2007) 676–684. https://doi.org/10.1016/j.polymertesting.2007.04.003.
[130] R. Caban, FTIR-ATR spectroscopic, thermal and microstructural studies on polypropylene-glass fiber composites, Journal of Molecular Structure 1264 (2022) 133181. https://doi.org/10.1016/j.molstruc.2022.133181.
[131] R. Morent, N. De Geyter, C. Leys, L. Gengembre, E. Payen, Comparison between XPS- and FTIR-analysis of plasma-treated polypropylene film surfaces, Surface and Interface Analysis 40 (2008) 597–600. https://doi.org/10.1002/sia.2619.
[132] E. Andreassen, Infrared and Raman spectroscopy of polypropylene, in: J. Karger-Kocsis (Ed.), Polypropylene, Springer Netherlands, Dordrecht, 1999: pp. 320–328. https://doi.org/10.1007/978-94-011-4421-6_46.
[133] V. Delbruel, H. Lajoie, V. Steiner, J.-F. Gérard, J. Duchet-Rumeau, J. Chevalier, Effects of polypropylene compositions and processing conditions on its aging resistance under tropical environments, Polymer Degradation and Stability 228 (2024) 110883. https://doi.org/10.1016/j.polymdegradstab.2024.110883.

[134] C. Badini, O. Ostrovskaya, G. Bernagozzi, R. Lanfranco, S. Miranda, Recycling of Polypropylene Recovered from a Composting Plant: Mechanical Behavior of Compounds with Virgin Plastic, Recycling 8 (2023). https://doi.org/10.3390/recycling8040062.
[135] L. Sangroniz, M. Fernández, A. Santamaria, Polymers and rheology: A tale of give and take, Polymer 271 (2023) 125811. https://doi.org/10.1016/j.polymer.2023.125811.
[136] I. Grigoriadou, K.M. Paraskevopoulos, K. Chrissafis, E. Pavlidou, T.-G. Stamkopoulos, D. Bikiaris, Effect of different nanoparticles on HDPE UV stability, Polymer Degradation and Stability 96 (2011) 151–163. https://doi.org/10.1016/j.polymdegradstab.2010.10.001.
[137] Z. Xu, G. Tang, Y. Liu, R. Yang, Interfacial effects on photooxidative aging of silica-filled polypropylene composites, Polymer Degradation and Stability 227 (2024) 110896. https://doi.org/10.1016/j.polymdegradstab.2024.110896.
[138] A. Shabir, C.M. Tan, P. Singh, Degradation Physics of Silicone Under UV-A Irradiation, IEEE Transactions on Device and Materials Reliability 23 (2023) 584–590. https://doi.org/10.1109/TDMR.2023.3324348.
[139] P. Singh, C.M. Tan, Time evolution of packaged LED lamp degradation in outdoor applications, Optical Materials 86 (2018) 148–154. https://doi.org/10.1016/j.optmat.2018.10.009.
[140] M. Lu, X. Gao, P. Liu, H. Tang, F. Wang, Y. Ding, S. Zhang, M. Yang, Photo- and thermo-oxidative aging of polypropylene filled with surface modified fumed nanosilica, Composites Communications 3 (2017) 51–58. https://doi.org/10.1016/j.coco.2017.02.004.
[141] J. Li, R. Yang, J. Yu, Y. Liu, Natural photo-aging degradation of polypropylene nanocomposites, Polymer Degradation and Stability 93 (2008) 84–89. https://doi.org/10.1016/j.polymdegradstab.2007.10.022.
[142] R. Seldén, B. Nyström, R. Långström, UV aging of poly(propylene)/wood-fiber composites, Polymer Composites 25 (2004) 543–553. https://doi.org/10.1002/pc.20048.
[143] T. Ojeda, A. Freitas, K. Birck, E. Dalmolin, R. Jacques, F. Bento, F. Camargo, Degradability of linear polyolefins under natural weathering, Polymer Degradation and Stability 96 (2011) 703–707. https://doi.org/10.1016/j.polymdegradstab.2010.12.004.
[144] P. Dahal, J.H. Kim, Y.C. Kim, Effects of linear low density polyethylene on physical properties and irradiation effectiveness of polypropylene, Korean J. Chem. Eng. 31 (2014) 1–5. https://doi.org/10.1007/s11814-013-0189-2.
[145] M.S. Rabello, J.R. White, Crystallization and melting behaviour of photodegraded polypropylene — I. Chemi-crystallization, Polymer 38 (1997) 6379–6387. https://doi.org/10.1016/S0032-3861(97)00213-9.
[146] C. Rouillon, P.-O. Bussiere, E. Desnoux, S. Collin, C. Vial, S. Therias, J.-L. Gardette, Is carbonyl index a quantitative probe to monitor polypropylene photodegradation?, Polymer Degradation and Stability 128 (2016) 200–208. https://doi.org/10.1016/j.polymdegradstab.2015.12.011.
[147] Y. Lv, Y. Huang, J. Yang, M. Kong, H. Yang, J. Zhao, G. Li, Outdoor and accelerated laboratory weathering of polypropylene: A comparison and correlation study, Polymer Degradation and Stability 112 (2015) 145–159. https://doi.org/10.1016/j.polymdegradstab.2014.12.023.

[148] I.H. Craig, J.R. White, P.C. Kin, Crystallization and chemi-crystallization of recycled photo-degraded polypropylene, Polymer 46 (2005) 505–512. https://doi.org/10.1016/j.polymer.2004.11.019.
[149] F.P. La Mantia, M. Baiamonte, S. Santangelo, R. Scaffaro, M.C. Mistretta, Influence of Different Environments and Temperatures on the Photo-Oxidation Behaviour of the Polypropylene, Polymers 15 (2022) 74. https://doi.org/10.3390/polym15010074.
[150] I. Yakimets, D. Lai, M. Guigon, Effect of photo-oxidation cracks on behaviour of thick polypropylene samples, Polymer Degradation and Stability 86 (2004) 59–67. https://doi.org/10.1016/j.polymdegradstab.2004.01.013.
[151] S.J. Park, H.-K. Lim, S.-J. Lee, S.H. Im, J. min Lee, Y. Jung, S.H. Kim, J.-S. Shim, J. Won, J.J. Chung, I.-S. Song, Enhancing Biodegradable Bone Plate Performance: Stereocomplex Polylactic Acid for Improved Mechanical Properties and Near-Infrared Transparency, Biomacromolecules 26 (2025) 2390–2401. https://doi.org/10.1021/acs.biomac.4c01768.
[152] C. Long, Z. Dong, K. Wang, F. Yu, C. He, Z.-R. Chen, Molecular weight distribution shape approach for simultaneously enhancing the stiffness, ductility and strength of isotropic semicrystalline polymers based on linear unimodal and bimodal polyethylenes, Polymer 275 (2023) 125936. https://doi.org/10.1016/j.polymer.2023.125936.
[153] K.-H. Nitta, M. Takayanagi, Role of tie molecules in the yielding deformation of isotactic polypropylene, Journal of Polymer Science Part B: Polymer Physics 37 (1999) 357–368. https://doi.org/10.1002/(SICI)1099-0488(19990215)37:4<357::AID-POLB9>3.0.CO;2-I.
[154] D. Dudic, D. Kostoski, V. Djokovic, Z. Stojanovic, Recrystallization processes induced by accelerated ageing in isotactic polypropylene of di erent morphologies, Polymer Degradation and Stability 67 (2000) 233–237. https://doi.org/10.1016/S0141-3910(99)00118-4.
[155] A. Ayadi, D. Kraiem, C. Bradai, S. Pimbert, Recycling effect on mechanical behavior of HDPE/glass fibers at low concentrations, Journal of Thermoplastic Composite Materials 25 (2012) 523–536. https://doi.org/10.1177/0892705711411343.
[156] F.J. Stadler, V. Karimkhani, Correlations between the Characteristic Rheological Quantities and Molecular Structure of Long-Chain Branched Metallocene Catalyzed Polyethylenes, Macromolecules 44 (2011) 5401–5413. https://doi.org/10.1021/ma200550c.
[157] F.J. Stadler, H. Münstedt, Correlations between the Shape of Viscosity Functions and the Molecular Structure of Long-Chain Branched Polyethylenes, Macromolecular Materials and Engineering 294 (2009) 25–34. https://doi.org/10.1002/mame.200800251.
[158] F.J. Stadler, H. Münstedt, Numerical description of shear viscosity functions of long-chain branched metallocene-catalyzed polyethylenes, Journal of Non-Newtonian Fluid Mechanics 151 (2008) 129–135. https://doi.org/10.1016/j.jnnfm.2008.01.010.
[159] S. Cheng, E. Phillips, L. Parks, Improving processability of polyethylenes by radiation-induced long chain branching, Radiation Physics and Chemistry 78 (2009) 563–566. https://doi.org/10.1016/j.radphyschem.2009.03.043.
[160] I.E. Nifant'ev, A.A. Vinogradov, A.A. Vinogradov, G.I. Sadrtdinova, P.D. Komarov, M.E. Minyaev, S.O. Ilyin, A.V. Kiselev, T.I. Samurganova, P.V. Ivchenko, Synthesis, molecular structure and catalytic performance of heterocycle-fused cyclopentadienyl-amido CGC of Ti (IV) in ethylene

(co)polymerization: The formation and precision rheometry of long-chain branched polyethylenes, European Polymer Journal 176 (2022) 111397. https://doi.org/10.1016/j.eurpolymj.2022.111397.
[161] F.J. Stadler, C. Piel, K. Klimke, J. Kaschta, M. Parkinson, M. Wilhelm, W. Kaminsky, H. Münstedt, Influence of Type and Content of Various Comonomers on Long-Chain Branching of Ethene/α-Olefin Copolymers, Macromolecules 39 (2006) 1474–1482. https://doi.org/10.1021/ma0514018.
[162] P.M. Wood-Adams, J.M. Dealy, A.W. deGroot, O.D. Redwine, Effect of Molecular Structure on the Linear Viscoelastic Behavior of Polyethylene, Macromolecules 33 (2000) 7489–7499. https://doi.org/10.1021/ma991533z.
[163] D. Yan, W.-J. Wang, S. Zhu, Effect of long chain branching on rheological properties of metallocene polyethylene, Polymer 40 (1999) 1737–1744. https://doi.org/10.1016/S0032-3861(98)00318-8.
[164] M. Celina, G.A. George, Characterisation and degradation studies of peroxide and silane crosslinked polyethylene, Polymer Degradation and Stability 48 (1995) 297–312. https://doi.org/10.1016/0141-3910(95)00053-O.
[165] D.J. Bullen, G. Capaccio, C.J. Frye, T. Brock, Crosslinking reactions during processing of silane modified polyethylenes, British Polymer Journal 21 (1989) 117–123. https://doi.org/10.1002/pi.4980210205.
[166] P. Sardashti, C. Tzoganakis, M.A. Polak, A. Penlidis, Radiation Induced Long Chain Branching in High-Density Polyethylene through a Reactive Extrusion Process, Macromolecular Reaction Engineering 8 (2014) 100–111. https://doi.org/10.1002/mren.201300134.
[167] J. Tian, W. Yu, C. Zhou, The preparation and rheology characterization of long chain branching polypropylene, Polymer 47 (2006) 7962–7969. https://doi.org/10.1016/j.polymer.2006.09.042.
[168] I. Vittorias, M. Wilhelm, Application of FT Rheology to Industrial Linear and Branched Polyethylene Blends, Macromolecular Materials and Engineering 292 (2007) 935–948. https://doi.org/10.1002/mame.200700120.
[169] V. García-Masabet, O.S. Pérez, J. Cailloux, T. Abt, M. Sánchez-Soto, F. Carrasco, M.L. Maspoch, PLA/PA Bio-Blends: Induced Morphology by Extrusion, Polymers 12 (2019). https://doi.org/10.3390/polym12010010.
[170] C.A. García-Franco, D.J. Lohse, C.G. Robertson, O. Georjon, Relative quantification of long chain branching in essentially linear polyethylenes, European Polymer Journal 44 (2008) 376–391. https://doi.org/10.1016/j.eurpolymj.2007.10.030.
[171] S. Trinkle, C. Friedrich, Van Gurp-Palmen-plot: a way to characterize polydispersity of linear polymers, Rheologica Acta 40 (2001) 322–328. https://doi.org/10.1007/s003970000137.
[172] A.H. Dekmezian, W. Weng, C.A. Garcia-Franco, E.J. Markel, Melt strength of blends of linear low density polyethylene and comb polymers, Polymer 45 (2004) 5635–5640. https://doi.org/10.1016/j.polymer.2004.03.075.
[173] P. Gupta, G.L. Wilkes, A.M. Sukhadia, R.K. Krishnaswamy, M.J. Lamborn, S.M. Wharry, C.C. Tso, P.J. DesLauriers, T. Mansfield, F.L. Beyer, Does the length of the short chain branch affect the mechanical properties of linear low density polyethylenes? An investigation based on films of copolymers of ethylene/1-butene, ethylene/1-hexene and ethylene/1-octene synthesized by a single site metallocene catalyst, Polymer 46 (2005) 8819–8837. https://doi.org/10.1016/j.polymer.2005.05.137.

[174] T. Kida, R. Tanaka, T. Shiono, H. Takeshita, K. Tokumitsu, Effect of short-chain branches in high-molecular-weight component on tensile properties of polyethylene solids, Polymer 298 (2024) 126906. https://doi.org/10.1016/j.polymer.2024.126906.
[175] R.K. Krishnaswamy, Q. Yang, L. Fernandez-Ballester, J.A. Kornfield, Effect of the Distribution of Short-Chain Branches on Crystallization Kinetics and Mechanical Properties of High-Density Polyethylene, Macromolecules 41 (2008) 1693–1704. https://doi.org/10.1021/ma070454h.
[176] R.N. Rothon, P.R. Hornsby, Flame retardant effects of magnesium hydroxide, Polymer Degradation and Stability 54 (1996) 383–385. https://doi.org/10.1016/S0141-3910(96)00067-5.
[177] A. Ares, R. Bouza, S.G. Pardo, M.J. Abad, L. Barral, Rheological, Mechanical and Thermal Behaviour of Wood Polymer Composites Based on Recycled Polypropylene, J Polym Environ 18 (2010) 318–325. https://doi.org/10.1007/s10924-010-0208-x.
[178] F. De Rosa, F. Palmeri, S. Laurenzi, Recycling Space Beverage Packaging into LDPE-Based Composite Materials, Aerospace 11 (2024) 957. https://doi.org/10.3390/aerospace11120957.
[179] T.R. Hull, A. Witkowski, L. Hollingbery, Fire retardant action of mineral fillers, Polymer Degradation and Stability 96 (2011) 1462–1469. https://doi.org/10.1016/j.polymdegradstab.2011.05.006.
[180] M.J. Wang, L.M. Bai, M. Zhang, Y.X. Ma, L.C. Zhao, S.Y. Li, Preparation of magnesium hydroxide by modifier-directed hydration and its effect on flame retardancy and mechanical properties of polypropylene, Physicochem. Probl. Miner. Process. 59 (2023). https://doi.org/10.37190/ppmp/175706.
[181] X. Chen, J. Yu, S. Guo, Thermal oxidative degradation kinetics of PP and PP/mg (OH)2 flame-retardant composites, Journal of Applied Polymer Science 103 (2007) 1978–1984. https://doi.org/10.1002/app.24965.
[182] Q. Zhang, H. Xing, C. Sun, H. Xiang, D. Jiang, L. Qin, The mechanical properties and thermal performances of polypropylene with a novel intumescent flame retardant, Journal of Applied Polymer Science 115 (2010) 2170–2177. https://doi.org/10.1002/app.31348.
[183] E.M. van der Merwe, C.A. Strydom, Quantitative thermogravimetric analysis of binary mixtures, Journal of Thermal Analysis and Calorimetry 76 (2004) 149–156. https://doi.org/10.1023/B:JTAN.0000027814.93703.0c.
[184] R. Édelobel, S. Bourbigot, M. Le Bras, Y. Schmidt, J. -Marie Leroy, Invariant values of kinetic parameters — Evaluation of fire retardancy application to the PP-APP/PER system, Makromolekulare Chemie. Macromolecular Symposia 74 (1993) 59–69. https://doi.org/10.1002/masy.19930740108.
[185] W. Gu, R. Wang, H. Qian, J. Zhang, J. Jing, H. Li, X. Gu, S. Zhang, Interaction modulation of diphosphate piperazine and melamine phosphate for enhanced water resistance and flame retardancy in polypropylene, Composites Part A: Applied Science and Manufacturing 199 (2025) 109177. https://doi.org/10.1016/j.compositesa.2025.109177.
[186] H. Vahabi, E. Movahedifar, B.K. Kandola, M.R. Saeb, Flame Retardancy Index (FRI) for Polymer Materials Ranking, Polymers 15 (2023) 2422. https://doi.org/10.3390/polym15112422.

[187] S. Bourbigot, Evaluation of condensed phase: Char/residue analysis, in: Analysis of Flame Retardancy in Polymer Science, Elsevier, 2022: pp. 191–231. https://doi.org/10.1016/B978-0-12-824045-8.00006-X.
[188] G. Bernagozzi, D. Battegazzore, R. Arrigo, A. Frache, Optimizing the Rheological and Thermal Behavior of Polypropylene-Based Composites for Material Extrusion Additive Manufacturing Processes, Polymers 15 (2023) 2263. https://doi.org/10.3390/polym15102263.
[189] N.K. Kim, R. Lin, D. Bhattacharyya, Effects of wool fibres, ammonium polyphosphate and polymer viscosity on the flammability and mechanical performance of PP/wool composites, Polymer Degradation and Stability 119 (2015) 167–177. https://doi.org/10.1016/j.polymdegradstab.2015.05.015.
[190] J. Dou, Y. Xie, R. Chen, Y. Qin, Study on the Dispersion and Processing Performance of Activated Aluminum Hydroxide/Ammonium Polyphosphate Composite Flame Retardant System for Vinyl Ester Resin, Polymers (Basel) 17 (2025) 667. https://doi.org/10.3390/polym17050667.
[191] Z. Hu, Z.-Q. Zhong, X.-D. Gong, Flame retardancy, thermal properties, and combustion behaviors of intumescent flame-retardant polypropylene containing (poly) piperazine pyrophosphate and melamine polyphosphate, Polymers for Advanced Technologies 31 (2020) 2701–2710. https://doi.org/10.1002/pat.4996.
[192] B. Schartel, T.R. Hull, Development of fire-retarded materials—Interpretation of cone calorimeter data, Fire and Materials 31 (2007) 327–354. https://doi.org/10.1002/fam.949.
[193] R. Carvalho Martins, S. Pereira da Silva Ribeiro, M. Jakeline Cunha Rezende, R.S. Veiga Nascimento, M.A. Chaer Nascimento, J.-M. Lopez-Cuesta, Evaluation of the thermal degradation and cone calorimeter parameters of an intumescent composite containing acidic montmorillonites, J Therm Anal Calorim 148 (2023) 7669–7686. https://doi.org/10.1007/s10973-023-12274-2.
[194] A. Coimbra, J. Sarazin, S. Bourbigot, G. Legros, J.-L. Consalvi, A semi-global reaction mechanism for the thermal decomposition of low-density polyethylene blended with ammonium polyphosphate and pentaerythritol, Fire Safety Journal 133 (2022) 103649. https://doi.org/10.1016/j.firesaf.2022.103649.
[195] E. Verret, A. Collin, S. Duquesne, M. Stievenard, Enhancing Flame Retardancy in Polypropylene Composites: A Bayesian Optimization Approach, Fire 8 (2025) 447. https://doi.org/10.3390/fire8110447.
[196] F. Cavodeau, R. Sonnier, B. Otazaghine, J.-M. Lopez-Cuesta, C. Delaite, Ethylene-vinyl acetate copolymer/aluminium trihydroxide composites: A new method to predict the barrier effect during cone calorimeter tests, Polymer Degradation and Stability 120 (2015) 23–31. https://doi.org/10.1016/j.polymdegradstab.2015.05.021.
[197] C. Cheng, S. Shuqian, S. Mingmei, W. Zhengwen, Z. Xingrong, T. Linsheng, Synergistic flame retardancy of ZnO with piperazine pyrophosphate/melamine polyphosphate in PP, Polymer Testing 117 (2023) 107878. https://doi.org/10.1016/j.polymertesting.2022.107878.
[198] T. Zhao, W. Wu, H. Hu, Z. Rui, X. Zhang, J. Li, The piperazine pyrophosphate intumescent flame retardant of polypropylene composites prepared by selective laser sintering, Polymer Composites 44 (2023) 305–317. https://doi.org/10.1002/pc.27046.

[199] Z. Yuan, H. Wen, Y. Liu, Q. Wang, Synergistic effect between piperazine pyrophosphate and melamine polyphosphate in flame retarded glass fiber reinforced polypropylene, Polymer Degradation and Stability 184 (2021) 109477. https://doi.org/10.1016/j.polymdegradstab.2020.109477.
[200] Z. Hu, T. Shi, Application of a piperazine pyrophosphate intumescent flame retardant in thin-walled glass fiber-reinforced polypropylene materials, Journal of Applied Polymer Science 140 (2023) e54498. https://doi.org/10.1002/app.54498.
[201] Y. Yu, L. Xi, M. Yao, L. Liu, Y. Zhang, S. Huo, Z. Fang, P. Song, Governing effects of melt viscosity on fire performances of polylactide and its fire-retardant systems, iScience 25 (2022) 103950. https://doi.org/10.1016/j.isci.2022.103950.
[202] X. Zheng, M. Deng, H. Jia, X. Chen, R. Wang, J. Sun, H. Li, X. Gu, S. Zhang, Surface Modification of Intumescent Flame Retardant and Its Application in Polypropylene with Excellent Fire Performance and Water Resistance, Polymers 17 (2025) 399. https://doi.org/10.3390/polym17030399.
[203] C. Lu, Q. Cao, X. Hu, C. Liu, X. Huang, Y. Zhang, Influence of morphology and ammonium polyphosphate dispersion on the flame retardancy of polystyrene/nylon-6 blends, Fire and Materials 38 (2014) 765–776. https://doi.org/10.1002/fam.2218.
[204] J. Jin, H. Wang, Z. Shu, L. Lu, Impact of selective dispersion of intumescent flame retardant on properties of polypropylene blends, J Mater Sci 52 (2017) 3269–3280. https://doi.org/10.1007/s10853-016-0615-z.
[205] J. Liu, R. Wang, D. Liang, S. Zhang, J. Feng, M. Xu, S. Du, B. Li, Highly efficient polyethylene composites with flame-retardant, smoke and toxicity suppression properties by incorporating urchin-like ZnO@C-N and intumescent flame retardant, Polymer Degradation and Stability 233 (2025) 111190. https://doi.org/10.1016/j.polymdegradstab.2025.111190.
[206] S. Chen, L. Ai, T. Zhang, P. Liu, W. Liu, Y. Pan, D. Liu, Synthesis and application of a triazine derivative containing boron as flame retardant in epoxy resins, Arabian Journal of Chemistry 13 (2020) 2982–2994. https://doi.org/10.1016/j.arabjc.2018.08.007.
[207] X. Almeras, F. Dabrowski, M. Le Bras, F. Poutch, S. Bourbigot, G. Marosi, P. Anna, Using polyamide-6 as charring agent in intumescent polypropylene formulationsI. Effect of the compatibilising agent on the fire retardancy performance, Polymer Degradation and Stability 77 (2002) 305–313. https://doi.org/10.1016/S0141-3910(02)00068-X.
[208] R. Jeencham, N. Suppakarn, K. Jarukumjorn, Effect of Flame Retardant on Flame Retardancy and Mechanical Properties of Glass Fiber/Polypropylene Composites, Advanced Materials Research 264–265 (2011) 652–656. https://doi.org/10.4028/www.scientific.net/AMR.264-265.652.
[209] N. Bahlouli, D. Pessey, C. Raveyre, J. Guillet, S. Ahzi, A. Dahoun, J.M. Hiver, Recycling effects on the rheological and thermomechanical properties of polypropylene-based composites, Materials & Design 33 (2012) 451–458. https://doi.org/10.1016/j.matdes.2011.04.049.
[210] A. Bata, D. Nagy, Z. Weltsch, Effect of Recycling on the Mechanical, Thermal and Rheological Properties of Polypropylene/Carbon Nanotube Composites, Polymers 14 (2022) 5257. https://doi.org/10.3390/polym14235257.
[211] K. Wang, N. Bahlouli, F. Addiego, S. Ahzi, Y. Rémond, D. Ruch, R. Muller, Effect of talc content on the degradation of re-extruded

polypropylene/talc composites, Polymer Degradation and Stability 98 (2013) 1275–1286. https://doi.org/10.1016/j.polymdegradstab.2013.04.006.
[212] C. Caicedo, A. Vázquez-Arce, O. Ossa, H. Cruz, A. Maciel, Physicomechanical behavior of composites of polypropylene, and mineral fillers with different process cycles, DYNA 85 (2018) 260–268. https://doi.org/10.15446/dyna.v85n207.71894.
[213] N. Shimodaira, A. Masui, Raman spectroscopic investigations of activated carbon materials, J. Appl. Phys. 92 (2002) 902–909. https://doi.org/10.1063/1.1487434.
[214] A. Orlando, F. Franceschini, C. Muscas, S. Pidkova, M. Bartoli, M. Rovere, A. Tagliaferro, A Comprehensive Review on Raman Spectroscopy Applications, Chemosensors 9 (2021). https://doi.org/10.3390/chemosensors9090262.
[215] F. Tuinstra, J.L. Koenig, Raman Spectrum of Graphite, J. Chem. Phys. 53 (1970) 1126–1130. https://doi.org/10.1063/1.1674108.
[216] R. Li, Y. Chen, D. Rao, X. Chen, Y. Meng, H. Wu, Breaking the flame retardancy-mechanical property dilemma in polypropylene composites with simultaneously imparted high thermal conductivity, Chemical Engineering Journal 525 (2025) 170051. https://doi.org/10.1016/j.cej.2025.170051.
[217] Y. Xu, H. Hu, B. Tao, R. Yin, L. Liu, B. Li, Safe and economical preparation of amino acid-derived bio-based triazine char-forming agent for efficient intumescent flame retardant polypropylene, Construction and Building Materials 484 (2025) 141876. https://doi.org/10.1016/j.conbuildmat.2025.141876.
[218] J. Chen, S. Dul, S. Lehner, M. Jovic, S. Gaan, M. Heuberger, R. Hufenus, A. Gooneie, Mechanical recycling of PET containing mixtures of phosphorus flame retardants, Journal of Materials Science & Technology 194 (2024) 167–179. https://doi.org/10.1016/j.jmst.2024.01.035.
[219] J. Honerkamp, J. Weese, A nonlinear regularization method for the calculation of relaxation spectra, Rheologica Acta 32 (1993) 65–73. https://doi.org/10.1007/BF00396678.

Appendix A

A.1 Materials

Polypropylene (PP) Moplen HP500N, with a melt flow rate of 12 g/10 min (230 °C/2,16 kg), was supplied in pellets by Lyondellbasell.

Recycled PP (rPP in Chapter 2.2), derived from post-consumer polypropylene trays, was collected from a recycling plant situated in Guarene (Cuneo, Italy) and it was supplied in the form of flakes.

High-density polyethylene (HDPE) Eraclene MS80U, having a melt flow rate of 27 g/10 min (190 °C/2.16 kg), was supplied in pellets by Versalis.

Nexamite® R201 (NEX in Chapters 2.1 and 2.2), composed of an ethylene copolymer comprising hydrolysable silicon-containing groups, was provided in pellets by Nexam Chemical. The additive was introduced in PP at 5 wt.%.

Nexamite® R305 (NEX in Chapter 2.3), composed of an ethylene copolymer comprising hydrolysable silicon-containing groups, was supplied in pellets by Nexam Chemical. The additive was introduced in HDPE at 5 wt.%.

Magnesium hydroxide (MH) Hydrofy TV 1.5 was supplied in powder form by Nuova Sima. The filler was introduced in PP at 60 wt.%.

Ammonium polyphosphate (APP) was supplied in powder form by Tecnosintesi S.p.A..

Pentaerythritol (PER) was supplied in powder form by Sigma-Aldrich.

The intumescent flame-retardant composed of APP and PER (AP) was introduced in PP at 30 wt.% in a mass ratio of 3:1.

Piperazine pyrophosphate (PAPP) was supplied in powder form by Zhongshan Complord New Materials Co., Ltd..

Melamine polyphosphate (MPP) was provided in powder form by Zhenjiang Senhua Flame Retardant Engineering Technology Co., Ltd..

The intumescent flame-retardant composed of PAPP and MPP (PM) was introduced in PP at 21 wt.% in a mass ratio of 2:1.

A.2 Processing

Xplore MC 15 (DSM) twin-screw mini-extruder was used in the work described in Chapter 2.1. The mini-extruder is equipped with a recirculation channel that allows selecting the desired residence time. The processing was carried out at 190 °C, with a screw rotation speed of 100 rpm for a residence time of 3 or 9 min.

Process 11 (Thermo Fisher Scientific) co-rotating twin-screw extruder was used in the research reported in Chapters 2.1, 2.2 and 2.3. The extruder is equipped with 11 mm diameter screws (L/D=40) and a screw profile with an alternance of conveying and kneading screw elements. The different processing parameters employed, namely barrel temperature, screw speed, and feed rate, are reported in Table 29.

Table 29. Processing parameters set with twin-screw extruder Process 11.

	Barrel temperature [°C]	**Screw speed [rpm]**	**Feed rate [kg/h]**
Chapter 2.1	190	150	0.6
Chapter 2.2	200	200	0.5
Chapter 2.3	190	250	0.8

A flat die (width: 25 mm, thickness: 1 mm) followed by a three-roll calendaring unit (Sheet Take Off for Process 11, Thermo Scientific) was employed for the production of films in Chapter 2.2. The films had a thickness ranging from 320 to 380 μm and a width of about 3 cm. The temperature of the flat die was set at 190°C.

Leistritz ZSE 18 HP is a co-rotating twin-screw extruder (screw profile composed of conveying and kneading screw elements) used in the activities reported in Chapters 3.1, 3.2, 3.3, and 3.4 for the production of recycled PP and for manufacturing flame-retardant composites. The recycled PP was obtained by subjecting virgin PP to eight consecutive extrusion cycles under the following parameters: flat temperature profile equal to 210 °C, 200 rpm and 3 kg/h. Virgin and recycled PP-based systems with MH and AP were melt compounded at 180 °C, 160 rpm and 0.6 kg/h. For the production of virgin and recycled PP-based systems with PM and for their reprocessing, the extrusions were carried out at 300 rpm, 3 kg/h and the following temperature profile (°C): 160, 170, 180, 180, 180, 180.

Rheospin apparatus (IdeaInstr) was used for the production of fibers, as described in Chapter 2.3. This apparatus is equipped with a series of pulleys that collect the hot filament coming from the extruder and transfer it to a final pulley rotating at a constant speed. In this way, the filament is subjected to a non-isothermal elongation flow, as it is uniaxially stretched while cooling by contact with the air; depending on the speed of the last pulley, it is possible to obtain fibers with different diameters. More specifically, fibers with diameters ranging from 200 to 800 μm (corresponding to different draw ratios ($DR = diameter^2_{extrudate}/diameter^2_{fiber}$)) were collected.

A compression molding machine Collin P200T was used for the production of samples for rheological characterization (Chapter 2.1), tensile, impact and

spectroscopic tests (Chapter 2.3), with the following parameters: 190 °C, 100 bar and 3 min. For the samples used for flammability and combustion tests reported in Chapters 3.1 and 3.2 the compression molding parameters were 180 °C, 100 bar and 3 min.

The specimens for the characterizations reported in Chapters 3.3 and 3.4 were prepared by injection molding, using a Haitian HTF86X 1 machine, using a temperature profile in the barrel equal to 165-175-180-180 °C and mold temperature of 30 °C.

A.3 Characterization methods

The rheological behavior of all investigated materials was evaluated using a strain-controlled rheometer ARES from TA Instruments equipped with parallel plate geometry (25 mm diameter). The tests were performed in nitrogen atmosphere to avoid the thermo-oxidative degradation of the sample during the measurement. Preliminary strain sweep experiments were carried out at 180 °C or 190 °C and ω = 10 rad/s. Subsequently, frequency sweeps measurements were carried out at 180 °C or 190 °C, from 10^2 to 10^{-1} rad/s, selecting a strain amplitude value within the linear viscoelastic region for each sample.

The Carreau model was used to fit the experimental complex viscosity data:

$$\eta(\omega) = \eta_0[1 + (\lambda\omega)^2]^{\frac{n-1}{2}} \quad (1)$$

where: η_0 is the zero-shear viscosity, λ is the characteristic relaxation time and n is the power law index.

Data coming from frequency sweep tests were used to calculate the weighted relaxation spectra of the materials in Chapters 2.1, 2.2, and 2.3, using the calculation procedure proposed by Honerkamp and Weese [219].

Attenuated total reflectance Fourier-transform infrared spectroscopy (ATR-FTIR) using a Frontier spectrophotometer (PerkinElmer) was employed for the chemical characterizations. The spectra were collected in the range of 4000–700 cm^{-1} at a resolution of 4 cm^{-1} and 16 scans for each measurement.

The thermal properties were assessed through Differential Scanning Calorimetry (DSC) using a Q20 equipment by TA Instruments. The samples were subjected to three runs of heating-cooling-heating in a nitrogen flow from 0°C to 250°C with a heating/cooling rate of 10 °C/min. The information gleaned from this assessment is the melting enthalpy (ΔH_m), which can be determined by measuring the area beneath the exothermal peak of the heat flow during the second heating. ΔH_m values are valuable indicators of the degree of crystallinity and, hence, of the molecular weight. Furthermore, the melting and crystallization temperatures, as well as the crystallization enthalpy (calculated as the area of the

crystallization peak) were evaluated. The crystallinity degree of the investigated materials was measured using the equation:

$$\chi = \frac{\Delta H_m}{\Delta H_{m0}} \times 100 \quad (3)$$

Where ΔH_m is the melting enthalpy and ΔH_{m0} is the melting enthalpy of 100% crystalline polymer (207 J/g for PP and 293 J/g for HDPE).

QUV SOLAR EYE (Q-PANEL) was used in order to perform the accelerated weathering and study the photo-oxidative degradation of materials in Chapter 2.2. This instrument allowed to expose the materials under controlled UV light and condensation conditions using fluorescent UV lamps with an irradiance equal to 0.77 W/m². The test conditions to which the films were subjected for their aging were the following:

- 8 hours under UVA (365-295 nm) at 50°C;
- 4 hours of water condensation (100% relative humidity) with lamps switched off at 40°C.

The films have been put inside the QUV instrument after die-cutting them into ISO 527-5A specimens. In order to record the changes induced by the photo-oxidative degradation in moisture environment, the specimens have been collected after a defined number of hours according to the characterization tests carried out.

The thermo-oxidative stability was assessed using a Discovery TGA instrument (TA Instruments) for samples analyzed in Chapters 3.1 and 3.2 and using a thermogravimetric analyzer TGA 8000 (PerkinElmer) for samples investigated in Chapters 3.3 and 3.4, in both cases at a heating rate of 10 °C/min under air atmosphere. T_{onset} (temperature at which 2% of weight loss occurs), T_{max} (temperature at which maximum weight loss rate is observed in dTG - derivative - curves), and the residue at 600°C were evaluated.

Flame-retardant performances reported in Chapters 3.1 and 3.2 were measured using UL-94 tests for flammability and using a cone calorimeter for the combustion behavior. UL-94 vertical burning tests were performed in a flammability test cabinet Noselab ATS according to ASTM D3801, using at least five specimens with standardized dimensions of 125×13×3.2 mm³. The combustion behavior was investigated by cone calorimetry according to the ISO 5660 standard, using a Noselab ATS instrument (Nova Milanese, Italy). Square specimens (100×100×3 mm³) were tested under a heat flux of 50 kW/m² in a horizontal configuration. The samples were placed in a sample holder at a distance of 25 mm from the cone heater. The cone calorimeter tests were carried out on three samples and the results averaged.

Flame-retardant performances reported in Chapters 3.3 and 3.4 were evaluated by the following standard methods. The limiting oxygen index (LOI) was determined with a JF-3 oxygen index tester (Jiangning, China) following ASTM D2863 standard and using specimens measuring 80×10×3 mm³. Vertical

burning behavior (UL-94) was assessed with a CZF-5 horizontal and vertical combustion tester (China Jiangning Analytical Instrument Co.) in accordance with ASTM D3801, employing at least five samples with dimensions equal to 130×13×3.2 mm^3. The combustion behavior was evaluated using a Vouch-6810 cone calorimeter according to ISO 5660, under a radiant heat flux of 50 kW/m^2, using specimens with dimensions of 100×100×4 mm^3. The cone calorimeter tests were carried out on three samples and the results averaged.

From the results of cone calorimeter tests, the following quantitative parameters were calculated: *(i)* SEA (Specific Smoke Extinction Area) indicates the total smoke produced per unit of mass lost, and measures the smoke production efficiency; *(ii)* EHC (Effective Heat of Combustion) is the heat released per kilogram of material burned, and reflects the combustion efficiency of the pyrolysis gases *(iii)* MARHE (Maximum Average Rate of Heat Emission) represents the highest rate of heat released during a fire, and provides insight into the intensity of the flame.

The morphology of the samples was observed using a scanning electron microscopy (SEM) ZEISS EVO 15 in Chapters 2.2, 3.1, and 3.2 and Thermo Scientific Apreo C in Chapters 3.3 and 3.4. The obtained SEM micrographs were further analyzed using the software ImageJ. More specifically, after setting the scale, images were processed using "Subtract Background" to improve the signal-to-noise ratio. The "Threshold" function was then applied to binarize the images, separating light clusters from the dark polymer matrix. This binary mask was refined using "Open" and "Close" operations to remove noise, "Watershed" to separate touching particles, and an edge filter to exclude objects at the borders. Finally, "Analyze Particles" was used to extract geometric data. The Feret Diameter was selected as the primary measurement because it is ideal for irregular shapes and rotationally invariant. This parameter represents the maximum distance between two parallel lines tangent to the particle's profile. For each system studied, at least three different SEM images have been analyzed.

Raman spectra were recorded at room temperature with a DXR2 Raman Microscope (Thermo Scientific) employing a 532 nm excitation laser.

Mechanical characterizations in Chapters 2.2 and 2.3 were performed through tensile tests with an Instron® 5966 machine equipped with a 2 kN (error < 0.25%) loading cell. The measurement parameters for testing ISO 527-5A specimens are the following: crosshead speed set at 5 mm/min in Chapter 2.2; in Chapter 2.3 the measurement included an initial strain rate of 1 mm/min, which increased up to 10 mm/min once a deformation of 0.25% was exceeded; the tests on the fibers reported in Chapter 2.3 were performed with a crosshead speed of 20 mm/min. The average values and corresponding standard deviations of the tensile modulus, tensile strength, stress at break, and elongation at break were calculated.

The mechanical properties reported in Chapters 3.3 and 3.4 were evaluated using an RGT-20A universal testing machine (Reger) using a crosshead speed of 25 mm/min for tensile tests and 15 mm/min for flexural tests. The average values and corresponding standard deviations of the flexural strength, tensile strength, and elongation at break were calculated.

Un-notched (Chapter 2.3) and notched (Chapters 3.3 and 3.4) Izod impact tests were performed using a 5.5 J pendulum impact tester HIT25P (Zwick Roell); the energy associated with the fracture after impact was recorded.

All the mechanical properties were carried out on at least five specimens and the results averaged.